From the Institute of Veterinary Pathology

Department of General Pathology and Pathological Anatomy

Chair: Prof. Dr. W. Hermanns

and the

Institute of Molecular Animal Breeding and Biotechnology/Gene Center

Head: Prof. Dr. E. Wolf

Ludwig-Maximilian-University Munich

Under the supervision of Prof. Dr. R. Wanke and Prof. Dr. E. Wolf

Effects of insulin-like growth factor-binding protein-2 (IGFBP-2) overexpression on adrenal and renal growth processes and functions: findings in transgenic mouse models

Inaugural – Dissertation

to achieve the doctor title of veterinary medicine

at the Faculty of Veterinary Medicine of the

Ludwig-Maximilian-University, Munich

by Thomas Martin Fisch

from Fürstenfeldbruck

Munich 2004

Gedruckt mit der Genehmigung der Tierärztlichen Fakultät der

Ludwig-Maximilians-Universität München

Dekan:	Univ.-Prof. Dr. A. Stolle
Referent:	Univ.-Prof. Dr. R Wanke
1. Korreferent:	Univ.-Prof. Dr. E. P. Märtlbauer
2. Korreferent:	Univ.-Prof. Dr. T. Göbel
3. Korreferent:	Univ.-Prof. Dr. R. Köstlin
4. Korreferent:	Univ.-Prof. Dr. M. Stangassinger

Tag der Promotion: 11. Februar 2005

Meinen Eltern

in Dankbarkeit gewidmet

Table of content

Acknowledgement

Curriculum vitae

1 Introduction

The growth hormone (GH)/insulin-like growth factor (IGF)-axis is a key endocrine regulatory system of growth and differentiation of cells, tissues and organs as well as the whole organism [1]. IGF binding proteins (IGFBPs) represent a crucial part of this axis and are capable to essentially modulate IGF-I and IGF-II actions *via* different mechanisms as well as to act IGF-independently [2,3].

The so far known six structurally related, high-affinity IGF binding proteins (IGFBP-1 to -6) are distributed in a highly defined fashion in various organs and tissues, and in biological fluids [4]. Their functions have been studied extensively *in vitro*, revealing a broad spectrum of actions for a given IGFBP. In order to unravel IGFBP actions *in vivo*, several mouse models lacking or overexpressing specific IGFBPs have been generated by transgenic technology in the last decade. However, the biological relevance of IGFBPs *in vivo* is only partially understood [5].

IGFBP-2 is the second most abundant IGFBP in the circulation and has been identified as an inhibitor of postnatal growth in mice *in vivo* [6]. The growth inhibitory effect of IGFBP-2 was even more pronounced in the context of GH and IGF-I excess in GH transgenic giant mice, than in animals with normal GH and IGF-I levels. The stimulated growth of the kidneys, the adrenal glands, and the carcass observed in GH transgenic mice was most potently reduced by IGFBP-2 excess [7].

Further findings implicate IGFBP-2 as a good candidate to modulate GH/IGF actions on the adrenal gland and on the kidney or to act by GH/IGF-independent mechanisms. IGFBP-2 attracted particular attention in the context of adrenal physiology and pathology since *1)* IGFBP-2 is co-regulated with IGF-II, an important factor inducing proliferation of adrenocortical cells and steroidogenesis [8]; *2)* overexpression of IGFBP-2 and secretion into the circulation are characteristic for adrenocortical carcinomas [9]; and *3)* overexpression of IGFBP-2 in mouse adrenocortical tumor cells (Y-1) increased their tumorigenic potential, *i.e.*, stimulation of anchorage-dependent and -independent proliferation and changes in cellular morphology [10].

Further, an involvement of IGFBP-2 in several physiological and pathological conditions of the kidney has been suggested, since *1)* serum IGFBP-2 levels are correlated with the degree of renal dysfunction and are inversely correlated with height in children suffering from chronic renal failure [11]; *2)* overexpression of IGFBP-2

in murine mesangial cells (MMC) avoids IGF-I-induced proliferation of those cells [12]; *3)* IGFBP-2 is overexpressed in cyst epithelia in human multicystic renal dysplasia [13].

GH transgenic mice represent a widely used experimental model for growth research. Phenotypical characterization of GH transgenic mice revealed a typical spectrum of alterations, including increased somatic growth and visceromegaly [14]. GH transgenic mice exhibit enlarged adrenal glands associated with corticosterone hypersecretion [15,16], so that studies concerning growth regulation of adrenocortical cells easily can be combined with a functional read-out, *i.e.*, plasma corticosterone secretion. The GH transgenic mouse further represents a valuable animal model for progressive glomerulosclerosis, chronic renal failure, and acquired cystic kidney disease (ACKD) [17].

The objective of this study was to characterize IGFBP-2 effects on growth and function of the adrenal gland and the kidney in normal and GH-stimulated conditions. Quantitative morphological and functional studies were performed on a collective of mice of four different genetic groups. The groups were generated by an experimental cross of hemizygous transgenic mice overexpressing murine IGFBP-2 under the transcriptional control of the cytomegalovirus (CMV) promoter with hemizygous transgenic mice overexpressing bovine GH under the transcriptional control of the rat phosphoenolpyruvate carboxykinase (PEPCK) promoter.

In particular, the following questions were addressed: *1)* Whether adrenal enlargement observed in G mice is due to cellular hyperplasia, hypertrophy, or both. *2)* How corticosterone hypersecretion is linked with these changes. *3)* Whether adrenal enlargement and function are affected by IGFBP-2. *4)* Which compartments of the kidney are involved in GH/IGF-I-induced renal hypertrophy. *5)* Whether IGFBP-2 overexpression affects GH/IGF-I-induced glomerular hypertrophy and damage. *6)* Whether overexpression of IGFBP-2 affects tubular cells under normal and GH/IGF-I-stimulated conditions.

2 Literature

2.1 Overview of the components of the GH/IGF-axis

The GH/IGF-axis displays a complex, interrelated and interactive system consisting of the peptide hormone GH, the peptide growth factors IGF-I and IGF-II, their specific receptors as well as a series of binding proteins, and multiple related proteases [1,18].

2.1.1 Growth hormone

GH belongs to a large family of cytokine peptides. It is synthesized and stored exclusively by somatotroph cells within the anterior pituitary [19], and is secreted in a pulsatile manner [20,21]. Its amino acid sequence is highly conserved between different species, *e.g.*, rat (r) and murine (m) GH show 95% and 92% identity with bovine (b) GH, respectively [22]. GH expression and secretion is mainly regulated by two hypothalamic peptides, the growth hormone-releasing hormone (GHRH) and the somatotropin release-inhibiting factor (SRIF, somatostatin) [23]. Apart from the neuro-endocrine regulation, various other hormones, including GH, IGF-I, ghrelin, as well as the metabolic status affect GH synthesis and release [24,25]. For example, IGF-I inhibits GH release by attenuating both the GH pulse frequency and amplitude [26].

2.1.2 Growth hormone receptor and growth hormone binding protein

The GH receptor (GHR) is a specific, high affinity cell-surface receptor that is activated by GH binding and mediates GH effects. When binding to its receptor, one GH molecule interacts with two GHR molecules, causing receptor dimerization [19]. Post receptor signaling initially occurs through phosphorylation of the associated tyrosine kinase Janus Kinase 2 (JAK2) [27]. GHR expression is highly tissue specific and regulated by numerous factors, including the developmental stage and nutritional status [28,29]. Further, various hormones have been shown to affect GHR expression [30,31].

The GH binding protein (GHBP) is the slightly modified, soluble form of the GHR extracellular ligand binding domain and occurs in serum [32]. GHBP binds up to 60% of circulating GH [33] and is suggested to act as a reservoir, buffering the secretory peaks

of GH [19]. Binding increases half-life of serum GH from about 20 minutes to several hours, mainly by decreasing renal clearance [34].

GH is able to influence GHR/BP expression dose-dependently [31] and in a tissue-specific fashion, as shown by *in vitro* and *in vivo* studies. In mice, hepatic GHR/BP mRNA levels are positively correlated with increased GH levels, whereas pituitary GHR/BP mRNA levels are not affected [35]. In contrast, in the kidney, GH binding sites are down-regulated by high serum GH levels [36].

2.1.3 Insulin-like growth factors

Together with their cognate receptors and binding proteins, IGF-I and IGF-II compose the IGF-system [37]. IGF-I and IGF-II are growth and differentiation promoting single-chain polypeptides, which share significant structural homology with insulin [38] and act as endocrine as well as auto-/paracrine growth factors [39]. Both IGF-I and IGF-II bind with high affinity to specific cell surface receptors (see 2.1.4), but are also able to interact with the insulin receptor and exhibit biological effects similar to those of insulin [40]. IGF-I is synthesized and released from multiple tissues. Postnatally, the vast majority of circulating IGF-I originates from GH-induced expression and secretion of the liver [41,42], as proposed by the somatomedin hypothesis [1,43]. IGF-I expression further depends on tissue type and developmental and physiological or pathological status. Contrary to IGF-I, expression of IGF-II is not stimulated by GH [40].

2.1.4 Insulin-like growth factor receptors

The type I IGF receptor (IGF-IR) and type II IGF receptor (IGF-IIR) represent specific cell-surface receptors, which mediate the effects of the IGFs [2]. According to the current view of IGF-IR and IGF-IIR functions, pre- and postnatal IGF signaling is mainly mediated through the IGF-IR [44,45], whereas the IGF-IIR mediates IGF binding, endocytosis and lysosomal degradation, thereby acting as a growth inhibitor [46].

The tetrameric IGF-IR consists of two extracellular, ligand-binding α-subunits and two transmembrane and cytoplasmatic, tyrosine residues containing β-subunits, linked by disulfide bonds [47]. IGF-IR binds IGF-I with K_D of 0.2-1 x 10^{-9} M, whereas its affinity to IGF-II and insulin is about 2-15 fold and 100-1000 fold lower, respectively [48].

IGF binding to the α-subunit of the IGF-IR causes autophosphorylation of different tyrosine kinases of the β-subunits [49,50]. The postnatal expression of IGF-IR is influenced by the nutritional status and various hormones [47], and by pathological conditions, especially in the kidney [51,52].

The mammalian IGF-IIR is identical to the cation-independent mannose 6-phospate (M6P) receptor (M6PR) and is thus referred as the IGF-IIR/M6PR. It binds IGF-I and IGF-II, but no known signal transduction mechanism is initiated by the IGF-IIR/M6PR [45,53]. An exception of the current view was recently given by Pantaleon *et al.* [45], who demonstrated an involvement of the IGF-IIR/M6PR in the regulation of growth of early mouse embryos.

The IGF-IIR/M6PR binds IGF-II with high affinity (K_D = 0.02-0.7 x 10^{-9} M) and IGF-I with 100-500 fold lower affinity, further, it binds various other ligands, including glyco-proteins bearing the M6P recognition marker [54]. The expression of IGF-IIR/M6PR is developmentally regulated [45]. It is high in multiple fetal tissues, and declines dramatically in most tissues during the late gestational and/or in the early postnatal period [55-57].

2.1.5 Insulin-like growth factor-binding proteins

The insulin-like growth factor-binding proteins (IGFBPs) comprise a family of six homologous peptides (IGFBP-1 to -6) that bind IGF-I and IGF-II with high affinity [4,44]. Together with nine IGFBP-related proteins (IGFBP-rP 1 to -9), which are able to bind the IGFs with low affinity [58], they create an IGFBP superfamily [59-61].

The IGFBPs occur in circulation, several other biological fluids and tissues in a specific pattern [4]. The expression of the different IGFBPs is tightly regulated in a development- and tissue-specific manner, depending on various factors, such as metabolic situation, hormones, and pathologic conditions [9,62].

The IGFBPs bind IGFs with high affinity (K_D ~ 10^{-10} M), thereby creating complexes of distinct molecular weight. In serum, approximately 75-80% of the IGFs are bound to IGFBP-3 comprising a 150 kDa ternary complex consisting of one molecule each of IGF-I or IGF-II, IGFBP-3, and a non-IGF binding glycoprotein, termed acid labile subunit (ALS) [2,63]. A smaller proportion (20-25%) of the serum IGFs is bound to the other IGFBPs, forming a 45 kDa binary complex, and less than 1% is found in an unbound form [4]. IGFBP-5 is able to form a 45 kDa binary complex or to form a

ternary complex of 130 kDa together with ALS [64]. IGFBP-2 is the second most abundant IGFBP in circulation [4].

IGFBPs are capable of inhibiting or enhancing IGF effects, but also exert IGF-independent effects [3]. IGF-dependent effects of IGFBPs refer to their ability of binding IGFs, thereby sequestering the IGFs from their receptors and manipulating their bioavailability, as well as supporting transport and storage of the IGFs [65]. IGFBP-binding prolongs half-life of serum IGFs from less than ten minutes of unbound IGFs to 20-30 minutes in the 45 kDa complex and to 12-15 hours in the ternary complex [66,67]. IGF-independent effects derive from the ability of the IGFBPs to interact with proteins other than the IGFs, including ALS, insulin, components of the cell surface, ECM proteins, and potentially, intracellular components [65,68].

Specific proteases are able to cleave every IGFBP. The IGFBP fragments show no or drastically reduced affinity to the IGFs, resulting in an altered bioavailability of the IGFs [69]. The group of proteases is heterogeneous and includes kallikrein-like serine proteases, cathepsins and matrix metalloproteinases [70].

2.2 Studying the role of the GH/IGF-axis in growth processes

The various components of the GH/IGF-axis are multifarious interacting and complex interrelated, thereby exhibiting pleiotropic effects on anatomic structures - from the single cell over tissues and organs to the whole organism [1,18]. Growth of a mammalian organism is a phenomenon effected predominately by proliferative events, outbalancing apoptosis and increasing total cell number, with some additional contributions of cell hypertrophy and deposition of extracellular matrix [71]. Beside its role in regulating physiological growth processes, the GH/IGF-axis is involved in various pathological growth processes, with diverse components of this axis being dysregulated [72-74]. In many physiological and pathological situations, it is difficult to predict, which individual members of the GH/IGF-axis are responsible for growth or altered growth, and which ones are only co-regulated without an intrinsic effect on growth processes [72,75,76].

Genetically modified mice represent a powerful tool for studying the contribution of individual members of the GH/IGF-axis to growth processes *in vivo*. Those animals, which either overexpress a particular gene or harbor a knockout of a particular gene, provide an unique opportunity for performing gain of function, or partial or complete loss of function studies regarding a particular gene [76,77]. Beside genetically modified mouse models, mouse strains that carry spontaneous mutations, leading to a partial or complete deficiency of an individual member of the GH/IGF-axis are of interest for studying the role of various components of the GH/IGF-axis in the regulation of growth and differentiation.

2.2.1 Studying the role of GH in growth processes

2.2.1.1 GH transgenic and GH deficient mouse models

The murine metallothionein-I (MT) promoter-hGH transgenic mouse, generated by Palmiter *et al.* in 1982 [78], was one of the first transgenic animals. Since then, several strains of transgenic mice overexpressing heterologous GH genes under the transcriptional control of various regulatory elements have been developed [79]. Frequently used promoters are the transcriptional regulatory elements from the MT gene [80] or the rat phosphoenolpyruvate carboxykinase (PEPCK) gene [81]. GH gene sequences

from several species, including human, rat, cow, and sheep, have been incorporated into the mouse genome. Different GH fusion genes introduced into the mouse genome are summarized by Wanke *et al.* [82] and Kopchick *et al.* [83].

GH transgenic mice display high serum levels of heterologous GH and increased serum IGF-I levels [84,85]. For example, a MT-hGH transgenic mouse strain was reported to exhibit heterologous GH levels ranging from 1.2 to 900 µg/ml, as well as about two- to three-fold increased serum IGF-I levels [79]. The most obvious phenotypical effect of GH transgene expression is the markedly stimulated overall body growth. From three weeks of age onwards, GH transgenic mice display an increased body weight, which is almost doubled in adult animals versus wild-type controls [86,87], as well as visceromegaly and disproportionate skeletal gigantism [88,89].

GH transgenic mice demonstrate a typical spectrum of pathomorphological alterations of inner organs, with the kidney and liver being predominantly affected [14,82]. Renal alterations result in chronic renal failure progressing to end-stage renal disease (see 2.4.3.1). The liver of GH transgenic mice is overproportionally enlarged in relation to body size. Sequential histological studies revealed a characteristic sequence of liver changes. Initial alterations are characterized by hepatocellular hypertrophy and single cell necroses. Subsequent stages include hypertrophic and regressive liver cell changes, oval cell proliferation, and focal growth of hepatocytes exhibiting no tendency to megalocytic change. Apart from non-neoplastic changes, hepatocellular tumors, including both adenoma and carcinoma, occur age-dependently at a high frequency in GH transgenic mice [14,90].

Further, transgenic GH male mice demonstrate stimulated skin growth, which results from an interaction of elevated GH levels with male sex hormones [91]. Life expectancy is significantly reduced in GH transgenic mice, primarily due to renal failure [92].

GH deficiency has been detected in several mouse strains, harboring spontaneous genetic mutations. GH deficient mice are growth retarded from two weeks of age onwards resulting in dwarfism [75]. Further, they usually show reduced fertility or are infertile, display additional severe endocrine alterations, and exhibit significantly prolonged longevity [93,94].

Snell dwarf mice (*dw/dw*) [95] carry a missense mutation in the gene encoding Pit-1, which is a pituitary-specific transcription factor that is responsible for differentiation of

somatotrophs, lactotrophs, and thyrotrophs during fetal development of the pituitary gland [96]. Snell dwarfs lack both GH and thyroid-stimulating hormone [75].

Ames dwarf mice (df/df) carry a missense mutation at the Prop-1 (Prophet of pit-1) locus. The gene product of Prop-1 is responsible for the development of Pit-1 positive cells [97]. The lack of Pit-1 positive cells in df/df mice apparently produces the same defects in pituitary development as in *dw/dw* mice, and thus, the phenotype of Ames dwarfs resembles that of Snell dwarfs [75].

So called ´little´ mice (*lit/lit*) bear a homozygous autosomal recessive *lit* mutation [98] and exhibit an isolated GH deficiency. The mutation consists of a single nucleotide substitution of the GH releasing hormone receptor gene. *lit/lit* mice possess only residual GH activity. Their pituitary and serum GH levels are reduced to less than 5% of normal [75].

Although of significant importance for a variety of studies, these spontaneous dwarf mice are not considered as ideal models to study the GH/IGF-axis in postnatal growth, as they exhibit combined pituitary hormone deficiencies or possess residual GH activity. Therefore, several investigators chose GHR knockout mice (see under 2.2.2.1) to study the effects of missing GH activity [75,99].

2.2.1.2 Effects of GH on somatic growth

GH promotes postnatal growth processes, whereas pre- and perinatal growth is GH independent [100] despite the presence of the GHR [101,102]. In the postnatal period, GH effects can be mediated directly through activation of the GHR, indirectly either by stimulating IGF-I expression and release from the liver into the bloodstream - as proposed in the somatomedin hypothesis by Salmon and Daughaday in 1957 [103] -, or by stimulating the local production of IGF-I in different organs [43,104].

In humans, prolonged hypersecretion of GH before puberty can yield gigantism [18]. GH hypersecretion in adults, mostly caused by pituitary adenomas [105], leads to a condition known as acromegaly [106]. Acromegalic patients are characterized by increased serum levels of GH and IGF-I and show a number of anatomic alterations, including acral and soft tissue overgrowth, skin thickening, and thyroid enlargement [106]. In contrast, hyposecretion or no secretion of GH before puberty results in dwarfism. Adult patients with GH deficiency exhibit increased adiposity and decreased

lean body mass [107], and a reduced life expectancy, despite apparently sufficient replacement therapies .

GH exerts a broad variety of biological actions [108]. Apart from promoting postnatal growth and differentiation, GH affects lipid, protein, carbohydrate, and mineral meta-bolism [19,106], and is assumed to modulate emotion, stress response, and behavior [109]. Acromegalic human patients develop severe hyperinsulinemia, impaired glucose tolerance, insulin resistance, and as many as 50% of the acromegalic patients develop overt diabetes mellitus [110,111]. Hyperinsulinemia associated with normoglyce-mia is a consistent finding in GH transgenic mice [86,112]. The reason for the apparent discrepancy in diabetogenesis between GH transgenic mice and human acromegalic patient is not clear [83]. Like acromegalic patients, PEPCK-bGH transgenic rabbits exhibit an acromegalic phenotype and frequently develop diabetes mellitus [113].

2.2.1.3 Effects of GH on other components of the GH/IGF-axis

GH levels influence serum and tissue concentrations of various other components of the GH/IGF-axis. Serum IGF-I levels are increased by GH excess and decreased in GH deficiency states [114,115]. Furthermore, serum GH levels and hepatic IGF-I mRNA and protein concentrations are positively correlated [104,116], whereas IGF-I mRNA levels of other organs are only partially GH-dependent or GH-independent [75,104].

Altered GH levels influence the expression and abundance of IGFBPs [59]. Hepatic mRNA as well as serum levels of IGFBP-2 are reduced by GH excess, but unaltered in GH deficiency states [117-119]. IGFBP-3 serum levels are elevated by GH [119,120], whereas IGFBP-3 liver mRNA levels are not affected [117,120]. An indirect effect of elevated IGF-I is discussed, which might protect IGFBP-3 from proteolysis by forming a ternary complex [121], or might promote the recruitment of IGFBP-3, attached to cell membranes [117]. Hepatic ALS mRNA and serum levels are increased due to elevated GH levels [63,117].

2.2.2 Studying the role of GHR/BP in growth processes

In order to evaluate the biological effects of GHR/BP on growth processes, different GHR/BP knockout mouse strains were generated [75,99]. Disruption of the GHR/BP gene causes failure of GHR/BP binding and signal transduction in homozygous (-/-)

mice resulting in the inability to utilize GH [122,123]. GHR/BP -/- mice exhibit normal birth weights [75], but show a dwarfing phenotype from two weeks of age onwards weighing about 40% to 45% of normal controls. GHR/BP -/- mice exhibit increased serum GH levels and drastically reduced IGF-I levels. Besides dwarfism, those mice demonstrate delayed sexual maturity and increased longevity [123].

The GHR/BP knockout mouse is discussed as a model for the human Laron syndrome (LS) [123,124], although the model differs in some aspects from human LS patients. Human LS patients tend to become obese and hypoglycemic, while GHR/BP -/- mice stay lean and normoglycemic. Insulin levels were found to be elevated in some LS patients, possibly due to obesity, while GHR/BP -/- mice show severely decreased insulin levels as compared to control mice [123,125].

2.2.3 Studying the role of the IGFs in growth processes

2.2.3.1 IGF-I and IGF-II transgenic mice

Overexpression of hIGF-I under the transcriptional control of the MT promoter in transgenic mice stimulates somatic growth from four weeks of age onwards and results in an about 1.4-fold elevated body weight, as compared to non-transgenic siblings [85,126]. MT-hIGF-I transgenic mice display an approximately 50% increase of serum IGF-I concentrations, as compared to controls [126]. Due to the negative feedback regulation on pituitary GH synthesis by transgene-encoded serum IGF-I, endogenous serum GH levels and, as a consequence, hepatic endogenous IGF-I mRNA levels are reduced [126]. Serum IGF-I concentrations in hIGF-I transgenic mice are markedly lower than those of GH transgenic mice, which is discussed to be at least partially responsible for the less stimulated body growth of hIGF-I transgenic mice [2].

hIGF-I transgenic mice exhibit a selective organomegaly, with kidneys, carcass, brain, and pancreas being mostly affected, but no apparent increase in skeletal growth as seen in GH transgenic mice [84,126]. Despite nephromegaly, IGF-I transgenic mice show no glomerulosclerotic lesions and only a moderate glomerular hypertrophy. The difference in renal pathology between GH- and IGF-I transgenic mice is discussed to be due to high serum GH levels and approximately doubled serum IGF-I levels in GH transgenic mice, as compared to IGF-I transgenic mice [84,127].

Several IGF-II transgenic mouse strains have been generated, harboring different IGF-II fusion genes [128]. Analysis of the various IGF-II transgenic mouse strains revealed that the postnatal overproduction of IGF-II may affect body and/or organ weights, depending on the expression level and tissue specificity of IGF-II overproduction as well as on the use of heterologous or homologous IGF-II coding regions. Several studies show a correlation between the sites where the transgene is expressed and the observed alterations in organ growth suggesting local actions of transgene-encoded IGF-II [128,129].

In several IGF-II transgenic mouse strains, increased serum IGF-II levels correlate negatively with serum IGF-I levels, probably through a negative feedback regulation of IGF-II on pituitary GH synthesis and concomitant reduction of IGF-I expression [130]. Another explanation for reduced serum IGF-I levels discussed, is the possibility that elevated serum IGF-II levels displace IGF-I from serum IGFBPs, leading to an accelerated plasma clearance rate of IGF-I [131]. Serum IGFBP levels were not affected by IGF-II overexpression, except for IGFBP-2, which serum levels were correlated positively with IGF-II levels in several IGF-II transgenic mouse strains. The authors suggest that IGF-II is a major regulator of IGFBP-2 [129].

2.2.3.2 IGF-I and IGF-II knockout mice

The knockout (-/-) of IGF-I or IGF-II in genetically engineered mice results in drastically reduced prenatal growth [132-135]. Newborn mice lacking IGF-I or IGF-II show birth weights 40% and 60% lower than wild-type littermates [132].

IGF-I -/- mice present a high neonatal death rate. In surviving animals, the postnatal absence of IGF-I impairs the body growth rate. At an age of seven to eight weeks, IGF-I knockout mice weigh only about 30% of controls emphasizing the relevance of IGF-I for normal postnatal growth [132]. Further, mice lacking IGF-I demonstrate developmental defects in brain, muscle, bone and lung, and are infertile [132,136]. The phenotype of IGF-I -/- mice resembles that of a known case of IGF-I gene deletion in a human patient. Deletion of the IGF-I gene in the human patient caused intrauterine and postnatal growth retardation leading to an extreme short stature [136].

In contrast to IGF-I -/- mice, mice lacking IGF-II do not have an increased neonatal death rate and show normal postnatal growth rates [132]. These findings support the hypothesis that IGF-II at physiologic concentrations has no relevance in postnatal

growth of mice [137]. However, IGF-II -/- mice do not catch-up the prenatal growth deficit [133].

Double knockout mice, lacking both IGF-I and IGF-II are more severely affected than single mutants, lacking either IGF-I or IGF-II. Their birth weight is decreased to approximately 30% of that of normal littermates indicating that the two ligands act, at least partially, independently. Those double knockout mice die within minutes after birth due to respiratory failure [132].

2.2.3.3 Mice carrying a conditional knockout of the hepatic IGF-I gene

Two different strains of liver IGF-I deficient (LID) mice were generated by gene targeting using the Cre/loxP system [138]. LID mice display a hepatocyte-specific inactivation of the IGF-I gene resulting in hepatic IGF-I mRNA levels that are reduced to approximately 5% of control values [41,42]. Contrary, IGF-I mRNA levels in non-hepatic tissues are normal, with exception of spleenic IGF-I mRNA levels, which in one strain are also significantly reduced [42]. As a consequence of hepatic IGF-I knockout, circulating IGF-I levels in LID mice are reduced by 75%, indicating that the liver is the main source of IGF-I in circulation. Serum GH concentrations in LID mice are elevated, which is supposed to result from the lack of IGF-I-mediated feedback regulation [41,42].

Despite the reduction of serum IGF-I levels, LID mice show normal somatic growth and development. However, LID mice demonstrate disproportionate organ growth, including significantly increased liver and decreased kidney weight [41,42]. These results demonstrate that liver-derived IGF-I is not required for postnatal somatic growth, which directly challenges the somatomedin hypothesis [42]. However, this conclusion must be regarded critically, since increased circulating GH levels might compensate for the lack of serum IGF-I [6]. Further studies revealed, that LID mice exhibit four-fold elevated serum insulin concentrations and muscle-specific insulin insensitivity [139] suggesting that IGF-I, together with GH and insulin, plays a role in maintaining a balanced carbohydrate metabolism [140].

2.2.4 Studying the role of the IGF-IR and IGF-IIR in growth processes

In order to study the role of the IGF-IR and IGF-IIR in growth processes, IGF-IR- and IGF-IIR knockout mice have been generated. IGF-IR -/- mice exhibit a dwarfing phenotype with birth weights of approximately 45% of that of controls, and appear to be normally proportioned. They exhibit histological abnormalities, consisting of cellular hypoplasia, chiefly in skeletal muscle, internal organs, and the stratum spinosum of the skin. IGF-IR knockout mice die immediately after birth due to respiratory failure [132,135]. In heterozygous knockout mice (IGF-IR +/-), growth as well as IGF-IR mRNA levels are normal, suggesting effective up-regulation of the second (wild-type, intact) IGF-IR allele. Thus, a single functional wild-type allele of the IGF-IR is sufficient to assure normal IGF-IR expression and growth [132,135]. In contrast, the reduction of the level of IGF-IR by either targeted partial invalidation of the IGF-IR gene or deletion of the essential exon 3 of the IGF-IR gene in genetically engineered mice, causes a modest postnatal growth deficit from four to five weeks of age onwards, with the weight differences affecting all tissues to a similar degree [141,142]. In those mice, transcripts of mutated alleles are present, but cannot be translated into functional protein, thus leading to approximately by half reduced IGF-binding sites. These findings support the current view that the levels of IGF-IR protein are regulated on the transcriptional stage [142].

Mouse mutants inheriting maternally a targeted disruption of the imprinted IGF-IIR gene (IGF-IIR knockout mice), which normally is only expressed from the maternal allele, have about 2- to 4.4-fold increased serum IGF-II levels and about 2-fold increased IGF-II protein contents in extracts of whole embryos [53,143,144]. The authors explain the elevated IGF-II concentrations of IGF-IIR knockout mice by a failure of IGF-II binding and degradation. The phenotype is characterized by fetal overgrowth (135% of normal birth weight), generalized organomegaly, kinky tail, postaxial polydactyly and edema. The enlargement of organs was reported to be attributed to cellular hyperplasia, but not to cellular hypertrophy [53]. IGF-IIR knockout mice usually die during the late fetal or perinatal period. A small minority of IGF-IIR knockout mice survives, depending on the genetic background. Since the paternal IGF-IIR allele is transcriptionally silent, the paternal transmission of the IGF-IIR mutation does not

affect the viability of heterozygous offspring, which are indistinguishable from wild-type siblings [53].

2.2.5 Studying the role of IGFBPs in growth regulation

For evaluating the specific roles of the IGFBPs on growth processes *in vivo*, several mouse models lacking or overexpressing specific IGFBPs have been generated by transgenic technology.

In contrast to the inactivation of ligands or receptors of the GH/IGF-I-axis, the knock-out approach applied to IGFBPs presents rather disappointing results [76]. IGFBP-2 knockout mice exhibit a reduction in spleen weight of adult males as the only anatomic alteration [145]. Mice lacking IGFBP-4 are slightly smaller than control animals, and the genetic ablation of IGFBP-6 does not result in any apparent phenotypical changes [146]. This phenomenon is discussed to be due to functional redundancy of the members of the IGFBP family, which prevent the appearance of dramatic phenotypes [76].

The alternative approach, overexpression of IGFBPs, has been far more successful in generating phenotypical changes [76]. Phenotypic analysis revealed features that are common for most IGFBPs, such as growth retardation, but also effects that are specific for individual IGFBPs [5]. Transgenic mice, overexpressing IGFBP-1 exhibit several organ-related alterations, with the brain and kidney being most affected (see under 2.4.2.4) as well as disturbed glucose homeostasis. IGFBP-2 transgenic mice are presented in depth below. IGFBP-3 transgenic mice display no alterations in somatic growth, but show significantly increased weights of heart, liver, and spleen. Surprisingly, the selective organomegaly develops in organs different from the sites of major IGFBP-3 transgene expression [76]. Findings in transgenic mice overexpressing IGFBP-4 under the control of the $H-2K^b$ promoter suggest that IGFBP-4 is a potential growth inhibitor of lymphoid tissues [147]. Local overexpression of IGFBP-4 in smooth muscle cells of transgenic mice resulted in decreased weights of bladder, aorta, and stomach as a consequence of hypoplasia of smooth muscle cells, and did not affect body weight [148]. Overexpression of IGFBP-5 under the control of the calcein promoter in transgenic mice results in a transiently impaired osteoblast function, in a decrease in trabecular bone, and osteopenia [149]. Local overexpression of IGFBP-5 in mammary gland epithelial cells of transgenic mice leads to impaired

mammary development, due to a decreased number of mammary gland epithelial cells [150]. Transgenic mice, overexpressing IGFBP-6 under the control of the glial fibrillary acidic protein promoter show high IGFBP-6 levels in the circulation and brain. They display reduced body weights at juvenile age as well as a reduced brain size, impaired ovary function and reduced litter sizes [151].

IGFBP-2 transgenic mice

Transgenic mice overexpressing homologous IGFBP-2 under the control of the cytomegalovirus (CMV) promoter show an expression of transgenic IGFBP-2 mRNA in numerous organs with exception of the liver [152]. They exhibit markedly elevated IGFBP-2 protein levels in several organs including kidney and adrenal gland. Serum IGFBP-2 levels are about three-fold increased in IGFBP-2 transgenic mice, if compared to their non-transgenic littermates, whereas serum concentrations of IGF-I, IGF-II, IGFBP-3, and -4 are not altered.

Phenotypic effects of IGFBP-2 overexpression in transgenic mice include reduced body weight gain from 23 days of age onwards. The reduction of body weight is mainly determined by decreased carcass weight, whereas absolute and/or relative (to body weight) organ weights are only partially and slightly reduced. Among the organs, pancreas, spleen, and liver are most prominently reduced in weight. Further evidence for a role of IGFBP-2 as a growth inhibitor *in vivo* derives from normal mice selected for low eight-week body weight, in which growth reduction is associated with increased hepatic IGFBP-2 mRNA expression and serum IGFBP-2 levels [153].

Interestingly, the phenotype of IGFBP-2 transgenic mice is inverse to that of IGF-I transgenic mice [126], indicating that *in vivo*, the growth inhibiting effect of IGFBP-2 maybe due to the suppression of IGF-I effects [152].

Crossbreeding of IGFBP-2 transgenic mice with transgenic mice overexpressing bovine (b) GH demonstrated that the growth inhibiting effect of IGFBP-2 is even more pronounced in high than in normal GH/IGF-I conditions [7]. Five-week-old double (IGFBP-2 and bGH) transgenic animals exhibit body weights that range at the level of non-transgenic controls demonstrating that IGFBP-2 overexpression normalizes GH-stimulated body growth in mice at this age. At an age of 15 weeks, the body weight of double transgenic mice is drastically reduced, as compared to bGH transgenic mice, ranging at an intermediate level between the body weight of controls and that of bGH

transgenic littermates. Various organs and tissues are differently affected by the growth inhibiting effect of elevated IGFBP-2. In double *vs*. bGH transgenic mice for example, the weight reduction of the adrenal gland and the kidney is even overproportional when compared to the reduction of body weight, pointing out the relevance of the GH/IGF-axis in regulation of adrenal gland and kidney growth *in vivo*.

2.3 The GH/IGF-axis and the adrenal gland

Apart from adrenocorticotropin (ACTH), which is the primary regulator of adrenocortical growth and function, the GH/IGF-axis is intimately involved in the developmental and functional regulation of the adrenal gland [154]. Both *in vitro* and *in vivo* studies demonstrated effects of single components of the GH/IGF-axis on fetal and adult as well as on neoplastic adrenal tissue.

2.3.1 Effects of GH on adrenal growth and function

In vivo, GH excess causes adrenal enlargement and corticosterone hypersecretion in various species. Administration of porcine (p) GH to barrows increases adrenal weight [155]. Transplantation of GH-producing tumors in rats leads to a 300% increase in adrenal weight and elevates serum corticosterone levels despite unaltered ACTH levels [156]. Chronic overexpression of hGH or bGH in transgenic mice results in adrenal enlargement [79], and increased serum corticosterone and plasma ACTH levels [15,16], whereas GH-deficiency in mice is associated with size reduction of adrenal glands [157] and unaltered corticosterone levels [118]. In children affected by isolated GH-deficiency, an elevated ACTH-induced steroidogenesis has been observed during short-term treatment with recombinant hGH [158]. Since the GH receptor is found in the adrenal gland of several species, including mouse, rat and man, a direct effect of GH on adrenal tissue is discussed by several authors [159-161].

However, hGH does not have a direct effect on basal or ACTH-induced steroidogenesis in fetal and adult human adrenocortical cells (HAC) [162,163]. Likewise, bGH is unable to induce steroidogenesis in murine adrenocortical tissue *in vitro* [15].

2.3.2 Expression of the IGFs in the adrenal gland and their effects on adrenal growth and function

The IGFs play a crucial role in growth and function of the adrenal gland. They exhibit mitogenic and differentiating effects on both fetal and adult adrenocortical tissue [154], and are assumed to act predominantly in a para-/autocrine manner at the adrenocortical level [164].

2.3.2.1 IGFs and the fetal adrenal gland

Fetal adrenal tissue of different species, including man [154,165], rhesus monkey [166], sheep [167], and rat [168] contains high levels of IGF-II mRNA and IGF-II protein. As shown in the fetal human and fetal rhesus monkey adrenal gland, the expression of IGF-II is restricted to the cortex [166,169]. Contrary, IGF-I mRNA and IGF-I protein is absent, or found only at minimal levels in the fetal adrenal gland. Similarly, in fetal HAC, mRNA levels encoding IGF-II are highly abundant, whereas IGF-I mRNA is not detectable [169]. Since the adrenal gland grows rapidly from midgestation until term [170], a central role of IGF-II in promoting growth of the fetal adrenal gland is postulated [154].

IGF-II expression in the fetal adrenocortex is regulated by numerous hormones and factors, such as GH, IGF-I, IGF-II and TGFβ [165,169]. However, pituitary ACTH has been shown to be the major promoter of adrenocortical IGF-II mRNA expression [154]. In fetal HAC, IGF-II mRNA concentrations are increased by ACTH in a time- and dose-dependent manner [165]. In rhesus monkey fetuses, elevated serum ACTH levels, which are achieved by *in uteri* metyrapone treatment, cause significantly increased adrenal IGF-II mRNA levels, as compared to untreated controls [166].

Depending on the species, IGF-I and/or IGF-II exhibit mitogenic and differentiating effects on the fetal adrenocortex. *In vitro*, both hIGF-I and hIGF-II stimulate proliferation of fetal HAC in a dose-dependent fashion [169]. In fetal rat adrenal cells, only IGF-II but not IGF-I acts mitogenic, pointing out the relevance of IGF-II in the fetal growth of the rat adrenal gland [171]. *In vivo*, increased adrenal IGF-II levels are associated with stimulated growth of the fetal rhesus monkey adrenal gland, due to hypertrophy of adrenocortical cells of the definitive, transitional and fetal zones, whereas the adrenal medulla is unaffected [166].

IGF-I and IGF-II show differentiating effects in fetal HAC, likely through interaction with the IGF-IR [154]. IGF-II augments ACTH-stimulated cortisol and androgen synthesis through up-regulation of several adrenal steroidogenic key enzymes [172,173]. Both IGF-I and IGF-II directly up-regulate basal expression of the steroidogenic key enzyme cytochrome P450 17α-hydroxylase [163].

2.3.2.2 IGFs and the adult adrenal gland

The expression and presence of the IGFs in the adult adrenal gland differs from that in the fetal adrenal gland [174]. In the adult human adrenal gland, IGF-II mRNA is almost undetectable, whereas IGF-I expression is comparably high in adult and fetal adrenals [175]. Likewise, IGF-I is expressed in the adrenal gland of adult mice, whereas no IGF-II mRNA is detectable [8].

Contrary, *in vitro* adult HAC secrete IGF-I and IGF-II, which might be due to culture conditions [176]. IGF-I and IGF-II secretion of adult HAC is stimulated by ACTH [176], but not by hGH [162] . Similarly, in adult bovine adrenocortical cells (BAC), IGF-I secretion can be stimulated dose-dependently by ACTH [177].

IGF-I and IGF-II stimulate growth and steroidogenesis of the adult adrenal gland. *In vivo*, infusion of IGF-I into guinea pigs causes an increase in the fractional weight of the adrenal glands. This effect is more pronounced with long R^3 IGF-I, an IGF-I anaogue with reduced affinity to IGFBPs [178]. hGH and bGH transgenic mice with increased systemic and adrenal IGF-I levels, display adrenal enlargement as well as elevated plasma corticosterone and ACTH levels [16,79,159]. Since hGH has no direct steroidogenic effect on adult HAC [162], IGF-I is likely to be responsible for the adrenal changes in hGH and bGH transgenic mice. PEPCK-hIGF-II transgenic mice, exhibiting increased IGF-II serum levels and adrenal IGF-II transgene expression, display an elevated adrenal weight resulting from an increased volume of the zona fasciculata [129]. hIGF-II transgenic mice exhibit two-fold elevated serum corticosterone concentrations, but unaltered plasma ACTH levels, as compared to non-transgenic control mice, excluding direct effects of hIGF-II on the hypothalamic or pituitary level [8]. Several lines of evidence indicate that in the adrenal gland, the IGFs act primarily at the local level in a paracrine/autocrine fashion [176]. In the transgenic mouse models mentioned above, however, it remains unclear, whether the IGFs act on the adrenal gland in an endocrine or rather a paracrine/autocrine fashion [8].

The steroidogenic effect of IGF-I and IGF-II has been confirmed *in vitro*. In adult HAC, IGF-I and more potently IGF-II stimulates basal as well as ACTH-induced steroid biosynthesis in a time- and dose-dependent manner through interaction with the IGF-IR [163]. The stimulation of steroid biosynthesis is linked to an up-regulation of steroidogenic key enzymes, and an increase in ACTH sensitivity due to an elevated

ACTH-receptor expression [163,174]. IGF-I and IGF-II display comparable effects in adult BAC, concerning cortisol secretion [179,180]. Furthermore, in adult BAC, IGF-I is involved in the regulation of Steroidogenic acute Regulatory Protein (StAR) [179], which is assumed to play a key role in the acute steroidogenic response of steroidogenic cells [181,182].

Results obtained from studies using rodent adrenocortical cells differ from those obtained with HAC or BAC. In rat adrenocortical cells, IGF-I exhibits an inhibitory effect on steroid biosynthesis [183], whereas in murine adrenocortical cells, IGF-I has no effect on adrenocortical steroid secretion [15]. The discrepancy in the steroidogenic potency of IGFs might be due to species differences or to methodic variations bet-ween the studies. Methodic variations for example, concern incubation times of the adrenocortical cells, which are two and four hours in the murine experiment, whereas they are up to 48 hours in time course studies using HAC and BAC. The maximum stimulation of basal and ACTH-induced cortisol secretion through IGF-I and IGF-II is reached after 36 or 48 hours in HAC and BAC.

2.3.3 Role of the IGF-IR and IGF-IIR/M6PR in adrenal growth

The mitogenic and differentiating effects of IGF-I and IGF-II on the adrenal gland are assumed to be mediated through interaction with the IGF-IR [154]. This is supported by bovine and human cell culture studies, demonstrating that both IGF-I and IGF-II stimulate steroidogenesis exclusively through activation of the IGF-IR [8,180]. The physiological role of the IGF-IIR/M6PR in the adrenal cortex remains controversial [164]. Since loss of heterozygousity at the IGF-IIR/M6PR locus represents a frequent event in human adrenocortical tumors, a tumor suppressing role is discussed for the IGF-IIR/M6PR [46,184].

Both the IGF-IR and IGF-IIR/M6PR are expressed in fetal and adult human adrenal glands to a comparable extend [175], and are abundant at a similar level in all zones of the adult adrenal cortex [185,186]. As shown in the fetal rhesus monkey adrenal gland, IGF-IR expression is restricted to the definitive, transitional, and fetal zone of the adrenal cortex [166]. Since IGF-IR expression levels decline to non-detectable levels from the end of the second trimester until term [166], the authors propose a growth regulative role of the decreasing IGF-IR expression, since 1) the IGF-IR expression changes perinatally, whereas no other components of the GH/IGF-axis is altered, and

2) the adrenal weight decreases significantly by the first week after delivery [170]. Besides the developmental regulation, ACTH stimulates adrenocortical expression of IGF-IR, as evidenced *in vivo* in the fetal primate adrenal gland [166] and *in vitro* in bovine adrenocortical cells [187].

2.3.4 Effects of the IGFBPs on adrenal growth

The occurrence of IGFBP mRNA and protein in the adrenal gland has been investigated in various species. Most detailed information derives from studies in primates. Both fetal and adult human adrenal glands express IGFBP-2 at equal levels, as determined by Northern blot analysis [175], and, like in fetal rhesus monkey adrenal tissue, the relative abundance of IGFBP-2 is greater than that of other IGFBPs [166]. These results indicate physiological significance of IGFBP-2 in both the fetal and adult adrenal gland. Conversely, IGFBP-1 and -3 are expressed in fetal but not adult human adrenal tissue, with IGFBP-1 expression levels being low. Furthermore, fetal and adult human adrenal tissue express IGFBP-4, -5 and -6 mRNA [175].

As determined by *in situ* hybridization, IGFBP-2 and -6 mRNA is localized in adrenocortical parenchymal cells in fetal rhesus monkey adrenal tissue. The authors therefore suggest an essential role of IGFBP-2 and -6 in the primate fetal adrenal gland [166]. In contrast, IGFBP-3, -4 and -5 mRNA are not localized in adrenocortical parenchymal cells, but in connective tissue surrounding the adrenal gland (IGFBP-3 and -4), and in endothelial cells of intra-adrenocortical blood vessels (IGFBP-5). Although IGFBP-3, -4 and -5 are not localized in parenchymal cells of the adrenocortex, a possible paracrine action of these IGFBPs must be considered [166].

Cultured adrenocortical cells secrete IGFBPs, and the *in vitro* expression pattern differs from that *in vivo*. In the medium of cultured fetal and adult HAC, IGFBP-3 is the most abundant IGFBP, whereas IGFBP-6 is not detectable, or at minimal levels [175,188]. Quantification of the IGF binding capacity in adult HAC medium reveals that IGFBP-3 accounts for almost half of the IGF binding capacity, whereas IGFBP-2 accounts for about 12% [188]. Adult BAC secrete a comparable pattern of IGFBPs [189].

The secretion of individual IGFBPs by adult HAC and BAC can be stimulated through ACTH and IGFs [188,189]. In adult HAC and BAC, ACTH treatment increases IGFBP-1 and -3 secretion, whereas incubation with IGFs elevates IGFBP-3 and -5 levels [177,189].

The enhanced secretion of IGFBP-1 and -5 by ACTH and IGFs, respectively, is paralleled by an increase in IGFBP-1 and -5 mRNA levels in these cells [188].

Locally expressed IGFBPs are able to modulate effects of the IGFs on adrenocortical cells. In HAC and BAC, the divergent steroidogenic potency of IGF-I and IGF-II (see 2.3.2.2) is caused by different interactions of IGFBPs with IGF-I and IGF -II. So far, it remains unclear, which particular IGFBP(s) is (are) responsible for this modulatory effect. Since some IGFBPs exhibit a greater affinity for IGF-II [4], the authors assume that the stronger steroidogenic potency of IGF-II is due to a preferential binding of IGF-II to IGFBPs that are capable of adhering to the cell surface and promote the interaction of IGF-II with the IGF-I receptor [174,180]. The potency of a single IGFBP to modulate IGF-stimulated steroidogenesis has been shown for IGFBP-1, which potentiates IGF-I effects [190].

In vivo, a characteristic change of the adrenal IGFBP pattern is associated with human adrenocortical carcinogenesis. In human adrenocortical neoplasms, IGFBP-2 concentrations are significantly higher in malignant than in benign tumors. Despite elevated levels of IGFBP-2 protein in malignant adrenocortical tumor tissue, no increase of IGFBP-2 mRNA levels is detectable, suggesting the influence of post-transcriptional mechanisms in the regulation of IGFBP-2 protein levels. In contrast to IGFBP-2, no change in the secretion of other IGFBPs is found in human adrenocorti-cal tumors [191]. Patients with metastasized adrenocortical carcinomas exhibit increased plasma IGFBP-2 levels, which correlate positively with tumor burden and inversely with survival [192]. *In vitro* studies using Y-1 mouse adrenocortical tumor cells provide further evidence for a role of elevated IGFBP-2 in adrenocortical tumorigenesis. Overexpression of IGFBP-2 in transfected tumor cells is associated with significant morphological alterations, enhanced cell proliferation, and increased colony formation, as compared to control cells [10].

2.4 The GH/IGF-axis and the kidney

The GH/IGF-axis plays a central role in renal growth and function. It is closely involved in growth and differentiation of the kidneys during nephrogenesis and development, but also in pathological processes of various renal disease states [193]. Furthermore, single components of the GH/IGF-axis show effects on glomerular hemodynamics as well as on distinct tubular functions. Both locally expressed and circulating components of the GH/IGF-axis affect the kidneys, and the kidneys influence systemic levels of individual members of the GH/IGF-axis by eliminating them from circulation [18].

2.4.1 Spatial distribution of the GH/IGF-axis in the kidney

Within the kidney, the expression of components of the GH/IGF-axis is highly organized and differs among the anatomical segments of the nephron [194]. Studies on the spatial distribution were performed predominantly in rats and mice, whereas less information is available about the expression pattern in human nephrons. Available data suggest that there are some species differences in the renal expression pattern of components of the GH/IGF-axis [195]. In rats and mice, the renal expression of members of the GH/IGF-axis is known to be altered in physiologic adaptive processes and in a number of experimental renal disease states [18].

2.4.1.1 Spatial distribution of GHR in the kidney

The GHR gene is expressed in the proximal tubule and the thick ascending limb of the loop of Henle (TALH), as demonstrated by *in situ* hybridization of rat kidneys [196]. Since IGF-I mRNA is not expressed in the proximal tubule, or only at minimal levels, the authors assume direct GH effects on this nephron segment [196]. This assumption is confirmed by *in vitro* studies demonstrating that GH stimulates gluconeogenesis in canine proximal tubular cells without induction of IGF-I expression [197]. In the proximal tubule, GHR and ALS (acid-labile subunit, see 2.1.5) are co-expressed, with both GHR mRNA and ALS mRNA levels are influenced by circulating GH levels. Since IGF-I and IGFBP-3 are not expressed in this nephron segment, a local intrinsic

function of ALS is speculated, independent of forming a 150 kDa complex together with one molecule each of IGF-I or IGF-II and IGFBP-3 [198].

IGF-I mRNA?
IGF-I?
IGF-II mRNA?
IGF-I Rec mRNA
IGF-I Rec
IGF-II Rec
IGFBP-2 mRNA
IGFBP-4 mRNA
IGFBP-5 mRNA

(GH Rec mRNA)
IGF-I Rec
IGF-II Rec
IGF-I mRNA?
IGF-I
IGFBP-4 mRNA
IGFBP-5 mRNAS
IGFBP-5

GH Rec mRNA
ALS mRNA

Vasculature:
IGF-II mRNA
IGFBP-2 mRNA
IGFBP-2

IGF-I mRNA
IGF-I
IGF-I Rec mRNA
IGF-I Rec
GH Rec mRNA
IGFBP-1 mRNA
IGFBP-1

IGF-I
IGFBP-1
IGF-II Rec
IGFBP-2

IGF-I R mRNA
IGF-I
IGFBP-1 mRNA
IGFBP-1
IGFBP-5 mRNA

IGF-I
IGF-II
IGF-I R mRNA
IGF-I R
IGFBP-1

Interstitium:
IGF-I Rec mRNA
IGF-II Rec mRNA
IGFBP-2 mRNA
IGFBP-3 mRNA
IGFBP-4 mRNA
IGFBP-5 mRNA

IGF-I mRNA
IGF-I
IGF-I Rec mRNA
IGF-I Rec
IGF-II Rec mRNA
IGF-II Rec
IGFBP-1
GFBP-2 mRNA
IGFBP-4 mRNA

Figure 1.2 Expression of components of the GH/IGF-axis in the rat nephron. The figure differentiates between proteins and mRNAs. Rec, Receptor; ?, *in vitro* finding, but not confirmed by *in vivo* studies. According to Feld and Hirschberg [18].

In the rat TALH, expression of the GHR is co-localized with the expression of IGF-I and IGF-IR. This constellation suggests that GH may act indirectly *via* local induction of IGF-I, which in turn acts through the IGF-IR by autocrine and/or paracrine modes [196]. The thick ascending limb of the loop of Henle is the only segment of the nephron, in which the triplet of GHR, IGF-I and IGF-IR is expressed [18].

Interestingly, in both the rat and human glomerulus, GHR expression has not been detected *in vivo*, which is important in sight of interpretations of GH actions in renal disease models [18]. Likewise, in glomeruli from C57B1/SJL mice, GHR mRNA is not detectable, however, GHBP is expressed [199]. In contrast to *in vivo* situations, *in vitro* studies demonstrate GHR/GHBP expression in human mesangial cells. In those cells, physiological doses of GH dose-dependently elevate GHR/GHBP gene transcription, whereas supraphysiological doses result in its down-regulation [31]. The

authors discuss dedifferentiation of glomerular cells under cell culture conditions as an explanation for the different GHR/GHBP expression of mesangial cells *in vivo* and *in vitro* [18,31].

2.4.1.2 Spatial distribution of the IGFs, IGF-IR and IGF-IIR/M6PR in the kidney

The renal expression of IGF-I and IGF-II varies greatly between species. The human kidney does not express IGF-I, whereas IGF-I mRNA is present in the rat kidney [18,195,200]. IGF-I expression is not detectable within the rat glomerulus *in vivo* [200], however, *in vitro*, rat and mouse glomerular mesangial cells express IGF-I [201,202]. The difference in IGF-I expression of rat mesangial cells between *in vivo* and *in vitro* situations is explained by dedifferentiation of those cells in the cell culture environment [18].

No or only minimal IGF-I mRNA content is detectable in rat proximal and distal tubule epithelial cells [200,203]. Contrary, IGF-I protein is found in proximal tubular epithelial (PTE) cells, being localized along the brush border and the basolateral membrane but not in cytoplasm. Thus, IGF-I protein detected in PTE cells most probably reflects bound IGF-I originating from the circulation and/or ultrafiltrate [204].

The rat TALH and collecting duct epithelia contain IGF-I mRNA and protein, with the greatest IGF-I expression within the kidney being localized in medullary collecting duct epithelia [196,204].

The human kidney expresses IGF-II, which is apparently limited to the vascular compartment and the medullary interstitium [205]. Conflicting data exist about the expression of IGF-II in the rat kidney. Chin & Bondy [196] did not detect IGF-II mRNA in the rat kidney, whereas Evan *et al*. [206] reported the occurrence of IGF-II mRNA, localized in the wall of the renal microvasculature.

The IGF-IR is expressed in rat glomeruli, which provides the basis for effects of IGF-I on glomerular function and growth. Glomeruli express IGF-IR even at a higher density than other parts of the nephron [200]. Since the glomerulus does not express IGF-I, as demonstrated by *in vivo* studies, the activation of glomerular IGF-IR by circulating but not by auto-/paracrine acting IGF-I is assumed [18]. Furthermore, rat glomeruli also contain IGF-IIR/M6PR mRNA [206] and IGF-IIR/M6PR protein [207].

IGF-IR and IGF-IIR/M6PR are expressed in rat PTE cells. The IGF-IIR/M6PR is localized exclusively in the apical part of PTE cells just below the brush border, but not in the basolateral part of the cells [208]. In contrast, the IGF-IR is abundant in both the apical and the basolateral part of PTE cells, with the higher concentration being located in the basolateral part [209]. However, functional studies in isolated-perfused rabbit proximal tubules indicate a greater sensitivity of apical IGF-IR. The stimulation of apical IGF-IR occurs at a 100-fold lower IGF-I concentration than of basolateral IGF-IR. Further, the magnitude of the maximal response (phosphate transport) of apical compared to basolateral IGF-IR to IGF-I stimulation is 3-fold greater [210]. *In vivo*, IGF-IR expression is further proved in the epithelium of rat TALH, distal tubules, and the collecting ducts [18,196].

2.4.1.3 Spatial distribution of the IGFBPs in the kidney

The IGFBPs are expressed in a specific spatial distribution within the kidney, suggesting that they tightly regulate IGF effects in a site-specific manner. Noticeably, rats and mice demonstrate comparable renal expression patterns of the IGFBPs [18].

In the glomerulus, both rats and mice express IGFBP-2 in the parietal epithelium of the Bowman's capsule and podocytes and IGFBP-5 in the glomerular mesangium [206,211,212]. Mice show an additional minor IGFBP-1 mRNA occurrence in the parietal epithelium of the Bowman's capsule [212]. Rat glomeruli additionally express IGFBP-4 at a minor level [213].

Mouse PTE cells contain high IGFBP-4 mRNA concentrations, and low IGFBP-1 and -5 mRNA levels [212]. The expression of IGFBP-4 mRNA [211,213] and IGFBP-5 mRNA [214] is also detectable in rat PTE cells.

In the epithelium of the thin limb of the loop of Henle of mice, IGFBP-2 mRNA and IGFBP-2 protein is demonstrable [212]. Similarly, IGFBP-2 mRNA has been detected in this nephron segment in rats [206,211]. Epithelial cells of the thick ascending limb of the loop of Henle of both mice and rats contain IGFBP-1 mRNA and IGFBP-1 protein [204,211,212]. Further, mouse and rat distal tubule epithelial cells express IGFBP-1 and -5, while collecting duct epithelium contains IGFBP-1, -2, and -4 mRNA [211,212].

The expression of IGFBP-3 is restricted to the cortical interstitium and to fibroblasts of large vessels and the ureter in the rat kidney. IGFBP-6 is expressed only weakly in the interstitium [211].

2.4.2 Renal processing of GH and IGFs

2.4.2.1 Processing of GH in the kidney

Besides effects of members of the GH/IGF-axis on the kidney, the kidney plays an important role in the turnover of the ligands. About 60% of GH is bound to GHBP, being prevented from renal degradation [33]. Unbound GH is handled similar to other microproteins by the kidney and undergoes glomerular ultrafiltration with a high sieving coefficient of 0.6, subsequent tubular absorption and lysosomal degradation, and minimal urinary excretion [215,216]. The kidney is the major organ causing plasma GH turnover [217,218]. Glomerular ultrafiltration of GH is the rate-limiting step in GH metabolism, which explains why renal dysfunction leads to increased serum GH levels and half-life of GH [18,219].

2.4.2.2 Processing of the IGFs in the kidney

Due to their low molecular mass, unbound IGFs undergo renal ultrafiltration with a sieving coefficient that approaches 1.0. Since more than 99% of the circulating IGFs are bound in 150 and 45 kDa complexes, their renal ultrafiltration is extremely low, and the healthy kidney plays only a modest role in degradation of circulating IGF-I [220-222]. Contrary, human patients and animals suffering from the nephrotic syndrome show an increased renal ultrafiltration of IGF-I, along with other growth factors [223] and stimulatory proteins [224].

Notably, in nephrotic rats, IGF-I is ultrafiltrated mainly in conjunction with IGFBP-2, and the concentration of IGF-I and IGFBP-2 is strongly increased in the proximal tubular fluid [220]. *In vitro*, proximal tubular fluid of nephrotic rats stimulates proliferation of opossum kidney (OK) cells [225] as well as the secretion of collagen type I and IV of mouse proximal tubular epithelial cells (PTE), confirming its ability of promoting tubulointerstitial fibrosis *in vivo* [220]. As demonstrated in mouse PTE, the effects of proximal tubular fluid of nephrotic mice are largely due to ultrafiltrated IGF-I and the activation of IGF-IR, indicating biological significance of ultrafiltrated IGF-I [220].

2.4.3 Role of components of the GH/IGF-axis in renal growth

The GH/IGF-axis is intimately involved in renal development. The components of the GH/IGF-axis, with exception of GH, are expressed in a varying degree in the embryonic metanephros as well as in fetal and postnatal renal tissue [18].

Beside its role in physiologic renal growth, the GH/IGF-axis plays an essential role in various adaptive and pathological growth processes of the kidney. Different human renal diseases states are characterized by altered expression of components of the GH/IGF-axis. Several rodent animal models have been established in order to study the role of the GH/IGF-axis in the pathogenesis of various renal diseases. These models include genetically engineered mice, lacking or overexpressing members of the GH/IGF-axis, unilateral and subtotal nephrectomized rodents, rodents with spontaneous or with induced diabetes mellitus, and nutritionally induced glomerulosclerosis of rodents [18].

2.4.3.1 Role of GH in renal growth processes

Systemic overexpression of GH in transgenic mice - either due to ectopic expression of heterologous GH transgenes or to stimulation of endogenous GH release by expression of a GHRH transgene (GH-releasing hormone) - regularly leads to a typical spectrum of renal alterations and results in chronic renal failure progressing to end-stage renal disease [17]. Both, morphological and clinical-chemical findings indicate renal failure as the primary cause of shortened lifespan of GH transgenic mice [92].

Detailed studies revealed a characteristic sequence of kidney alterations in GH transgenic mice. Initial changes include renal hypertrophy and hypertrophy of the glomeruli, which are overproportionally enlarged in relation to both kidney and body weight, indicating that the glomeruli may exhibit individual growth responses to GH [82]. Glomerular enlargement in GH transgenic mice is progressive with age and associated with the development of glomerulosclerotic lesions. Hypertrophic changes of GH transgenic mouse glomeruli include mesangial extracellular matrix expansion due to an increased extracellular matrix synthesis and a decreased extracellular matrix degradation [226], and proliferation of both endothelial and mesangial cells. However, there is no change in the number of podocytes, which demonstrate hypertrophy and

foot process effacement [227]. These early podocyte changes are associated with albuminuria. Concomitant with an age-related further increase of glomerular size in GH transgenic mice, severe maladaptive podocyte lesions including detachment of podocytes from the glomerular basement membrane do occur. The resultant denudation of the glomerular basement membrane is associated with severe proteinuria, glomerular hyalinosis, synechia formation, and collapse of glomerular capillaries [227]. These lesions progress to glomerular obsolescence that is associated with atrophy of the adjacent tubule and interstitial fibrosis. Thus, the progressive kidney lesions in GH transgenic mice appear to be attributable to a considerable extent to podocyte damage resulting from the limited capacity of this highly specialized cell type [228] to keep up with progressing overall glomerular growth. End-stage renal lesions are characterized by a marked atrophy of nephrons, interstitial fibrosis, and pronounced tubulocystic alterations. Remnant glomeruli demonstrate diffuse-segmental or focal-global sclerosis and/or hyalinosis [82,229].

The nephropathological alterations of GH transgenic mice, therefore, represent a valuable and well characterized model to study the pathogenesis of glomerulosclerosis and the mechanisms involved in the progression of chronic renal failure. Further, advanced kidney lesions of GH transgenic mice provide a model for aquired cystic kidney disease [17].

Similar renal effects of GH excess are also detectable in various other species. Rats treated with GH, and rats bearing GH-secreting tumors develop renal and glomerular hypertrophy, glomerulosclerosis, and severe proteinuria [230,231]. In dogs, GH treatment for 14 weeks causes enlarged kidneys, glomerular hypertrophy and mesangial thickening, suggesting that the development of pathological changes of the kidney due to overexposure to GH is not restricted to rodents [232]. Likewise, PEPCK-bGH transgenic rabbits develop severe glomerulosclerotic and tubulointerstitial lesions [113]. Contrary, in healthy humans, short-term administration of recombinant hGH causes only a transient, slight proteinuria [18]. Even acromegalic patients, showing high serum GH and IGF-I concentrations for long periods, exhibit only minor renal changes, including increased kidney weight, and moderate proteinuria [233,234]. Single cases of acromegalic patients have been reported with glomerulosclerotic lesions [235,236]. The renal enlargement of acromegalic patients is partially reversible by the reduction of GH secretion through either surgery or somatostatin treatment [233].

In contrast, dwarf rats, which are selectively deficient for GH exhibit reduced renal mass and glomerular tuft volume, as compared to normal rats [237]. Furthermore, GH absence prevents from development of renal and glomerular hypertrophy and glomerulosclerosis. Thus, GH-deficient rats do not develop spontaneous age-related glomerulosclerosis [238]. Likewise, subtotally nephrectomized GH-deficient rats [239] or subtotally nephrectomized normal rats that are treated with a somatostatin analogue [240] do not develop compensatory renal and glomerular growth. Similarly, adult uninephrectomized mice that are treated with a specific GHR antagonist are prevented from renal and glomerular hypertrophy, which occur in untreated mice. Noteworthy, both GHR antagonist treated and untreated mice exhibit equal serum GH levels [241]. Additionally, renal and glomerular hypertrophy following the induction of experimental diabetes in rodents, can be abolished by eliminating GH secretion or blockade of GHR [19].

Circulating GH levels were found to correlate with the degree of nephropathological changes in various rodent models [83]. For example, co-expression of bGH and GH *antagonist* genes at different levels in transgenic mice results in renal alterations, which reflect the relative expression levels of each transgene [83]. The lifespan of GH transgenic mice negatively correlates with serum GH levels, and the lifespan of those animals is shortened primarily due to chronic renal failure [92]. Furthermore, the severity of spontaneously developing glomerulosclerosis in aging rats is correlated with plasma GH levels [238].

2.4.3.2 Role of IGF-I and IGF-II in renal growth processes

IGF levels have been shown to be able to influence the nephron number in the pre-natal period. *In vitro*, the nephron population of mouse metanephroi in organ culture are increased when exposed to IGF-I [242]. Likewise, IGF-II elevates the number of nephrons in cultured rat metanephroi in a dose-dependent manner, whereas IGF-I is not able to influence nephron numbers [243]. Contrary, surviving IGF-I knockout mice exhibit a 20% nephron deficit associated with generalized organ hypoplasia at birth and growth retardation [244].

Doublier *et al.* [243] reported that overexpression of hIGFBP-1 in mice affects nephron number. A 15% to 20% nephron deficit associated with intrauterine growth

retardation was found in normal mice born from hIGFBP-1 transgenic mothers suggesting prenatal growth deficits by hIGFBP-1 overexpression. Furthermore, transgenic mice overexpressing hIGFBP-1 from embryonic day 15 onwards and born from normal mothers were reported to have normal body and kidney weights at birth, however, to show a significant nephron deficit at an age of three months. The authors, therefore, suggested postnatally affected nephrogenesis. They explained the phenotypes by reduced amounts of circulating IGFs, presumably IGF-II, due to transgene hIGFBP-1 expression, although direct hIGFBP-1 effects cannot be excluded [243].

In the postnatal period, IGF-I mediates many of the effects of GH in the kidney, and both circulating as well as renal IGF-I participates in renal and glomerular growth processes *via* endocrine and auto-/paracrine pathways, respectively [245,246]. In GH-deficient dwarf rats characterized by low systemic and renal IGF-I levels, both the reduced renal mass and glomerular tuft volume can be normalized to a similar degree by administration of either IGF-I or GH [237]. Moreover, an increase in GFR can be induced in those dwarf rats by either IGF-I or GH administration. These findings indicate that IGF-I may mimic and/or mediate much of the renal effects of GH [237].

Treatment of normal rats with IGF-I or overexpression of IGF-I in transgenic mice causes body weight gain and selective growth of certain organs including the kidneys [85,247], although endogenous GH and IGF-I expression is inhibited in IGF-I transgenic mice [126]. Proximal tubular epithelial (PTE) cells are the dominant cell type in the renal cortex making up 80% of the mass of the kidney, and their growth accounts for most of renal hypertrophy [248]. IGF-I is a strong mitogen for PTE cells and causes hyperplasia of cultured PTE cells of various species, including man [249], mouse [250], rat [251], and rabbit [252]. The PTE cell proliferative effect of IGF-I is mediated *via* activation of the IGF-IR [250,253]. Beside its mitogenic effect, IGF-I has an anti-apoptotic effect on PTE cells [254].

As shown in the rat kidney *in vivo*, the renal mass increase in IGF-I excess states is due to cellular hypertrophy in addition to hyperplasia, as indicated by an increase of DNA/protein ratio, mitosis and proliferating cell nuclear antigen expression [255]. Likewise, in various rodent models, renal hypertrophy associated to increased renal IGF-I levels has been shown to be due to a combination of hyperplasia and hypertrophy, or

only to hypertrophy of renal cells [256]. In compensatory renal growth following uninephrectomy in mice and rats, the proximal tubule growth is a hypertrophic, but not a hyperplastic growth form, and is mediated by a cell cycle-dependent process [257]. The mechanism in cell cycle-dependent hypertrophy involves the coordinated effects of a mitogen and an anti-proliferative agent, *e.g.*, transforming growth factor β (TGF-β). The mitogenic stimulus moves quiescent PTE cells into the G_1 phase of the cell cycle. The anti-proliferative stimulus blocks the PTE cells to cross the restriction point and move to the S phase. Having undergone increased protein synthesis and growth associated with the early G_1 phase, the cells are now "trapped" in a hyper-trophied state [258].

Glomerular alterations in IGF-I transgenic mice include glomerular hypertrophy and mesangial cell proliferation, but IGF-I transgenic mice did not show progressive glomerulosclerotic or tubulointerstitial lesions or albuminuria up to an age of 19 weeks [84,85]. However, the degree of glomerular enlargement does not reach that of GH transgenic mice, which exhibit a significantly higher mean glomerular volume as well as an increased mean glomerular volume-to-either kidney or -body weight-ratio than IGF-I transgenic mice [85,127]. The absence of glomerulosclerotic lesions in only moderately hypertrophied glomeruli of IGF-I transgenic mice is in line with the hypothesis that overproportional overall tuft growth and resultant podocyte damage, plays a significant role in the initiation and progression of glomerulosclerotic lesions in GH transgenic mice [227]. *In vitro*, IGF-I has been shown to promote mesangial cell hyperplasia, by acting both as a mitogen [259,260] and as an inhibitor of apoptosis [261] through activation of the IGF-IR [262]. Further, IGF-I is able to induce mesangial cell hypertrophy [263]. In addition, IGF-I stimulates the expression of extracellular matrix components, including proteoglycans and type I and type IV collagen by cultured mesangial cells [245,260].

2.4.3.3 Involvement of IGFBPs in renal growth processes and renal disease states

The renal levels of the IGFBPs show changes in normal growth physiology and particulary under pathological conditions[18]. However, it is difficult to predict whether altered IGFBPs have intrinsic effects or merely represent an epiphenomenon of developmental processes and diseases [5]. Contrary, altering the level of IGFBPs, in particular that of IGFBP-1, results in a renal phenotype [264].

Renal changes have been shown in transgenic mice overexpressing hIGFBP-1 [265]. hIGFBP-1 transgenic mice are characterized by decreased nephron numbers [243] and develop glomerulosclerosis without glomerular hypertrophy or hypercellularity [264]. At three months of age, hIGFBP-1 transgenic mice present a significantly increased mesangial extracellular matrix. The expansion of mesangial extracellular matrix is related to a marked increase in laminin and type IV collagen and to the appearance of type I collagen. Several possibilities are discussed to explain the renal phenotype of hIGFBP-1 transgenic mice, including impaired glucose and lipid metabolism, as seen in another IGFBP-1 transgenic mouse strain, reduced nephron numbers, reduced renal IGF-I bioavailability, and IGF-independent effects of high IGFBP-1 levels [264].

In several renal disease states, including chronic renal failure (CRF) [11,222,266,267] and multicystic renal dysplasia [13] in humans, and the nephrotic syndrome in experimental animals [268,269], circulating as well as renal patterns of the IGFBPs are dysregulated [72]. In human patients with CRF and end stage renal disease (ESRD), serum levels of intact or fragmented IGFBP-1 to -4 and IGFBP-6 are elevated [266,270], as a consequence of multiple factors, including increased synthesis, increased proteolysis (of IGFBP-3), and altered renal excretion [11].

Children suffering from CRF commonly display severe growth retardation and tissue catabolism resulting from an excess of serum IGFBPs and concomitant reduction of IGF-I bioavailability [11,266]. Those children demonstrate by half reduced serum concentrations of unbound and presumably bioactive IGF-I, as compared to healthy controls [222]. Their total serum IGF-I concentrations tend to cluster in the normal-low range [11], despite elevated plasma GH levels due to a prolonged half-life and an increased production of GH [271,272]. In children with CRF, serum concentrations of unbound IGF-I are inversely correlated with serum IGFBP-1 and -2 levels [222]. More, IGFBP-2 is the only binding protein, which has been shown to be inversely correlated with the height of prepuberal children with CRF. Further, compared to other IGFBPs, IGFBP-2 serum concentrations are most markedly elevated and this increase correlates with the degree of renal dysfunction [11,266].

Elevated serum IGFBP-2 levels were also detected in two different nephrotic rat models and found to be due to increased hepatic expression of IGFBP-2 [268,269]. In human patients with CRF, serum IGFBP-2 levels do not decrease within 14 days

after renal transplantation, indicating that serum IGFBP-2 levels are not, or only in part regulated by an intact kidney function, which is the case for IGFBP-3 and -6 [273]. Elevated serum IGFBP-2 levels are assumed to shift IGF-I from the 150 kDa (ternary) to 45 kDa (binary) complexes, resulting in an augmented renal excretion of IGF-I [194]. As shown in the proximal tubule fluid of nephrotic rats, the glomerular ultrafiltration of IGF-I occurs primarily in association with IGFBP-2 [220].

Multicystic renal dysplasia displays the most common form of renal dysplasia that leads to ESRD in children [274]. Renal expression of IGFBP-2 and -3 as well as of IGF-II are altered in multicystic renal dysplasia. IGFBP-2 is overexpressed in multicystic dysplastic kidneys from early gestation fetuses to postnatal stages, with both IGFBP-2 mRNA and IGFBP-2 protein being localized to the cyst epithelium. The authors speculate that IGFBP-2 may serve to potentiate and target the mitogenic and proliferative effects of IGF-II. However, a direct, IGF-independent effect of IGFBP-2 on the cyst epithelium cannot be excluded [13]. IGF-II mRNA is abundantly expressed in the mesenchyme surrounding the cysts, whereas IGF-II peptide is present in the cyst epithelium, suggesting that IGF-II may act in a paracrine fashion on the neighboring cyst epithelium. Expression of IGFBP-3 mRNA, which has been shown in metanephric blastema and in the ureteric duct and collection duct epithelia of normal developing kidneys, is absent in cyst epithelia maybe due to dedifferentiation of cyst epithelial cells [13].

Contrary to the proliferative effect, associated with IGFBP-2 overexpression in cyst epithelium in human multicystic renal dysplasia, elevated IGFBP-2 expression in murine mesangial cells (MMC) has an IGF-dependent, anti-proliferative effect [12]. In MMC, IGF-I dose-dependently up-regulates IGFBP-2 expression and secretion, and as a consequence of high IGFBP-2 levels, IGF-I is not able to stimulate MMC proliferation. When the IGF-I-induced stimulated IGFBP-2 synthesis is inhibited, IGF-I is able to enhance proliferation of MMC [12]. The authors speculate that the discrepancy in glomerulosclerosis development between GH and IGF-I transgenic mice (see 2.4.3.1 and 2.4.3.2) may be caused by a diverse mesangial expression of endogenous IGFBP-2. They speculate that mesangial cells of IGF-I transgenic mice secrete elevated levels of IGFBP-2 in response to elevated IGF-I levels and, thus limit IGF-I effects, like mesangial proliferation and extracellular matrix secretion. Contrary, high

GH levels in GH transgenic mice reduce IGFBP-2 production (see 2.2.1.3), and thereby may strongly increase the sensitivity of mesangial cells to elevated IGF-I [12].

In summary, these findings demonstrate that IGFBPs represent essential regulators of IGF-actions in different renal cell types. In particular, IGFBP-2 has been implicated to modulate proliferative effects on glomerular cells and proximal tubular cells. Further, IGFBP-2 is considered to play a central role in regulation/dysregulation of IGF-I bioavailability in chronic renal failure.

3 Research design and methods

3.1 Animals

3.1.1 Crossbreeding and animal husbandry

Hemizygous transgenic female mice overexpressing murine (m) IGFBP-2 under the transcriptional control of the cytomegalovirus (CMV)-promoter were mated with hemizygous transgenic male mice overexpressing bovine (b) GH under the transcriptional control of the rat phosphoenolpyruvate carboxykinase (PEPCK)-promoter, generating four different genetic groups of offspring. In the present study, male mice of the following genetic groups were investigated: non-transgenic controls (C), animals harboring the mIGFBP-2 (B) or the bGH (G) transgene, and those harboring both transgenes (GB) (Fig. 3.1).
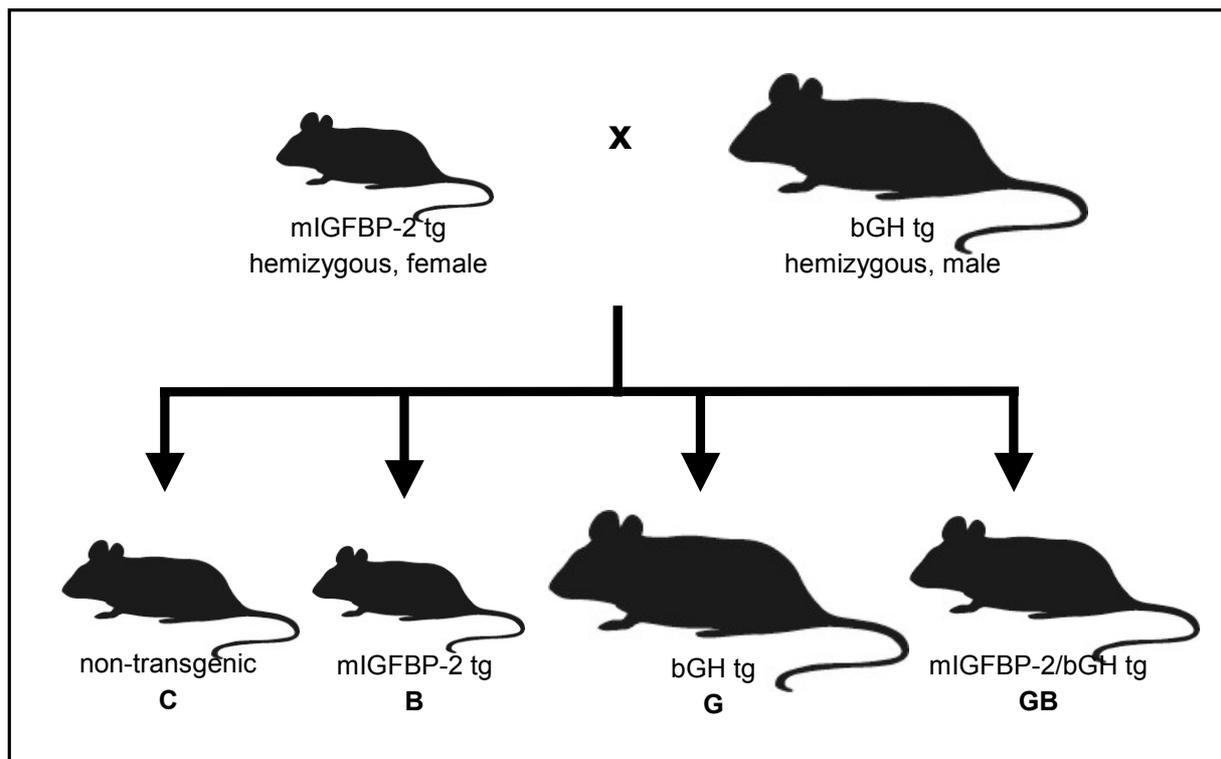

Figure 3.1 Breeding regime. Female hemizygous CMV-mIGFBP-2 transgenic (tg) mice were crossed with male hemizygous PEPCK-bGH transgenic mice. According to the Mendelian transmission, all experimental groups were produced within the same litters: non-transgenic controls (C), single mIGFBP-2 (B) or bGH (G) transgenic mice, and mice carrying both transgenes (GB).

mIGFBP-2 transgenic mice were generated as previously described by Hoeflich *et al*. [152] and bred onto a C57BL/6 background (Charles River Laboratories, Inc.-Wiga, Germany). The generation of bGH transgenic mice is reported elsewhere in detail [81]. bGH transgenic mice were derived from the 12th generation of sequential crossing with NMRI outbred mice (Charles River Laboratories, Inc.-Wiga, Germany). The used breeding regime ensures a similar genetic background of the four generated experimental groups.

All mice were maintained under standard (non-barrier) conditions (21±1°C, 55±3% relative humidity; 12/12-hours light/dark cycle) and had free access to standard diet (V1534; Ssniff, Germany) and tap water. At an age of three weeks, animals were weaned, separated according to gender, marked by piercing the ears, and tail tip biopsies were taken for genetic analysis.

The experimental setup summarized 175 animals. Of the four genetic groups, 44 mice at 38 days of age and 44 mice at 75 days of age were analyzed for several parameters. Age, number, and genotype of animals used for analyses of individual parameters are listed in table 3.1.

Additionally, 44 mice (C: n=15, B: n=11, G: n=10, GB: n=8) of the four genetic groups at four months of age were used for plasma corticosterone determination. Plasma ACTH levels were measured from 31 mice (C: n=8, B: n=7, G: n=8, GB: n=8) of the four genetic groups at an age of four to seven months. To exclude strain-specific effects on plasma ACTH levels, this parameter was also investigated in a different transgenic mouse strain overexpressing bGH under the control of the MT promoter. Blood samples from 6 four-month-old MT-bGH transgenic male mice and 6 male littermate controls were used for plasma ACTH determination.

Table 3.1 Age, number, and genotype of mice used for the analyses of single parameters. n(x) indicates the number of mice of the genotype that is given in brackets; $V_{(cortex, adrenal\ gland)}$, volume of the adrenal cortex; $V_{(medulla, adrenal\ gland)}$, volume of the adrenal medulla; $V_{(z.\ fasciculata)}$, volume of the zona fasciculata; $V_{(z.\ glomerulosa)}$ volume of the zona glomerulosa; $v_{(z.\ fasciculata\ cells)}$, mean volume of zona fasciculata cells; $N_{(z.\ fasciculata\ cells,\ animal)}$, total number of zona fasciculata cells per animal; $N_{(glomeruli,\ animal)}$, number of glomeruli per animal; $V_{(x\ zone,\ kidney)}$, volume of a particular (renal) zone; $V_{(x\ nephron\ segment)}$, volume of a particular nephron segment; $v_{(PTE\ cells)}$, mean volume of proximal tubular epithelial (PTE) cells; $N_{(PTE\ cells,\ animal)}$, total number of PTE cells per animal; $v_{(glom)}$ mean glomerular volume; WLB, Western ligand blot.

Table 3.1

Investigation/ Parameter	38 days of age	75 days of age
Body weight	7(C), 7(B), 7(G), 7(GB)	6(C), 8(B), 7(G), 7(GB)
Serum parameters		
IGF-I-, IGFBP-2 concentration	11(C), 11(B), 11(G), 11(GB)	10(C), 12(B), 11(G), 11(GB)
Clinical-chemical parameters	11(C), 11(B), 11(G), 11(GB)	10(C), 12(B), 11(G), 11(GB)
Adrenal gland weight		3(C), 3(B), 3(G), 3(GB)
Quantitative stereology of the adrenal gland		
$V_{(cortex,\ adrenal\ gland)}$, $V_{(medulla,\ adrenal\ gland)}$		3(C), 3(B), 3(G), 3(GB)
$V_{(z.\ fasciculata)}$, $V_{(z.\ glomerulosa)}$		3(C), 3(B), 3(G), 3(GB)
$V_{(z.\ fasciculata\ cells)}$, $N_{(z.\ fasciculata\ cells,\ animal)}$		3(C), 3(B), 3(G), 3(GB)
Kidney weight	7(C), 7(B), 7(G), 7(GB)	6(C), 8(B), 7(G), 7(GB)
Quantitative stereology of the kidney		
$N_{(glomeruli,\ animal)}$	4(C), 4(B), 4(G), 4(GB)	
$V_{(x\ zone,\ kidney)}$	5(C), 5(B), 5(G), 5(GB)	5(C), 5(B), 5(G), 5(GB)
$V_{(x\ nephron\ segment)}$	5(C), 5(B), 5(G), 5(GB)	5(C), 5(B), 5(G), 5(GB)
$V_{(PTE\ cells)}$, $N_{(PTE\ cells,\ animal)}$		4(C), 4(B), 4(G), 4(GB)
$V_{(glom)}$	5(C), 5(B), 5(G), 5(GB)	5(C), 5(B), 5(G), 5(GB)
Glomerulosclerosis index	4(C), 4(B), 4(G), 4(GB)	4(C), 4(B), 4(G), 4(GB)
Urine protein analyses		
Pattern of proteinuria	11(C), 11(B), 11(G), 11(GB)	10(C), 12(B), 11(G), 11(GB)
Urinary albumin concentration	11(C), 11(B), 11(G), 11(GB)	10(C), 12(B), 11(G), 11(GB)
WLB analysis	3(C), 3(B), 3(G), 3(GB)	
Immunohistochemistry	3(C), 3(B), 3(G), 3(GB)	
In situ Hybridization	3(C), 3(B), 3(G), 3(GB)	

3.1.2 Polymerase chain reaction (PCR)

Transgenic mice were identified by polymerase chain reaction (PCR). Tail tip biopsies of approximately 0.4 cm length were taken and stored at -80°C until assayed. Genomic DNA was extracted using the proteinase K lysis buffer-method [37]. The tail tips were digested over night in 450 µl lysis buffer and 30 µl proteinase K solution by incubation at 56°C in a type 1030 waterbath (Gesellschaft für Labortechnik mbH, Germany). Subsequently, the samples were cleared by adding 400 µl of phenol-chloroform/isoamyl alcohol (C/IA), gently shaking the tubes for 10 min, centrifuging them (3 min, 10.000 rpm, RT), and transferring the aquatic, DNA-containing supernatant in a new tube. Next, 400 µl C/IA was added to the revealed supernatant, tubes were gently shaken for 3 min and again, the supernatant containing the DNA was saved in a new tube. This step was repeated once. The DNA was precipitated with 40 µl 3 M sodium acetate solution and 700 µl 100% ethanol, became visible and was pelleted by shortly vortexing. The pellet of genomic DNA was washed in 70% ethanol, dried, and dissolved in 50 µl re-distilled water.

Subsequently, the sample was prepared for amplification. 19 µl of the Master Mix and 1 µl of a 1:5 dilution of the genomic DNA solution were mixed carefully in PCR-analysis cups, which were then placed in a thermocycler (Mastercycler gradient®; Eppendorf, Germany) and the program (see 3.1.2.2) was run. As positive control, the DNA solution of a known transgenic animal was used in the PCR approach, whereas the Master Mix with 1 µl of PCR water instead of DNA solution served as negative control. For detection of the bGH transgene, 5' CGG ACC GTG TCT ATG AGA AGC 3' sense (bGH #1) and 5' GGA AAG GAC AGT GGG AGT GG 3' anti-sense (bGH #2) oligonucleotides were used. For mIGFBP-2 PCR analysis, primers were used as follows: 5' GCG CGG GTA CCT GTG AAA 3' sense (CMV #3) and 5' TCC CTC AGA GTG GTC GTC ATC 3' antisense (IGFBP-2 #4).

After amplification, 4 µl 6x loading dye (MBI Fermentas, Germany) was added to each sample. Then the sample was transferred into the sample wells of a 2% agarose gel containing 1.0 µl ethidium bromide per 100 ml, and was positioned in a Easy Cast™ gel chamber (PeqLab, Germany) filled with 1*TAE running buffer. At the beginning of each sample well row, 12 µl PUC Mix Marker #8 (MBI Fermentas, Germany) was placed in order to allow estimation of amplified fragment size.

Electrophoresis was run for approximately 45 min at 90 V with an output of approximately 200 mA. Subsequently, the amplified products were visualized under UV light (306 nm) and a Polaroid picture (AGS, Germany) was taken for result documentation. bGH transgenic mice showed a distinct fragment with a size of 608 bp, in mIGFBP-2 transgenic mice, a fragment of 332 bp was acquired (Fig. 3.2).
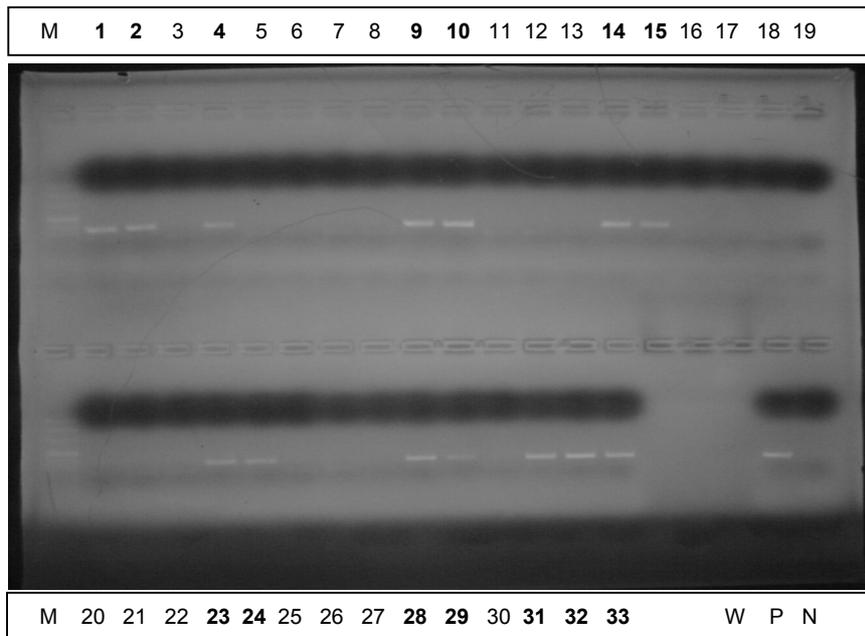
Figure 3.2 Polaroid picture for PCR result documentation. Bands at 608 bp meet the size of bGH fragment. At the beginning of each row, the PUC Mix Marker #8 (M) is placed. The identification number of the animals is shown above and underneath the Polaroid print; transgenic mice are written in bold numbers. W, PCR water (Quiagen, Germany); P, positive control; N, negative control.

Beside the material mentioned in the text above, the following reagents and pro-grams have been used:

Proteinase K solution: 20 mg/ml diluted in re-distilled water (Roche, Germany):

C/IA   24 vol/1 vol: chloroform/isoamyl alcohol (both Roth, Ger.)

Phenol-C/IA   25 vol/25 vol: phenol (Roth, Germany)-C/IA

Sodium acetate, 3 M   18.6 g/100 ml distilled water

Lysis buffer: 10 ml Tris, pH 8.0, 1 M

                                 40 ml EDTA, pH 8.0, 0.5 M

                                  5 ml Sodium chloride, 4 M

                                 20 ml SDS, 10 %

                                 125 ml distilled water

Tris, pH 8.0, 1 M

                                 6.06 g Tris-(hydroxymethyl)-aminomethane (Roth, Ger.)

                                 ad 50 ml dist. water, adjust pH with 1 N HCl (Merck, Ger.)

EDTA, pH 8.0, 0.5 M

                                 14.89 g EDTA (Roth, Germany)

                                 ad 80 ml distilled water, adjust pH with 1 N NaOH

Sodium chloride, 4 M

                                 11.69 g Sodium chloride (Merck, Germany)

                                 ad 50 ml distilled water

SDS, 10 %   10.0 g SDS (Sigma, Germany)

                                 ad 100 ml distilled water

Primer concentration: 100 pmol/μl each (Genzentrum/DNSynthese, Germany)

dNTPs: 100 mM each (Eppendorf, Germany):

PCR-KIT Master Mix: (Quiagen, Germany)

dNTP 1mM	4.0 μl
10*Buffer	2.0 μl
$MgCl_2$	1.25 μl
Primer sense	1.0 μl
Primer antisense	1.0 μl
PCR water	5.7 μl
Q-solution	4.0 μl
Taq polymerase	0.125 μl

50* TAE stock solution:

           121 g Tris base (Roth, Germany)

           28.55 ml glacial acetic acid (Sigma, Germany)

           50 ml EDTA, 0.5 M, pH 8.0

           ad 500 ml distilled water

Agarose gel: 2 g agarose (Gibco BRL, Germany)/100 ml 1*TAE buffer,

           add 1 μl (1 mg/ml) ethidium bromide (Merck, Germany)

Program for bGH DNA fragment amplification

           a) 4 min 94°C

           b) 1 min 94°C

           c) 1 min 65°C

           d) 2 min 72°C

           e) 10 min 72°C

           f) Hold on 4°C

Steps b) - d): 35 cycles

Program for mIGFBP-2 DNA fragment amplification

           a) 4 min 94°C

           b) 1 min 94°C

           c) 1 min 56°C

           d) 2 min 72°C

           e) 10 min 72°C

           f) Hold on 4°C

Steps b) - d): 35 cycles

3.2 Urine protein analysis

Urine protein analyses were applied to determine the consequence of expression of the bGH and/or IGFBP-2 transgene on kidney function. In order to exclude potential differences in urine protein excretion over the day, spot urine samples were taken constantly between twelve and one o'clock in the afternoon. The urine samples were immediately frozen and stored at -80°C until assayed. Usually, spontaneous urine could be obtained. If this was not the case, samples were taken by carefully squeezing the bladder with two fingers.

Details of mice used for urine protein analyses are listed in table 3.1. The pattern of proteinuria was determined using sodium dodecyl sulphate- (SDS-) polyacrylamide gel electrophoresis (PAGE). The urinary albumin concentration was measured using the murine microalbuminuria enzyme linked immunosorbent assay (ELISA) Albuwell M™ (Exocell Inc., USA).

3.2.1 Analysis of the pattern of proteinuria by SDS-PAGE

A 12% separating and a 5% stacking SDS-polyacrylamide gel was casted in a Mini-Protean III gel-casting chamber (Biorad, Germany). A comb for forming sample wells was immediately placed in the still fluid stacking gel until fully polymerisation. The comb was removed and the gel was placed into a Protean III electrophoresis cell (Biorad, Germany), which next was filled with running buffer.

All urine samples were examined within one week. First, the creatinine concentration of the urine samples was measured using an automated analyser technique (Hitachi, Merck, Germany). Urine samples were then standardized by dilution with sample buffer to a constant creatinine content of 250 µmol/l. A mouse albumin standard (Biotrend, Germany) was diluted 1:100 in sample buffer. Protein was denatured by heating the diluted samples and the mouse albumin standard thermoblock TB1 (Biometra, Germany) for 10 min at 100°C. The samples, an additional broad range molecular weight standard (Biorad, Germany), and the mouse albumin standard were then loaded onto the gel and electrophoresis was run for 60 min at 200 volt. Subsequently, the gel was stained with the Coomassie blue staining solution for 30 min and destained in the Coomassie destaining solution for approximately 1.5 hours until clear background. Visible protein bands were registered and gels were digitally

photographed for documentation. Finally, gels were dried for long-term storage using the DryEase™ Mini-Gel Drying System (Novex, Germany) according to the manufacturers protocol.

Beside the material mentioned in the text above, the following reagents have been used:

12% SDS-polyacrylamide gel:

        3.5 ml distilled water

        2.5 ml Tris/HCl, 1.5 M, pH 8.8

        100 µl SDS, 10%

        4.0 ml Acrylamide, 30% (Roth, Germany)

        50 µl Ammonium persulphate 10% (Biorad, Germany)

        5 µl Tetraethylethylenediamine (TEMED; Sigma, Germany)

    Tris/HCl, 1.5 M, pH 8.8:

        18.5 g Tris base

        ad 100 ml distilled water, adjust pH with 1N HCl

5% SDS-polyacrylamide gel:

        6.1 ml distilled water

        2.5 ml Tris/HCl, 0.5 M, pH 6.8

        100 µl SDS, 10%

        1.3 ml Acrylamide, 30%

        50 µl Ammonium persulphate, 10%

        5 µl TEMED

    Tris/HCl, 0.5 M, pH 6.8:

        6.075 g Tris

        ad 100 ml dist. water, adjust pH with 1N HCl

Running buffer (stock):

        30.3 g Tris

        144 g Glycerol (Merck, Germany)

        ad 1 l distilled water

Running buffer (ready to use):

        40 ml running buffer stock solution

        4.0 ml SDS, 10%

        ad 400 ml distilled water

Sample buffer: 1 ml distilled water

        0.25 ml Tris/HCl, 0.5 M, pH 6.8

        0.2 ml Glycerol

        0.4 ml SDS, 10%

        0.125 ml Bromphenol blue, 0.05% (Sigma, Germany)

Coomassie staining solution:

        625 mg Coomassie Brilliantblau G250 (Merck, Germany)

        12.5 ml 100% acetic acid (AppliChem, Germany)

        125 ml 100% ethanol

        ad 250 ml distilled water

Coomassie destaining solution:

        17.5 ml 100% acetic acid

        12.5 ml 100% ethanol

        ad 250 ml distilled water

3.2.2 Determination of urinary albumin concentration by ELISA

For quantitative determination of urinary albumin concentrations, the murine micro-albuminuria ELISA Albuwell M™ (Exocell Inc., USA) was applied, representing a conventional indirect competitive ELISA.

The murine albumin standard dilutions were prepared due to manufacturers recommendations with a provided diluent. The proper dilution of urine specimens ranged from 1:13 to 1:150, as shown by a pilot study. For the first incubation step (30 min), 50 µl of the standard solutions and the diluted specimens were added to the albumin-precoated wells of the ELISA plate together with 50 µl of a rabbit anti-murine albumin antibody solution. Then, the plate was washed ten times with a Columbus plate washer (Tecan AG, Germany). In a second incubation step (30 min), the probe was labeled by adding 100 µl of a horseradish peroxidase-conjugated goat anti-rabbit antibody. Next, the plate was washed as described above. Subsequently, the antibody-conjugate that bound to the albumin of the stationary phase was detected through a chromogenic reaction. 100 µl of a provided color developer was added for 5 to 10 min. The color intensity was measured by determining the absorbance at 450 nm using a computer-assisted (Magellan; Tecan AG, Germany) microplate reader (Sunrise; Tecan AG, Germany). The values of the specimen wells were in the linear segment of the calibration curve.

3.3 Serum and plasma parameters

For determination of clinical-chemical serum parameters and serum IGFBP-2 and IGF-I levels, blood was collected from mice (see table 3.1) under ether anesthesia by puncture of the retroorbital plexus. Serum was separated by centrifugation (10 min, 10,000 rpm) and stored at -80°C until assayed. Various clinical-chemical serum parameters, including sodium, potassium, calcium, chloride, phosphate, total protein, creatinine, urea, cholesterol, and triglycerides were determined using an Olympus AU400 autoanalyser (Olympus Diagnostica GmbH, Germany) and adapted reagents from Olympus Diagnostica GmbH (Germany). The measurement of clinical-chemical serum parameters was kindly carried out by Martina Klempt, Institute of Experimental Genetics, National Research Center for Environment and Health (GSF), Neuherberg, Germany.

Serum IGF-I and IGFBP-2 concentrations were quantified as described previously [275-277] using specific RIAs. The determinations were kindly performed by Martin Elmlinger, University Children's Hospital, Pediatric Endocrinology, Tübingen, Germany. For both assays, dilution curves of mouse serum samples were linear and paralleled those of human standards.

Plasma corticosterone levels were measured in 44 mice (C: n=15, B: n=11, G: n=10, GB: n=8) at four months of age. The animals were housed singly in opaque cages for two weeks before measurement of basal plasma corticosterone levels. Blood samples were taken between 16.00 and 18.00 hours. Mice were anesthetized individually in a glass jar containing saturated ether vapor and retroorbital blood was collected within 30 sec of the initial disturbance from the cage. To measure stimulated corticosterone levels, the anesthetized animals were treated intraperitoneally with 1 IU/100 g body weight ACTH (Synacthen®, Ciba-Geigy, Switzerland), and a second blood sample was obtained 60 min later. Blood was collected in ice chilled EDTA-coated Eppendorf tubes containing 200 IU aprotinin (Trasylol®, Bayer AG, Germany). Plasma samples were stored at -80 C until assayed.

For measurement of basal plasma ACTH concentrations, blood samples were taken from additional 31 mice (C: n=8, B: n=7, G: n=8, GB: n=8; four to seven months of age) of the four genetic groups between 8.00 and 9.00 hours and between 16.00 and 17.00 hours. The blood samples from the six MT-bGH transgenic mice and six littermate controls were collected in the morning. The blood samples for basal plasma ACTH determination were taken from the tail vein of conscious animals, because this is the least stressful method of blood sampling, if only a small amount of blood is needed and if the animals are used to be handled. Blood samples were collected in EDTA-coated tubes. The measurement of plasma corticosterone and ACTH concentrations was kindly carried out by Matthias M. Weber, Laboratory of Endocrine Research, Medical Department II Köln-Merheim, University of Cologne, Germany.

3.4 Body and organ weights

The body weight of mice listed in table 3.1 was constantly recorded between twelve and one o'clock in the afternoon after urine collection, and was determined to the nearest 0.1 g (PM 3000; Mettler, Switzerland).

The adrenal gland and kidney weight was determined after perfusion fixation of the mice (for details, see table 3.1). After fixation, the adrenal glands and kidneys were excised and adjacent tissues were carefully removed under a dissecting microscope (Stemi DV4, Zeiss, Germany). The adrenal glands were weighed to the nearest 0.1 mg, the kidneys to the nearest 1.0 mg on a precision balance (AE 200; Mettler, Switzerland).

3.5 Tissue preparation

3.5.1 Perfusion fixation

After blood collection under ether anesthesia, the mice were sacrificed by ether inhalation. Subsequently, the abdominal cavity and thorax were opened and the animals were fixed by orthograde perfusion *via* the left heart ventricle. The vascular system was preflushed with phosphate-buffered saline (PBS, pH 7.4, 37 °C) for 20 sec and perfused with a 3% glutaraldehyde-PBS solution (pH 7.4, 37 °C) for 5 min under a constant pressure of 100 mm Hg. An incision of the inferior vena cava served as outlet for the perfusate. After perfusion fixation, the adrenal glands and kidneys were postfixed *in situ* for an additional 48 h in the same fixative.

3.5.2 Immersion fixation

The kidneys for immunohistochemistry and *in situ* hybridization were collected from mice sacrificed by bleeding from the retroorbital sinus under ether anesthesia, and cut perpendicular to the longitudinal axis into four slices. The kidney slices were placed in tissue-embedding capsules and fixed by immersion in a 4% paraformaldehyde-PBS solution (pH 7.2) at 4°C for 12 hours.

3.5.3 Materials

The following materials were used for perfusion fixation and immersion fixation:

Phosphate-buffered saline (PBS)

0.25 g potassium dihydrogen phosphate (AppliChem, Germany)

8.0 g sodium chloride

1.46 g di-sodium hydrogen phosphate dihydrate (AppliChem, Germany)

ad 1 l distilled water, adjust to pH 7.4

3% glutaraldehyde-PBS solution (pH 7.4):

880 ml PBS, pH 7.4

120 ml glutaraldehyde, 25% (Serva, Germany)

4% paraformaldehyde-PBS solution (pH 7.2):

1000 ml PBS, pH 7.4

40 g paraformaldehyde (Serva, Germany)

adjust to pH 7.2 with 1 n NaOH

3.6 Histological techniques

3.6.1 Paraffin histology

The left, perfusion fixed, complete adrenal glands and the immersion fixed kidney slices were routinely dehydrated in a Histomaster 2050/DI (Bavimed, Germany) and embedded in paraffin (Paraplast®, Tyco Health Care, USA). Approximately 3 to 5 µm thick sections were obtained using a HM 315 microtome (Microm GmbH, Germany). The sections were mounted on glass slides (Marienfeld, Germany) and stained with hematoxylin and eosine (H&E), and Periodic Acid Schiff stain (PAS) according to standard procedures (see appendix).

3.6.2 Plastic histology

Perfusion fixed, sliced (see below) kidneys were dehydrated in a Citadel 1000 (Shandon, Germany). In order to avoid distorsion, the kidney slices were fixed with a piece of foam-rubber sponge in the tissue-embedding capsules. Subsequently, the kidney slices were processed in a hydroxymethylmethacrylate (Fluka Chemie, Germany)/methylmethacrylate (Riedel de Haën, Germany) solution at 4°C on a shaker for 18 hours. The kidney slices were then shifted into "solution 1", composed of benzoylperoxide (338 mg; Merck, Germany), methylmethacrylate (20 ml), hydroxymethylmethacrylate (60 ml), ethyleneglycol monobutylether (16 ml; Merck, Germany), and polyethylene glycol 400 (2 ml; Merck, Germany). After immersion at 4°C on a shaker for four hours, the kidney slices were placed in plastic cups and embedded using 60 µl of dimethylanilin (Merck, Germany) in 40 ml of "solution 1" as starter for polymerisation. Embedding cups were immediately placed into a water bath (4°C) and polymerisation took place at 4°C over night [278]. Sections of 1.5 µm thickness were cut from the casted blocks on a Reichert-Jung 2050 rotary microtome (Cambridge Instruments, Germany). The sections were routinely processed and stained with H&E, PAS, and Periodic acid silver methenamine combined with PAS (PASM-PAS), respectively. Staining procedures are listed in the appendix.

3.6.3 Epon histology

Since Epon is a trademark of the Shell Company (USA), Serva (Germany) distributes the identical chemical substance under the designation "glycid ether 100". In the present study the terms "Epon" and "glycid ether 100" are used synonymous.
Cubes with a maximal carve length of 1 mm of the renal cortex and complete adrenal glands were washed for 3 hours in Sörensen phosphate buffer at room temperature, postfixed in 1% osmium tetroxide [279] for 2 hours at 4°C, and washed in Sörensen phosphate buffer three times for 2 min at room temperature. Subsequently, the specimens were dehydrated through a series of acetone solutions at 4°C before they were infiltrated with a 100% acetone/Epon mixture for 1 hour, and twice with pure Epon for 30 min, respectively, at room temperature. Then, the Epon infiltrated samples were embedded in an Epon-embedding mixture in dried gelatin capsules (Plano, Germany). Polymerization took place at 60°C for approximately 48 hours.

Epon blocks were trimmed with a TM60 Reichert-Jung milling machine (Leica, Germany) and 0.5 µm semi-thin sections were obtained with a Reichert-Jung "Ultracut E" microtome (Leica, Germany).

The following materials were used for Epon histology:

Sörensen phosphate buffer, 0.067 M, pH 7.4

        80.8 ml solution I

        19.2 ml solution II

        adjust to pH 7.4

Solution I: 9.08 g potassium dihydrogen phosphate

        ad 1 l distilled water

Solution II: 11.88 g di-sodium hydrogen phosphate dihydrate

        ad 1 l distilled water

Osmium tetroxide, 1%

        5.0 ml osmium tetroxide, 2% (Merck, Germany)

        2.0 ml veronal acetate buffer, pH 7.6

        2.0 ml hydrogen chloride 0.1 M (Merck, Germany)

        1.0 ml distilled water

        0.45 g saccharose (Merck, Germany)

veronal acetate buffer, pH 7.6:

        2.95 g sodium veronal (barbitone sodium) (Merck, Germany)

        1.94 g sodium acetate (Merck, Germany)

        ad 100 ml distilled water

Epon-embedding mixture

        3.5 ml solution A and 6.5 ml solution B

        0.15 ml para-dimethyl aminomethyl phenol (Serva, Germany)

Solution A: 62 ml glycid ether 100 (Serva, Germany)

100 ml 2-dodecenyl succinicacid anhydride (Serva, Germany)

Solution B: 100 ml glycid ether 100

89 ml methylnadic anhydride (Serva, Germany)

3.7 Stereological investigations of the adrenal glands

Stereological analyses of the adrenal glands were carried out on 12 male mice (n=3 per genetic group, chosen by random numbers) at the age of 75 days.

3.7.1 Determination of the zonal composition

The left, paraffin-embedded (see 3.6.1) adrenal gland was exhaustively sectioned at a nominal thickness of 3 μm on a HM 315 microtome (Microm GmbH, Germany) equipped with a section counter. Every 20th section of the series was saved, mounted on consecutively numbered glass-slides, and stained with H&E. Morphometric evaluation was carried out on a Videoplan® image analysis system (Zeiss-Kontron, Germany) coupled to a light microscope (Orhoplan; Leitz, Germany) *via* a color video camera (CCTV WV-CD132E; Matsushita, Japan). The total number of paraffin sections sampled per adrenal gland ranged from 14 to 28. On these sections, the cross-sectional areas of cortex and medulla were planimetrically determined. Furthermore, the cross-sectional areas of the adrenocortical zones were measured by point counting at a 340 $\times$ final magnification, which was provided by a 10 $\times$ objective. For calibration, an object micrometer (Zeiss, Germany) was used.

Since in mice the zona fasciculata and zona reticularis are not distinguishable at the light microscopic level [280], these zones were calculated jointly and for simplicity will henceforth be denoted zona fasciculata only. The volume fractions of the cortex ($V_{V(cortex/adrenal\ gland)}$) and the medulla ($V_{V(medulla/adrenal\ gland)}$) of the adrenal gland were estimated following the principle of Delesse [281]. They were calculated as the sum of cross-sectional areas of cortical and medullary tissue, respectively, divided by the sum of cross-sectional areas of the whole adrenal gland [282]. The fractional volume of

the zona fasciculata in the adrenal cortex ($V_{V(zona\ fasc./cortex)}$) was estimated from the corresponding point fraction.

The absolute volume of the adrenal cortex ($V_{(cortex,\ adrenal\ gland)}$) and the medulla ($V_{(medulla,\ adrenal\ gland)}$) was obtained as the product of the corresponding volume fractions ($V_{V(cortex/adrenal\ gland)}$ and $V_{V(medulla/\ adrenal\ gland)}$, respectively) and the volume of the adrenal gland. The latter was calculated by dividing the weight of the adrenal gland by the specific weight, which is reported to correspond to 1.039 mg/mm^3 for adrenal glands [283]. The volume of the zona fasciculata ($V_{(zona\ fasciculata,\ cortex)}$) was obtained as the product of $V_{V(zona\ fasciculata/cortex)}$ and $V_{(cortex,\ adrenal\ gland)}$.

3.7.2 Determination of number and size of zona fasciculata cells

For quantitative determination of the changes of the zona fasciculata at a cellular level, the disector method was applied. The disector is a three-dimensional stereologic probe, which allows unbiased assumption-free counting and sizing of particles [284]. The physical disector, which consists of a pair of physical section planes separated by a known distance and an unbiased two-dimensional counting frame, in combination with systematic point counting was used to estimate the numerical density and the mean volume of zona fasciculata cells.

The right, Epon-embedded adrenal glands were analyzed. After trimming of the Epon blocks, at least 8 serial semi-thin sections (0.5 µm) comprising the whole organ were cut from each adrenal gland with a Reichert-Jung "Ultracut E" microtome (Leica, Germany), mounted on consecutively numbered glass-slides, fixed over a flame, and stained with toluidine blue and safranine.

From the stack of serially cut semi-thin sections, one section was drawn at random by means of a random number (R) between 2 and 8 (the baseline section was not used for sampling) as a reference section in a disector. The second section (look-up section) was sampled among no. 2-8 by means of R±3, *i.e.*, the disector height was equivalent to the thickness of three semi-thin sections (1.5 µm). Five fields were systematically sampled at random in the zona fasciculata of the reference section and the corresponding fields were identified in the look-up section (Fig. 3.3). Light microscopic images of the selected fields were acquired with a color video camera using a 63 × oil immersion objective and color prints were prepared at a constant final

magnification (2,300×). A plastic transparency with equally spaced test points (n=70) and an unbiased counting frame [285,286], representing an area of 8,800 µm^2, was superimposed on the printed images (Fig. 3.3).

All profiles of zona fasciculata cell nuclei sampled in the reference section, which were not present in the look-up section, were counted (Q$^-$). On the reference sections, the number of points hitting zona fasciculata cells (P$_{(zona\ fasc.\ cells)}$) was counted as well as the points hitting the zona fasciculata (P$_{(zona\ fasc.)}$). The volume density of zona fasciculata cells in the zona fasciculata (V$_{V(zona\ fasc.\ cells/zona\ fasc.)}$) was estimated from the corresponding point fraction [282]. The operation of counting of Q$^-$ (cell nuclei) was then repeated by interchanging the roles of the look-up section and the reference section, thereby increasing the efficiency by a factor of two.
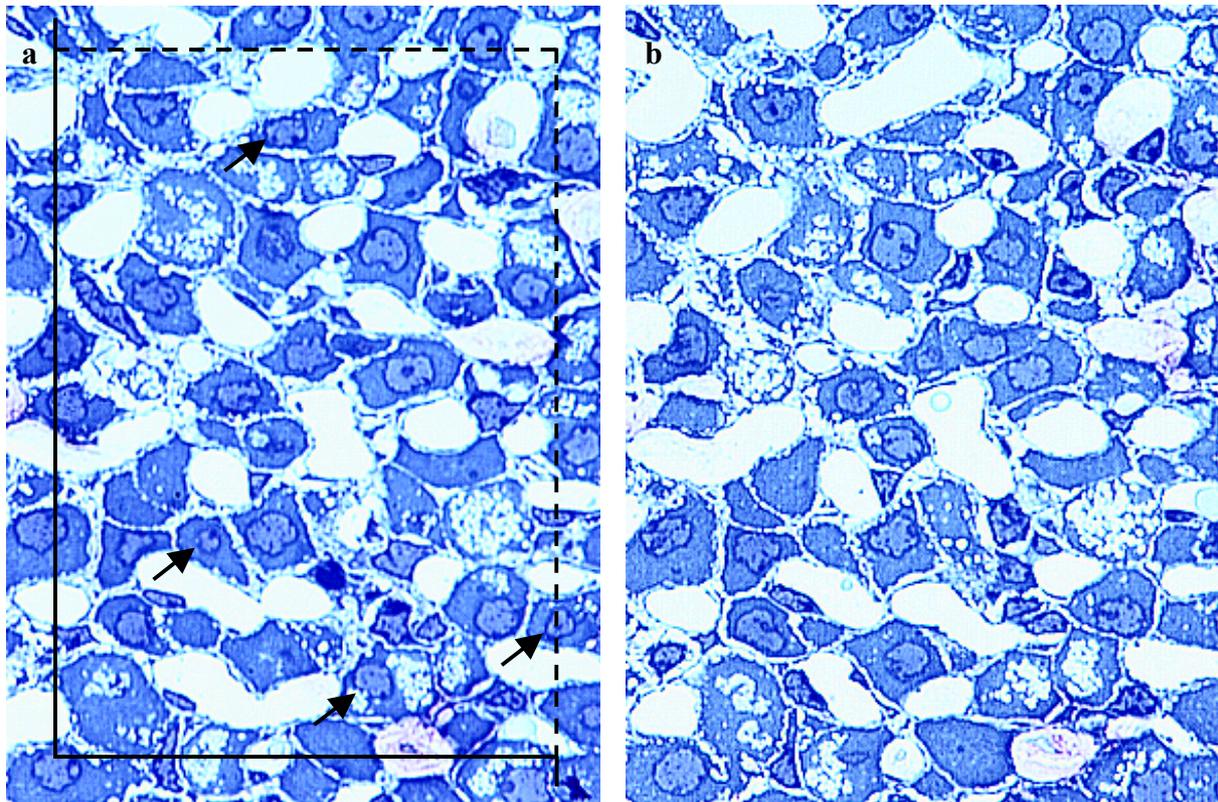
Fig. 3.3: Counting of zona fasciculata cells with the physical disector. A visual field, selected by systematic random sampling in the zona fasciculata on the reference section (a) and the corresponding visual field on the look-up section (b, 1.5 µm apart) are shown. An unbiased counting frame is superimposed on the reference section. Profiles of zona fasciculata cell nuclei were sampled, if they were located completely in the frame, or were partially in the frame and intersected or touched by the "allowed" (dotted) lines. Profiles of zona fasciculata cell nuclei were not sampled, if they were touched or intersected by the "forbidden" (solid) lines. Cell nuclei sampled in the reference section were counted (Q$^-$; arrows), if they were not present in the look-up section.

Given that zona fasciculata cells have only one nucleus, which is documented in the literature [280] and was also observed in this study, no cell is counted twice with this procedure. On the average, 61 nuclei (range: 45-83) were counted with the five disector pairs per adrenal gland. The numerical density of epithelial cells in the zona fasciculata ($N_{V(zona\ fasc.\ cells/zona\ fasc.)}$) was calculated by dividing the total number of cells counted in all disectors in an adrenal gland by the cumulative volume of the disectors (area of the unbiased counting frame × disector height × number of disectors) sampled in the adrenal gland. Assuming the same numerical density of epithelial cells in the zona fasciculata in both (right and left) adrenal glands and neglecting the small amount of tissue shrinkage when using Epon-embedding [282], the total number of zona fasciculata cells per adrenal gland ($N_{(zona\ fasc.\ cells,\ adrenal\ gland)}$) was calculated as the product of the numerical density of epithelial cells in the zona fasciculata ($N_{V(zona\ fasc.\ cells/zona\ fasc.)}$) and the volume of the zona fasciculata ($V_{(zona\ fasc.,\ adrenal\ gland)}$).

The mean volume of zona fasciculata cells ($v_{(zona\ fasc.\ cells)}$) was obtained by dividing the volume density ($V_{V(zona\ fasc.\ cells/zona\ fasc.)}$) by the numerical density of the epithelial cells in the zona fasciculata ($N_{V(zona\ fasc.\ cells/zona\ fasc.)}$).

To control the nominal thickness of semi-thin sections (0.5 µm), a resectioning technique was used. Five semi-thin sections, which were not used for sampling, were selected from different section series and re-embedded in Epon (see under 3.6.3). Ultra-thin sections (approximately 70 nm) of the semi-thin sections were stained with uranyl acetate and lead citrate and examined with a Zeiss EM 10 electron microscope (Zeiss, Germany). Electron micrographs (final magnification 10,500×) were taken from segments of the primary section, showing every evidence of having been re-sectioned normally to their surface. For calibration, a waffle grating replica with 2,160 lines/mm (Plano, Germany) was used. The measured mean thickness of the semi-thin sections was 0.497±0.020 µm. Thus, the precision of the ultramicrotome was confirmed.

3.8 Stereological investigations of the kidneys

Stereological analyses of the kidneys were carried out on male mice, chosen by random numbers from the different age and genetic groups. Detailed information on number, age, and genotype of the mice used for investigations of single stereological parameters is given in table 3.1.

3.8.1 Determination of the zonal composition

After weighing, the length of each kidney was determined. Then the kidneys were cut perpendicular to the longitudinal axis into parallel slices of approximately 1 mm thickness, with the first cut positioned randomly in a 1 mm interval from one of the poles. The total number of slices per kidney ranged from 7 to 14. Before further processing, specimens of the renal cortex were taken for Epon-embedding and subsequent stereological analysis of the mean volume and the total number of proximal tubular epithelium (PTE) cells (see 3.8.2). Cortex specimens were selected by systematic random sampling using a plastic transparency with regularly spaced (3 mm) test points that was superimposed on the kidney slices [287]. The cortex specimens sized approximately 1 mm^2 × 1 mm thickness of the kidney slice.

Using PASM-PAS stained sections of plastic-embedded kidney slices, the quantitative stereological determination of the volume fractions of the individual renal zones was performed following the principle of Delesse [281]. For this purpose, micrographs of the sections were produced using an Orthoplan photomicroscope (Leitz, Germany) at a final magnification of 30 ×, provided by a 2.5 × objective. An object micrometer was used for calibration, which was photographed and printed under the same conditions as the kidney sections. The distinct renal zones, as defined in the literature [288,289] - cortex, outer stripe of medulla (OSM), and inner stripe of medulla together with the inner zone of medulla (ISM/IZM) - were highlighted on the prints. Their cross-sectional areas were determined planimetrically on the photographs by circling the cut surface using a Videoplan® image analysis system (Zeiss-Kontron, Germany).

The volume fractions of the renal zones ($V_{V(cortex/kidney)}$, $V_{V(OSM/kidney)}$, and $V_{V(ISM/IZM/kidney)}$) were calculated separately in each kidney as the sum of cross-sectional areas of the individual zones, divided by the sum of cross-sectional areas of the whole kidney. The absolute volumes of the renal zones ($V_{(cortex, kidney)}$, $V_{(OSM, kidney)}$, and $V_{(ISM/IZM, kidney)}$) were obtained as the product of the corresponding volume fractions and the volume of the kidney. The volume of the kidney was calculated by dividing the weight of the kidney by its specific weight, which is reported to correspond to 1.05 mg/mm^3 [290].

3.8.2 Determination of the volume of nephron segments

The fractional volume of the proximal tubular epithelium (PTE) within cortex and OSM ($V_{V(PTE/cortex\&OSM)}$) was determined by point counting. Further, the fractional volumes of other nephron segments were obtained, like that of other tubular epithelia (OTE, $V_{V(OTE/cortex\&OSM)}$), and that of miscellaneous structures, like glomeruli, interstitium, and blood vessels (MIS, $V_{V(MIS/cortex\&OSM)}$). Sections of every third kidney slice were selected. Within one section, every 8th to 15th visual field (depending on the cross-sectional area of the kidneys) was evaluated. The visual fields were projected from a microscope on a monitor with a final magnification of 340 $\times$, provided by a 10 $\times$ objective. Per kidney, 90 to 138 points (six points per visual field) were counted. The point fraction of the individual nephron segments (*e.g.*, for the PTE: $P_{P(PTE/cortex\&OSM)}$) of hitting points (for the PTE: $P_{(PTE)}$) as a function of the total number of points ($P_{(total)}$) is equivalent to the fractional volume of the individual nephron segments in the cortex and OSM (for the PTE: $V_{V(PTE/cortex\&OSM)}$) [282,291]. The absolute volume of the individual nephron segments (for the PTE: $V_{(PTE, cortex\&OSM)}$) was obtained as the product of the corresponding volume fraction and the volume of the cortex and OSM.

3.8.3 Determination of the mean volume and total number of PTE cells

The mean volume and the total number of cortical PTE cells were determined applying the disector method in combination with systematic point counting, analogous to the stereological investigation of parameters of adrenal zona fasciculata cells (see 3.7.2).

Two specimens of the renal cortex were taken per kidney (four samples per animal) as described in 3.8.1, and embedded in Epon. At least 10 serial, toluidine blue and safranine stained semi-thin sections (0.5 μm) were obtained from each cortex specimen. One section out of the stack of serially cut semi-thin sections was drawn at random by means of a random number (R) between 2 and 10 as a reference section in a disector. The look-up section was sampled among no. 2-10 by means of R±3, destining a disector height of 1.5 μm. In this approach, two visual fields were systematically sampled at random in the renal cortex of the reference section and the corresponding fields were identified in the look-up section.

Color prints of light microscopic images of the selected fields were prepared (1,450 × final magnification, provided by a 40 × objective) and were overlaid with a plastic transparency with equally spaced test points (n=70) and an unbiased counting frame, representing an area of 22,360 $μm^2$.

Profiles of PTE cell nuclei were sampled in the reference section and counted (Q^-), if they were not present in the look-up section. The operation of counting of Q^- (cell nuclei) was then repeated by interchanging the roles of the look-up section and the reference section. As documented in the literature [292] as well as confirmed in this study, PTE cells have one nucleus. Thus, no cell is counted twice with this method. To calculate the numerical density of PTE cells in the cortex ($N_{V(PTE\ cells/cortex)}$), the total number of PTE cells counted per kidney (Q^-=87 PTE cell nuclei/kidney on average, range: 60 - 102) was divided by the cumulative volume of the disectors per kidney. The total number of PTE cells in the cortex ($N_{(PTE\ cells,\ cortex)}$) was calculated as the product of ($N_{V(PTE\ cells/cortex)}$ and the volume of the cortex ($V_{(cortex,\ kidney)}$).

The number of points hitting PTE cells ($P_{(PTE\ cells)}$) was counted on the reference sections, as well as the points hitting the reference space, *i.e.*, the renal cortex ($P_{(cortex)}$). The volume density of PTE cells in the renal cortex ($V_{V(PTE\ cells/cortex)}$) was estimated from the corresponding point fraction [282]. The mean volume of PTE cells ($v_{(PTE\ cells)}$) was obtained by dividing the volume density of PTE cells in the cortex ($V_{V(PTE\ cells/cortex)}$) by the numerical density of PTE cells in the cortex ($N_{V(PTE\ cells/cortex)}$).

3.8.4 Determination of the mean glomerular volume

The mean glomerular volume ($v_{(Glom)}$) was estimated following the method of Hirose et al. [293]. In this model-based stereological approach, the glomeruli were considered as rotation ellipsoids. The mean glomerular area ($a_{(glom)}$) was obtained from planietric measurements of glomerular profile areas. In the calculation, a shape coefficient (β, =1.40) and a size distribution coefficient (κ, =1.04) were considered. The results were corrected for embedding shrinkage [293]. The values for the shape and size distribution coefficient as well as for the shrinkage correction factor for plastic embedded murine renal tissue were taken from Wanke [229]. The mean glomerular volume was calculated with the following equation [293]:

$$v_{(glom)} = \frac{\beta}{\kappa} \cdot a_{(glom)}{}^{1,5}$$

$v_{(glom)}$:   mean glomerular volume

β :   shape coefficient

κ :   size distribution coefficient

$a_{(glom)}$:   mean area of glomerular profiles

PASM-PAS stained sections of every third kidney slice were selected. Images of the sections were displayed on a color monitor using a Videoplan® image analysis system (Zeiss-Kontron, Germany). The final magnification on the monitor was 1380 × (40 × objective). An object micrometer (Zeiss) served for calibration. Within the section, these glomerular profiles were sampled, which appeared on the monitor while systematically meandering through the section. The lateral lines of a frame displayed on the monitor were used as "allowed and forbidden lines", as meant by the unbiased counting rule [285,294]. These glomerular profiles, which were between the lines, or which were touched or intersected by "allowed lines" were sampled, whereas these, which were touched or intersected by "forbidden lines" were not sampled. The contours of the sampled glomerular profiles were circled with a cursor. Between 114 and 316 glomerular profiles were evaluated per kidney (on average

165 glomerular profiles). The difference between right and left kidney of the same animal was seen as an internal quality control and ranged from 0.02 to 8.98%, and was on average 4.61 %.

3.8.5 Determination of the nephron number

For determination of the nephron number, the number of glomeruli per kidney ($N_{(glom, kidney)}$) was estimated following the method of Weibel [282]. The analysis was performed on images of PASM-PAS stained sections that were projected on a color monitor in combination with a Videoplan® image analysis system. An object micrometer served for calibration. A plastic transparency with a grid (four lines per mm) was super-mposed on the sections to enable an area-based selection of the cortical areas to be evaluated. The selection of cortical areas was performed at a final magnification of 25 × (2.5 × objective). By changing the objective, the selected cortical areas were investigated at a final magnification of 350 × (10 × objective).

In a first step, the fractional area of glomerular profiles in the renal cortex ($A_{A(glom/cortex)}$) was determined. This was achieved by planimetrically measuring the areas of glomerular profiles located completely or partially within a frame with known area that is displayed on the monitor. $A_{A(glom/cortex)}$ was determined in 24 to 55 test fields (average 40) per kidney representing 5.2 to 11.3 % (average 7.6%) of the total cortical area of the sections of the kidneys investigated.

In a second step, the number of glomerular profiles per cortical area ($Q_{A(glom/cortex)}$) was counted using the identical fields as used for estimation of $A_{A(glom/cortex)}$. In those fields, the frame lines generated by the monitor were used according to the unbiased counting rule [285]. Analogous to the determination of the mean glomerular volume (see 3.8.4), a shape coefficient and a size distribution coefficient were considered in the calculation, and the results were corrected for embedding shrinkage. The numerical volume density of glomeruli in the renal cortex was calculated by the following equation [282]:

$$N_{V(glom/cortex)} = \frac{\kappa}{\beta} \sqrt{\frac{Q_{A(glom/cortex)}^{3}}{A_{A(glom/cortex)}}}$$

$N_{V(glom/cortex)}$:   numerical volume density of glomeruli in the renal cortex

β :   shape coefficient

κ :   size distribution coefficient

$Q_{A(glom/cortex)}$:   number of glomerular profiles per unit of cortex area

$A_{A(glom/cortex)}$:   fractional area of the glomerular profiles in the cortex

The number of glomeruli per kidney was calculated from the product of the numerical volume density of glomeruli in the renal cortex ($N_{V(glom/cortex)}$) and the volume of the renal cortexglomerular area fraction in the cortex ($V_{(cortex, kidney)}$).

3.9 Evaluation of the glomerulosclerosis index

The degree of glomerular lesions was assessed semi-quantitatively on a scale of 0 - 4 following the method of El Nahas *et al*.[295]. The glomerular score was: Grade 0, glomeruli without light-microscopic structural changes; Grade 1, presence of mesangial expansion; Grade 2, segmental glomerular sclerosis/hyalinosis involving less than 50% of the glomerular tuft profile; Grade 3, glomerular sclerosis/hyalinosis involving more than 50% of the tuft profile; Grade 4, global glomerulosclerosis with total tuft obliteration.

The glomerulosclerosis index was evaluated on images of PASM-PAS stained sections that were projected on a color monitor *via* a color video camera. The final magnification on the monitor was 1380 × (40 × objective). Two randomly selected sections of each kidney were investigated by systematically meandering through the section. The lateral lines of a frame generated by the monitor were used as "allowed and forbidden lines". Glomerular profiles between the lines or touching the "allowed" line were sampled, and those touching the "forbidden" line were excluded, to give an unbiased sample [285]. Between 107 and 164 glomerular profiles were evaluated per mouse (on average 143 glomerular profiles). The ultimate glomerular sclerosis index was obtained by averaging the scores of all glomerular profiles surveyed in each animal.

3.10 Detection of IGFBP-2 mRNA and protein in renal tissue

Three mice per genetic group at 38 days of age were used for immunohistochemistry and *in situ* hybridization analysis of the kidneys. Animals were sacrificed under ether anesthesia. Subsequently, the left kidney of each mouse was removed, cut transversally into four slices, shock frozen in liquid nitrogen, and stored at -80°C until used for Western ligand blot (WLB) analysis. The right kidney and the pancreas were immersion fixed (see 3.5.2) and paraffin-embedded (see 3.6.1) for immunohistochemistry and *in situ* hybridization. The pancreata of B and GB mice were taken as positive control tissue for IGFBP-2 immunohistochemistry since the highest IGFBP-2 protein levels were found in pancreatic islets [152].

3.10.1 Immunohistochemical detection of IGFBP-2

The indirect immunoperoxidase technique [296] served to localize IGFBP-2 protein within the kidney. Approximately 5 μm thick paraffin sections were cut with a HM 315 microtome and mounted on 3-aminopropyltriethoxy-silane-treated glass slides. The treatment of the sections was carried out at room temperature and all incubation steps were performed in a humidity chamber. Sections were deparaffinized in xylene, rehydrated in a descending ethanol series and washed in distilled water. Then, they were incubated in a preheated Target Retrieval Solution (Dako Diagnostika, Germany) for 10 min at 96°C and another 20 min in the down-cooling solution in order to improve the accessibility of the antibodies to target sites within the tissue. The slides were rinsed with distilled water and washed in PBS for 10 min. Next, tissue sections were treated with 1% hydrogen peroxide phosphate-buffered saline (PBS) for 10 min to block endogenous peroxidase activity, followed by a 10-min washing in PBS. Subsequently, the tissue sections were pre-incubated with 2% normal rabbit serum (Dako Diagnostika, Germany) PBS solution for 60 min to reduce non-specific binding. The pre-incubation serum was decanted before the slides were incubated with a goat anti-humanIGFBP-2 antibody (sc-6002, Santa Cruz Biotechnology Inc., Germany) for 45 min that was diluted 1:100 in PBS solution containing 2% (vol/vol) normal rabbit serum. According to the manufacturers description, the epitopes the antibody recognizes are identical between human and murine IGFBP-2 and presents the identical amino acid sequence. After a 10-min washing in PBS, horseradish

peroxidase conjugated rabbit anti-goat IgG antibody (Dako Diagnostika, Germany), diluted 1:100 in PBS solution containing 5% (vol/vol) mouse serum was applied for 45 min. Then slides were washed in PBS solution for 10 min and immunoreactivity was visualized using DAB tablets (3,3 diaminobenzidine; ENTEC Diagnostics, Denmark) tablets. The DAB tablet was dissolved in 10 ml distilled water containing 10 µl 30% hydrogen peroxide, and the tissue sections were incubated with the solution for 5 min. Tissue sections were counterstained with Mayer`s hemalaun (AppliChem, Germany) solution, dehydrated in an ascending series of alcohols, cleared in xylene and mounted under glass coverslips (Menzel GmbH & Co KG, Germany) using Histofluid® (Superior, Germany).

Specificity controls included substitution of the primary antibody with non-immune serum and omission of the secondary antibody.

3.10.2 Detection of IGFBP-2 mRNA by *in situ* hybridization

Approximately 5 µm thick paraffin sections were cut with a HM 315 microtome, mounted on SuperFrost®Plus (Menzel GmbH & Co KG, Germany) glass slides, and kept at 4°C until assayed. Serial sections from the identical paraffin blocks as used for immunohistochemistry allowed a direct comparison of IGFBP-2 mRNA expression and protein occurrence in individual kidney structures.

Section pre-treatment included deparaffination and rehydration through successive graded alcohol solutions. Tissue sections were then postfixed in ice-cold 4% para-formaldehyde-PBS solution, digested with Proteinase K (20 µg/ml; Roche, Germany), acetylated in acetic anhydride (0.25 %; Sigma, Germany) in triethanolamine (10 mM; Sigma, Germany), and equilibrated, due to a standard protocol. RNA riboprobes were generated by *in vitro* transcription. To this end, IGFBP-2 cDNA (kindly donated by Stenvert L. S. Drop, Department of Pediatrics, Division of Endocrinology, Sophia Children's Hospital, Erasmus University, Rotterdam, The Netherlands) as well as the vector pGEM4Z were digested and the resulting fragments were ligated. The plasmid pGEM4Z-IGFBP2 was linearized with restriction enzymes and subsequently used as template for Digoxigenin (DIG)–UTP-labeled riboprobe synthesis. After transcription, the template cDNAs were digested by RNase-free DNase (Desoxyribonuclease; Invitrogen, Germany) and the riboprobes were precipitated. Concentration and length of the riboprobes were determinated by agarose gel electrophoresis.

For *in situ* hybridization, pre-treated tissue sections were prehybridized with hybridization solution (mRNA *in situ* hybridization Solution; Dako Diagnostika, Germany) at 65°C. The probes were denatured for 5 min at 80°C and added to hybridization mix. The hybridization reaction was carried out at 65°C over-night in a closed sealed box in a water bath. Afterwards, the tissue sections were washed several times and RNase (RNaseA; Roche, Germany) treated. The slides were then blocked (DIG Wash and Block Buffer set; Roche, Germany) and subsequently labeled with alkaline phosphatase-coupled anti-digoxigenin antibody (DIG RNA Labeling Mix; Roche, Germany). Excess antibody was removed by several washes. Prior to the cytochemical detection of hybridized probe sections were equilibrated. Color development was performed under visual inspection with BM Purple (Roche, Germany), staining was stopped with distilled water. Sections were mounted with Vectashield® (Vector Laboratories, USA) mounting medium.

In situ hybridization for detection of IGFBP-2 mRNA was kindly performed by Dagmar Kress, Institute of Molecular Animal Breeding and Biotechnology/Gene Center, University of Munich.

3.10.3 Western Ligand Blot analysis

In order to evaluate binding capacity of IGFBP-2 within the distinct renal zones, the right kidneys of three 38-day-old mice per genetic group were investigated by Western ligand blot (WLB) analysis [297].

The kidney samples were thawed on a 4°C aluminum padding. Subsequently, three to four about 1 mm^3-sized pieces were excised from the renal zones (cortex, OSM, and ISM/IZM) with a scalpel and were in part embedded in paraffin, sectioned, and stained with H&E, in order to control their purity. A microscopic evaluation of the control pieces confirmed that no neighbored renal zones were catched.

The majority of renal zone samples were saved in 15 ml plastic tubes and 5 ml of 4°C tempered extraction buffer were added immediately. Then the samples were homogenized for about 1 min with a Polytron® PT-K 7 K1 homogenizer (ART, Germany). Next, the protein content of the extracts was standardized. For that purpose, the actual protein content was determined using the bicinchinoic acid (BCA) protein assay. A 96 well plate was prepared with 4 µl of bovine serum albumin dilutions as

standards as well as 4 µl of the extracts, before addition of 200 µl of BCA (Sigma, Germany) and $CuSO_4$ (4%) (Sigma, Germany) in a 50:1 relation. The plate was incubated at 37°C for 30 min and evaluated by measuring the absorbance at 562 nm with a microplate reader. The results of the tissue extraction samples were in the linear range of the standard dilution curves. After determining the protein contents, the tissue extraction samples were standardized for constant protein content by dilution with adequate amounts of extraction buffer.

Next, 20 µg of protein per tissue extraction sample was separated by SDS-PAGE, as described under 3.2.1. After electrophoresis, the separated proteins were transferred onto a polyvinylidene difluoride Q (PVDF) membrane (Millipore, Germany), using semi-dry electroblotting. Six layers of transfer buffer-moistened absorbent paper (Schleicher & Schüll, Germany) and a PVDF membrane were placed on the cathode of a semi-dry blotting chamber (Millipore, Germany). The PVDF membrane had been incubated in 100% methanol (AppliChem, Germany) for 10 min and subsequently washed in transfer buffer. Next, the SDS-PAGE gel was positioned on the PVDF membrane. The absorbent paper that was not covered by the PVDF membrane and the SDS-PAGE gel was enclosed with parafilm "M" (Am. National Can™, USA), in order to obtain an accurate currency through the gel. The SDS-PAGE gel was covered with six layers of absorbent paper and the anode. The transfer was run for 90 min with an initial currency of 60 mA. A correct blotting was confirmed by staining the membrane with ponceau S red solution for 1 to 2 min and destaining until clear background with distilled water.

For detection of the IGFBPs, the PVDF membrane was positioned in a 50 ml tube and incubated with different solutions. All incubations and washing steps were carried out at 4°C in a tube rotator (Bachhofer, Germany). First, a 3% NP-40 Tris-Saline solution was added for 20 min, replaced by a blocking 1% fish gelatine Tris-Saline solution for 60 min in order to avoid non-specific binding of the ligand to the membrane. Subsequently, the membrane was treated with a 0.1% Tween-20 Tris-Saline solution for 15 min before over night incubation with the tracer containing 10^6 cpm [^{125}I]-IGF-II per blot. The following steps included two washings with 0.1% Tween-20 Tris-Saline solution and three washings with Tris-Saline solution for 30 min, respectively. Membrane bound [^{125}I]-IGF-II was visualized using a Phospho-

Imager Storm (Molecular Dynamics, Germany). The densitometric analysis of the IGFBP-2 bands was performed using the ImageQuant™ Software Package (Molecular Dynamics, USA).

The following materials were used for Western Ligand blot analysis:

Extraction buffer   388 mg Tris base (Roth, Germany)

                           3.2 ml Triton X-100, 2% (Sigma, Germany)

                           40 ml Laemmli buffer (5x)

                           ad 160 ml distilled water, adjust to pH 7.4

     Laemmli buffer (5x)

                           7.5 g Tris base (Roth, Germany)

                           10 g SDS

                           50 g Glycerol (Merck, Germany)

                           1.0 ml EDTA, 1 mM (Sigma, Germany)

                           10 ml Bromphenol blue, 0.05%

                           ad 100 ml distilled water, adjust to pH 6.8

Transfer buffer   3.03 g Tris base

                           14.4 g Glycerol

                           200 ml Methanol (Applichem, Germany)

                           800 ml distilled water

Tris-Saline   1.21 g Tris base

                           8.765 g sodium chloride

                           ad 1000 ml distilled water, adjust to pH 7.4

3% NP-40 Tris-Saline

                           485 ml Tris-Saline, pH 7.4

                           15 ml Nonidet P-40 (Fluka Chemie, Germany)

1% fish gelatine Tris-Saline

        5.0 ml Tris-Saline, pH 7.4

        50 µl fish gelatine (Amersham Pharmacia GmbH, Germany)

0.1% Tween-20 Tris-Saline

        500 ml Tris-Saline, pH 7.4

        500 µl Tween 20 (Sigma, Germany)

Tracer   5.0 ml 0.1% Tween-20 Tris-Saline, pH 7.4

        50 µl fish gelatine

        0.5×10^6 cpm/ml $[^{125}I]$-IGF-II (Amersham Pharmacia GmbH,

                                   Germany)

3.11 Statistical Analysis and Data Presentation

Data were analyzed by ANOVA taking the effect of genetic group into account. Means were compared by using LSD post-hoc tests (SPSS program package; SPSS, Inc., Chicago, IL, USA). P values < 0.05 were considered significant. Data are presented as means and standard deviations (SDs) throughout the study.

4 Results

4.1 Body weight

Body weight of male mice transgenic for mIGFBP-2 (B), bGH (G), or for both
transgenes (GB), and of non-transgenic littermates (C) was recorded in 28 animals at
38 days of age (n=7 per genetic group) and in 28 animals at 75 days of age (C: n=6;
B: n=8; G: n=7; GB: n=7).

In both 38- and 75-day-old B *vs*. C mice, the body weight was significantly decreased
by 18% and 15%, respectively (Fig. 4.1). In contrast, the body weight of G mice was
increased by 29% (p<0.001) at 38 days of age and by 76% (p<0.001) at 75 days of
age, as compared to that of non-transgenic littermates.
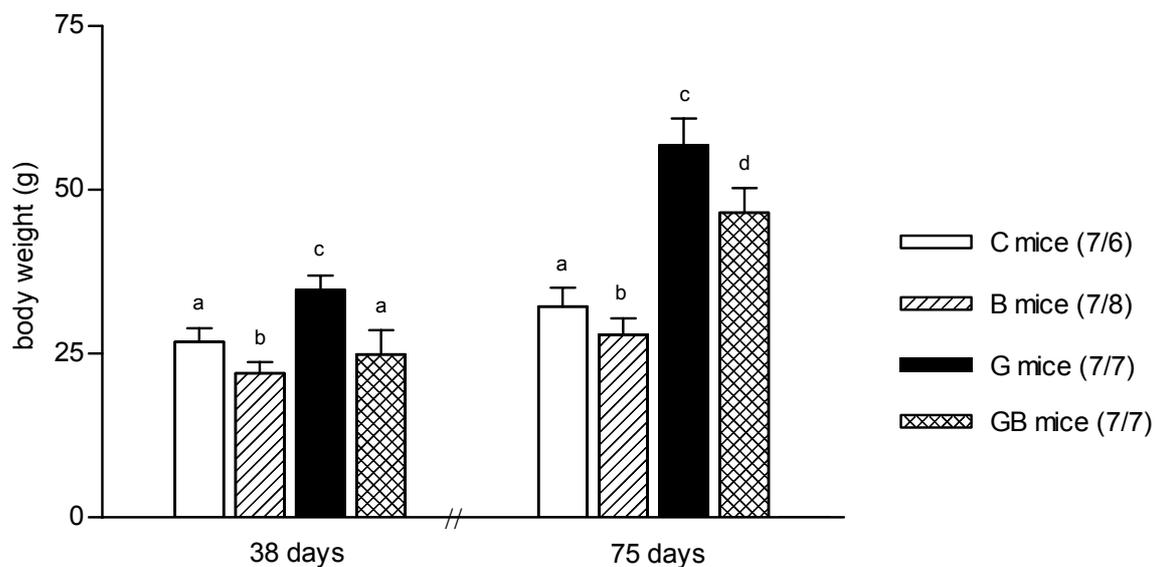
Figure 4.1 Body weights of mice of the four different genetic groups. At both ages
investigated, the body weight of G mice was markedly increased, compared to that of non-transgenic
littermates. GB *vs*. G mice demonstrated a markedly reduced body weight, which in the 38-day-old
group even was reduced as a tendency compared to C mice. (n/n): number of mice investigated at an
age of 38 and 75 days, respectively. The data are shown as means and SDs. Significant differences
(at least p<0.05) between the genetic groups are indicated by different superscripts (a, b, c, d).

In GB *vs*. G mice, the body weight was significantly decreased at both ages investigated. In the 38-day-old group, the body weight of GB mice was even slightly lower than that of non-transgenic controls. Thus, the body growth stimulation seen in G mice was completely abolished in 38-day-old GB mice. Regarded from the other side, as GB *vs*. B mice exhibited a significantly higher body weight, the growth inhibiting effect observed in B mice was reduced in 38-day-old GB mice.

At 75 days of age, the body weight of GB mice ranged at an intermediate stage between those of G and C mice, being significantly different from both.

In both age groups, GB *vs*. G mice demonstrated a more pronounced relative growth inhibiting effect than B *vs*. C mice (B *vs*. C mice: -18% (38 d), -13% (75 d); GB *vs*. G mice: -28% (38 d), -18% (75 d)). The absolute reduction of body weight between B and C mice and between GB and G mice was virtually constant at both ages investigated (B *vs*. C mice: -4.8 g (38 d), -4.3 g (75 d); GB *vs*. G mice: -9.8 g (38 d), -10.3 g (75 d)).

4.2 Serum IGFBP-2 and IGF-I concentrations

Serum concentrations of IGFBP-2 and IGF-I were determined in 44 mice at 38 days of age (n=11 per genetic group) and in 44 mice at 75 days of age (C: n=10; B: n=128; G: n=11; GB: n=11).

The serum IGFBP-2 levels of 38-day-old B and GB *vs*. C mice were about 2-fold increased (p<0.001; Fig. 4.2). In the 75-day-old group, the serum IGFBP-2 levels of B and GB mice displayed a 2.8-fold and 2.6-fold increase (p<0.001), respectively, compared to these of non-transgenic littermates. The findings demonstrate similarly elevated serum IGFBP-2 levels in both IGFBP-2 overexpressing groups.

In G mice, the serum levels of endogenous IGFBP-2 were reduced to about one fifth in the 38-day-old group (p<0.001) and to about one third in the 75-day-old group (p<0.001), compared to these of littermate controls.
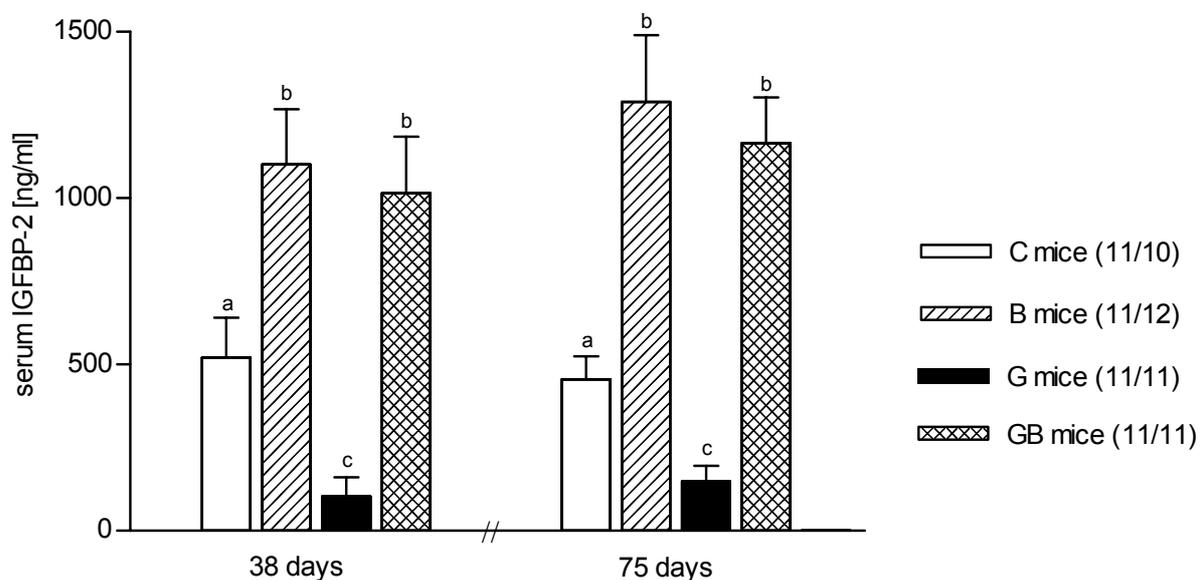
Figure 4.2 Serum IGFBP-2 levels of mice of the four genetic groups. At both ages investigated, B and GB mice exhibited similarly increased serum IGFBP-2 levels, whereas in G mice, the serum level of endogenous IGFBP-2 was significantly reduced, compared to non-transgenic littermate controls. (n/n): number of mice investigated at an age of 38 and 75 days, respectively. The data are shown as means and SDs. Significant differences (at least p<0.05) between the genetic groups are indicated by different superscripts (a, b, c).

The serum IGF-I levels in G and GB *vs*. C and B mice were significantly increased: 38-day-old G and GB *vs*. C mice displayed an approximately 1.7-fold increase, 75-day-old G and GB *vs*. C mice an approximately 2-fold increase in this parameter (Fig. 4.3). Between G and GB mice and between C and B mice, the circulating IGF-I levels were not significantly different at both ages investigated, demonstrating that IGFBP-2 overexpression had no effect on serum IGF-I levels.

Within the four different genetic groups, no significant differences were detected in either serum IGFBP-2 or serum IGF-I levels between the 38- and 75-day-old group.
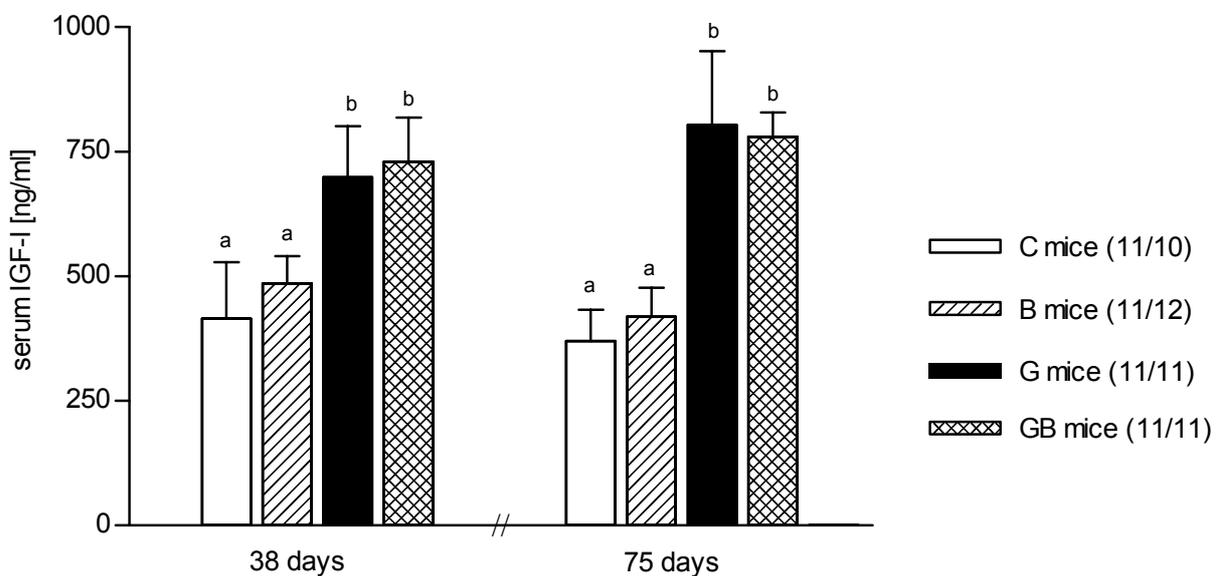
Figure 4.3 Serum IGF-I levels of mice of the four genetic groups. In both G and GB *vs*. C mice, circulating IGF-I levels were elevated to a similar extend in the 38- and 75-day-old group. Between C and B mice, serum IGF-I levels were not significantly different. (n/n): number of mice investigated at an age of 38 and 75 days, respectively. The data are shown as means and SDs. Significant differences (at least $p<0.05$) between the genetic groups are indicated by different superscripts (a, b).

4.3 Clinical-chemical serum parameters

Various clinical-chemical serum parameters were screened in 44 mice at the age of 38 days (n=11 per genetic group) and in 44 mice at the age of 75 days (C: n=10; B: n=12; G: n=11; GB: n=11). The data are summarized in tables 4.1 and 4.2.

The serum sodium concentrations did not significantly differ between the four genetic groups at both ages investigated.

In both age groups, the serum chloride levels did not significantly differ between B and C mice, but were significantly reduced in G and GB vs. corresponding C mice.

In the 38-day-old group, the serum potassium concentrations were slightly reduced in B and GB *vs*. C mice, and were significantly reduced in G *vs*. C mice (-38%). Contrary, at an age of 75 days, B and G *vs*. C mice showed slightly elevated serum potassium levels, and GB mice exhibited significantly increased serum potassium levels (by 36%), as compared to C mice.

The serum calcium levels of both G and GB *vs*. C mice were equally increased by 42% (p<0.001) at an age of 38 days, and by 39% (p<0.001) at an age of 75 days. Between B and C mice, this serum parameter did not significantly differ at both ages investigated.

In the 38-day-old group, the serum phosphate concentrations did not significantly differ between mice of the four genetic groups. Contrary, in the 75-day-old group, the serum phosphate concentrations of B and G *vs*. C mice were slightly elevated, and these of GB *vs*. C mice were significantly elevated.

The serum creatinine levels of C and B mice were comparable at both ages. G *vs*. C mice of both age groups exhibited significantly increased serum creatinine levels. In GB mice, this serum parameter ranged at an intermediate level between those of C and G mice, being not significantly different from both in the 38-day-old group. In the 75-day-old group, the serum creatinine levels of GB *vs*. C mice were significantly elevated, and were significantly reduced, compared to G mice.

The serum urea concentrations did not differ between the four genetic groups at an age of 38 days. In the 75-day-old group, the serum urea concentrations of G and GB *vs*. C mice were reduced by 41 and 37% (p<0.001), respectively. The serum urea concentrations did not differ between 75-day-old C and B mice.

Table 4.1

Parameter	C mice	B mice	G mice	GB mice
	n=11	n=11	n=11	n=11
Sodium [mmol/l]	157.2^a (4.3)	158.1^a (3.2)	155.7^a (4.8)	156.0^a (3.2)
Chloride [mmol/l]	113.5^a (3.3)	114.5^a (2.0)	108.5^b (3.4)	109.8^b (3.2)
Potassium [mmol/l]	7.8^a (2.0)	6.0^{ab} (2.3)	4.8^b (0.7)	5.6^{ab} (2.1)
Calcium [mmol/l]	1.9^a (0.2)	2.1^a (0.3)	2.7^b (0.1)	2.7^b (0.1)
Phosphate [mmol/l]	2.8^a (0.4)	2.7^a (0.3)	2.8^a (0,4)	3.0^a (0.3)
Creatinine [mg/dl]	0.29^a (0.04)	0.31^{ab} (0.03)	0.36^c (0.02)	0.34^{bc} (0.04)
Urea [mg/dl]	41.5^a (5.8)	45.6^a (12.2)	44.5^a (10.8)	46.9^a (8.9)
Total protein [g/dl]	5.5^a (0.5)	5.6^a (0.3)	6.6^b (0.2)	7.0^c (0.3)
Cholesterol [mg/dl]	111.7^a (16.0)	127.8^a (13.7)	181.2^b (21.8)	185.3^b (15.6)
Triglyceride [mg/dl]	179.7^a (105.9)	176.0^a (71.3)	159.0^a (36.5)	206.3^a (75.4)

Table 4.1 Clinical-chemical serum parameters of 38-day-old mice of the four different genetic groups. n: number of mice analyzed per genetic group. The data are shown as means and (SDs). Significant differences (at least $p<0.05$) between the genetic groups are indicated by different superscripts (a, b, c).

The total serum protein concentrations were significantly elevated to a similar extend in both G and GB mice at 38 and 75 days of age, as compared to C mice, but were not different in B *vs*. C mice.

Likewise, the serum cholesterol levels were similarly increased in 38- and 75-day-old G and GB *vs*. C mice ($p<0.001$). The serum cholesterol concentrations did not differ between C and B mice of both ages.

The serum triglyceride concentrations of mice of the four genetic groups were not significantly different at the age of 38 days. In the 75-day-old group, the serum triglyceride levels of G *vs*. C mice were reduced ($p<0.02$), whereas these of B and GB mice were not significantly different from that of controls.

Table 4.2

Parameter	C mice n=10		B mice n=12		G mice n=11		GB mice n=11	
Sodium [mmol/l]	161.0^a	(1.9)	155.7^a	(12.1)	156.9^a	(5.4)	154.3^a	(6.4)
Chloride [mmol/l]	116.8^a	(1.6)	114.1^a	(7.0)	108.6^b	(2.0)	109.5^b	(3.8)
Potassium [mmol/l]	6.9^a	(2.2)	8.0^{ab}	(2.0)	8.0^{ab}	(1.9)	9.4^b	(1.6)
Calcium [mmol/l]	1.8^a	(0.3)	1.9^a	(0.3)	2.5^b	(0.4)	2.5^b	(0.4)
Phosphate [mmol/l]	2.3^a	(0.3)	2.6^{ab}	(0.4)	2.8^{ab}	(0,6)	3.0^b	(0.6)
Creatinine [mg/dl]	0.28^{ab}	(0.05)	0.25^a	(0.08)	0.43^c	(0.05)	0.34^b	(0.07)
Urea [mg/dl]	54.1^a	(6.6)	48.9^a	(9.4)	31.9^b	(12.5)	34.2^b	(6.1)
Total protein [g/dl]	5.6^a	(0.3)	5.9^a	(0.7)	7.1^b	(0.4)	6.7^b	(0.4)
Cholesterol [mg/dl]	112.0^a	(22.4)	125.9^a	(17.2)	168.5^b	(28.2)	188.8^b	(12.3)
Triglyceride [mg/dl]	184.0^a	(34.6)	165.6^{ab}	(35.4)	142.5^b	(21.5)	178.5^{ab}	(42.3)

Table 4.2 Clinical-chemical serum parameters of 75-day-old mice of the four different genetic groups. n: number of mice analyzed per genetic group. The data are shown as means and (SDs). Significant differences (at least $p<0.05$) between the genetic groups are indicated by different superscripts (a, b, c).

4.4 Data of the adrenal gland

Parts of the findings of the adrenal gland have recently been published (Hoeflich, A., Weber, M. M., Fisch, T., Nedbal, S., Fottner, C., Elmlinger, M. W., Wanke, R. & Wolf, E. Insulin-like growth factor binding protein 2 (IGFBP-2) separates hypertrophic and hyperplastic effects of growth hormone (GH)/IGF-I excess on adrenocortical cells in vivo. FASEB J., 16, 1721-31 (2002)).

The perfusion fixed adrenal glands of 12 mice (n=3 per genetic group) at 75 days of age were investigated.

4.4.1 Weight of the adrenal gland

G and GB mice exhibited a markedly increased adrenal gland weight (by 68% and 32%, respectively; $p < 0.001$), compared to non-transgenic controls (Fig. 4.3). In B *vs*. C mice, this parameter was only reduced as a tendency (by 15%, $p = 0.111$), whereas in GB *vs*. G mice the adrenal gland weight was markedly reduced by 22% ($p < 0.001$).
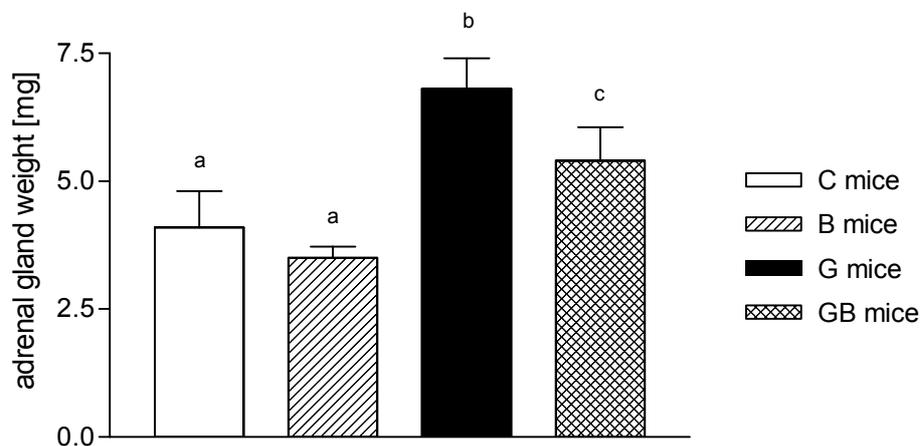
Fig. 4.3 Adrenal gland weight from 75-day-old mice of the four different genetic groups. The demonstrated weight of the adrenal glands represents the sum of the weights of right and left adrenal gland per animal. n=3 mice were analyzed per geneic group. The data are shown as means and SDs. Significant differences (at least $p < 0.05$) between the genetic groups are indicated by different superscripts (a, b, c).

The adrenal gland-to-body weight-ratio (relative adrenal gland weight) ranged between 1.13 ± 0.10 x 10^{-4} and 1.17 ± 0.09 x 10^{-4} and did not significantly differ between the genetic groups (data not shown).

4.4.2 Volume fractions and volumes of the adrenal cortex and medulla

The volume fractions of the adrenal cortex ($V_{V(cortex/adrenal\ gland)}$) and medulla ($V_{V(medulla/adrenal\ gland)}$) ranged from 81% to 85% and from 19% to 15%, respectively, and did not differ significantly between the four genetic groups (data not shown).

The volume of the adrenal cortex ($V_{(cortex,\ adrenal\ gland)}$) of G and GB *vs*. C mice was 2-fold and 1.7-fold (p<0.001) increased, respectively (Fig. 4.5 *a*). The adrenocortical volume of GB mice was significantly decreased (by 18%), compared to G mice, ranging at an intermediate level between those of G and C mice. Likewise, the adrenocortical volume was reduced by 25% in B *vs*. C mice (p<0.01).

The volume of the adrenal medulla ($V_{(medulla,\ adrenal\ gland)}$) of G mice was 1.7-fold (p<0.01) larger, as compared to that of C mice (Fig. 4.5 *b*). In GB mice, the adrenomedullary volume was significantly reduced (-26%), compared to G mice, reaching the level of non-transgenic controls. Between B and C mice, this parameter was not significantly different.

The data show that GH excess stimulates growth of the adrenal cortex and medulla implicating that both contribute to adrenal enlargement in bGH transgenic mice. Similarly, both compartments are affected by IGFBP-2 overexpression. Representative sections of adrenal glands from the different groups are shown in figure 4.5 *c*.
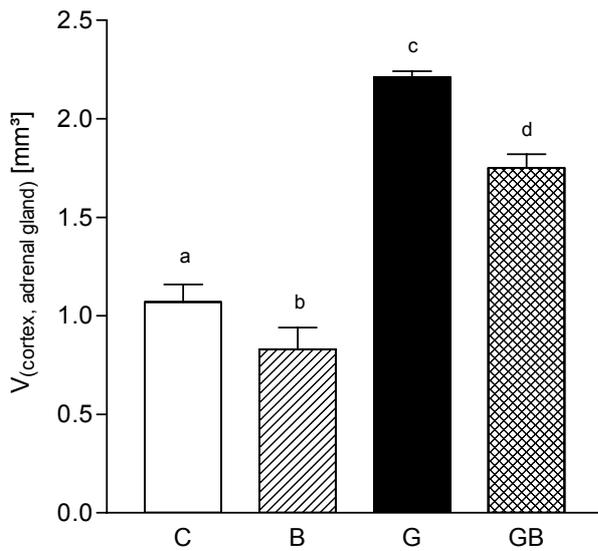
Fig. 4.5 *a*
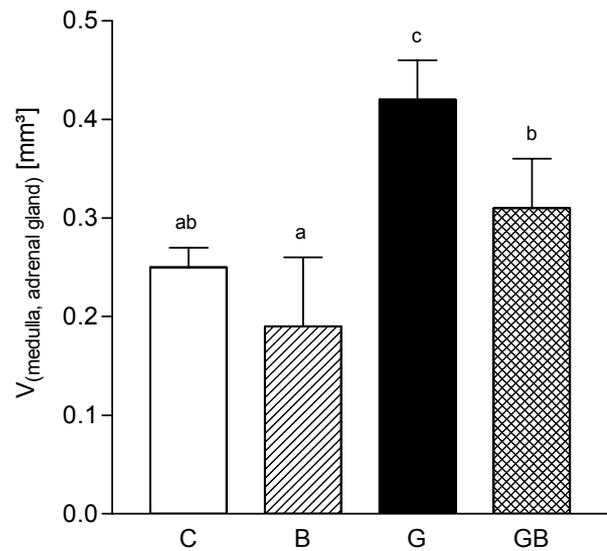
Fig. 4.5 *b*

C   B   G   GB
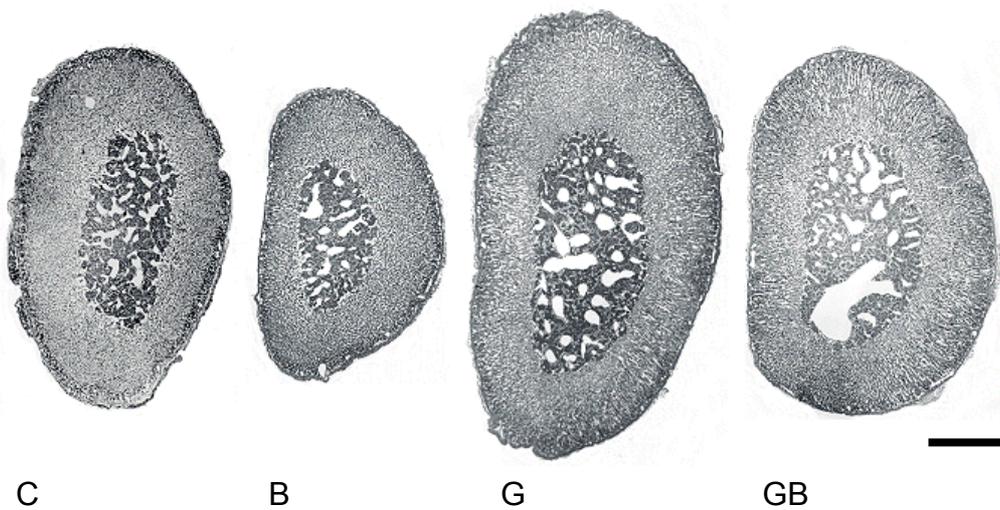
Fig. 4.5 *c*

Figure 4.5 Volumes of the adrenal cortex (*a*) and medulla (*b*). Both the adrenal cortex and medulla are enlarged by bGH expression and contribute to adrenal enlargement in bGH transgenic mice. Likewise, the volumes of both adrenocortex and -medulla are reduced by IGFBP-2 overexpression. The left, perfusion fixed adrenal glands of n=3 mice per genetic group were investigated. The data are shown as means and SDs. Significant differences (at least $p<0.05$) between the genetic groups are indicated by different superscripts (a, b, c, d).

(*c*) Representative histological sections of the adrenal gland from mice of the four different genetic groups. H&E stained paraffin sections; identical magnification; bar = 0.5 mm

4.4.3 Volume fractions and volumes of the zona fasciculata and zona glomerulosa

The volume fractions of the zona fasciculata ($V_{V(zona\ fasc./cortex)}$) and zona glomerulosa ($V_{V(zona\ glom./cortex)}$) ranged from 70.4 to 71.4% and from 28.6 to 29.6%, respectively, and did not significantly differ between the four genetic groups (data not shown).

The volume of the zona fasciculata ($V_{(zona\ fasc.,\ cortex)}$) was markedly increased in G *vs*. C mice (by 115%; $p<0.001$). $V_{(zona\ fasc.,\ cortex)}$ was slightly reduced in B *vs*. C mice, whereas in GB *vs*. G mice, the volume of the zona fasciculata was significantly lowered by 24%, ranging at an intermediate level between that of G and C mice (Fig. 4.6 *a*).
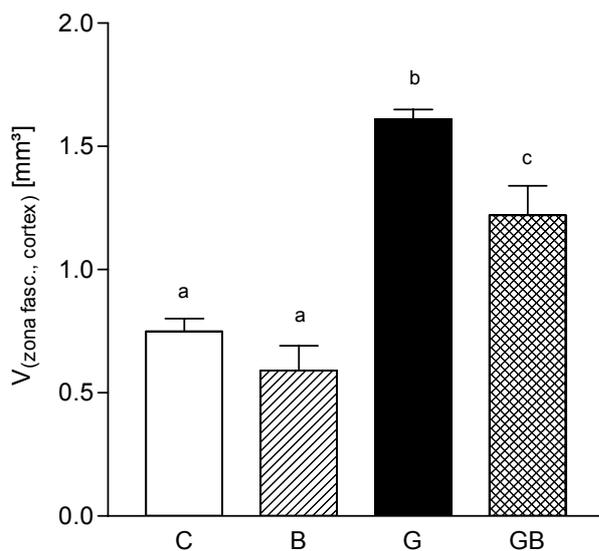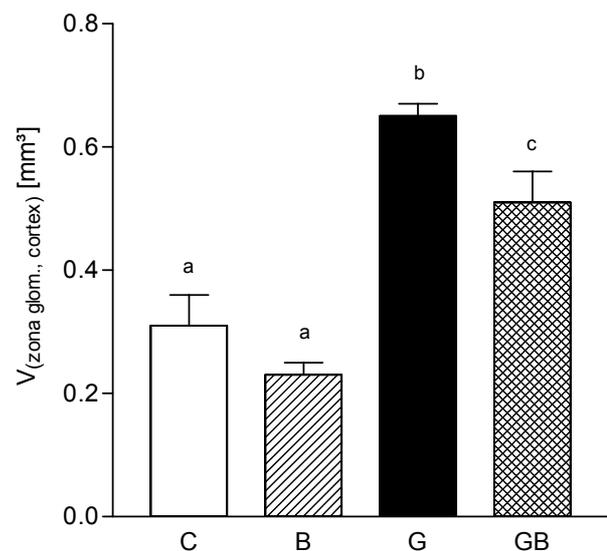
Fig. 4.6 *a*   Fig. 4.6 *b*

Figure 4.6 Volumes of the zona fasciculata (*a*) and zona glomerulosa (*b*). The volumes of both zona fasciculata and zona glomerulosa are markedly increased in G mice, and both parameters are decreased in GB *vs*. G mice and slightly decreased in B *vs*. C mice. The left, perfusion fixed adrenal glands of n=3 mice per genetic group were investigated. The data are shown as means and SDs. Significant differences (at least $p<0.05$) between the genetic groups are indicated by different superscripts (a, b, c).

The volume relations of the zona glomerulosa between the four genetic groups resembled those of the zona fasciculata (Fig. 4.6 *b*). In G and GB mice, the volume of the zona glomerulosa ($V_{(zona\ glom.,\ cortex)}$) was markedly increased, as compared to C and B mice. No significant difference in $V_{(zona\ glom.,\ cortex)}$ was detectable between C and B mice, whereas the reduction in $V_{(zona\ glom.,\ cortex)}$ of GB vs. G mice reached level of statistical significance.

4.4.4 Mean volume and total number of zona fasciculata cells

In G mice, the mean volume of zona fasciculata cells (Fig. 4.7 *a*) was enlarged by 44% ($p<0.005$) and the total number of zona fasciculata cells (Fig. 4.7 *b*) was increased by 50% ($p<0.005$), as compared to non-transgenic controls. Strikingly, in GB mice, the mean zona fasciculata cell volume was similar to that of controls, *i.e*., the bGH-associated zona fasciculata cell hypertrophy was completely abolished, whereas the total number of zona fasciculata cells was elevated, comparable to that of G mice. Thus, a clear-cut effect of IGFBP-2, to inhibit hypertrophy, but not hyperplasia of zona fasciculata cells can be demonstrated in this model. In B *vs*. C mice, no significant difference in either mean volume or total number of zona fasciculata cells was found.

Representative segments of the adrenal cortex from mice of the different genetic groups are shown in figure 4.7 *c*.
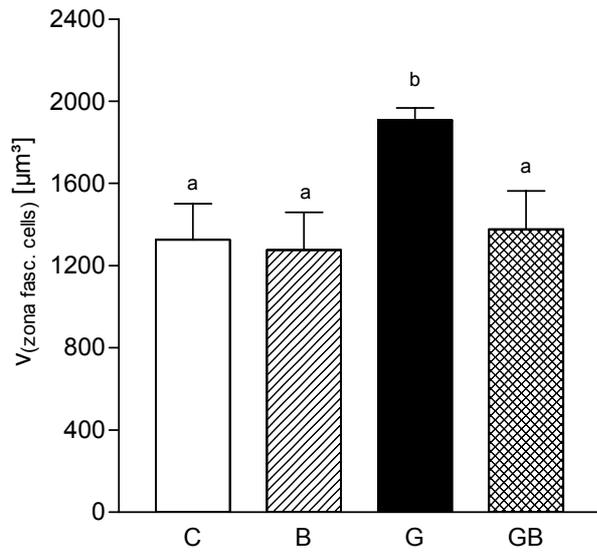
Fig. 4.7 *a*
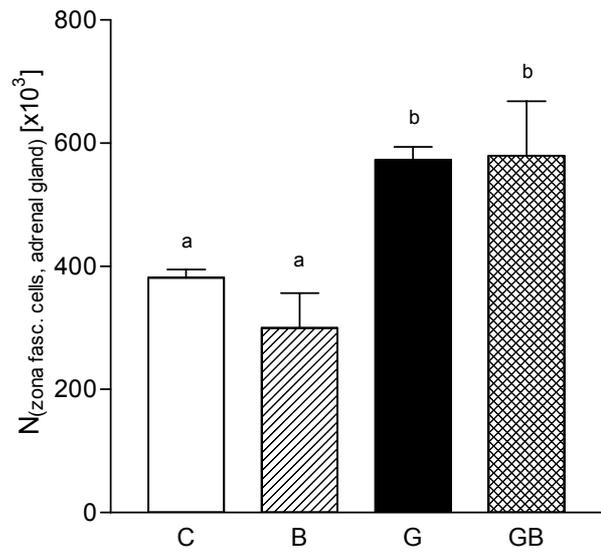
Fig. 4.7 *b*
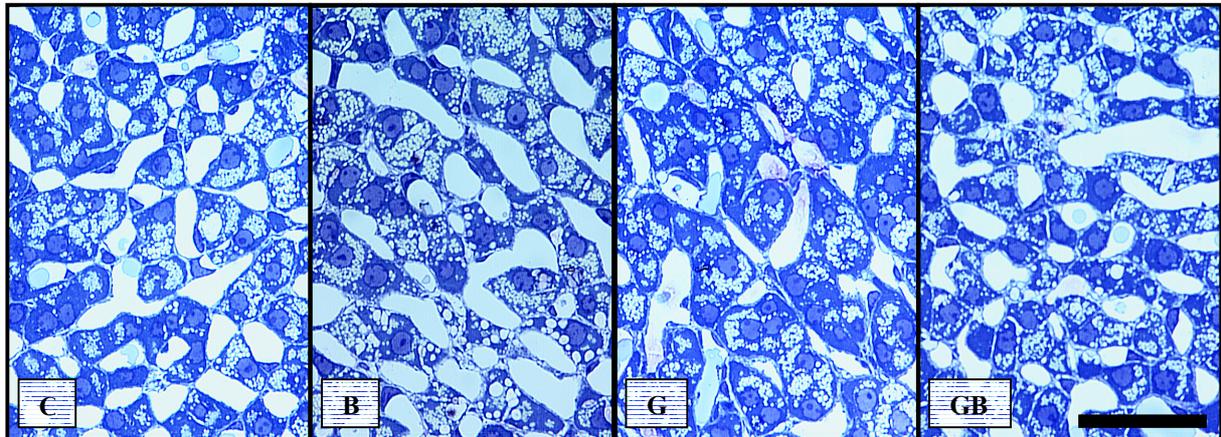
Fig. 4.7 *c*

Figure 4.7 Mean volume (*a*) and total number (*b*) of zona fasciculata cells. G mice exhibited hypertrophy and hyperplasia of zona fasciculata cells. In GB mice, hypertrophy was completely abolished, whereas the hyperplasia of zona fasciculata cells was not affected. The right, perfusion fixed adrenal glands of n=3 mice per genetic group were investigated. The data are shown as means and SDs. Significant differences (at least $p<0.05$) between the genetic groups are indicated by different superscripts (a, b).

(*c*) Representative segments of the zona fasciculata from 75-day-old mice of the four different genetic groups. Semi-thin sections, toluidine blue and safranine stained; bar = 50 µm.

4.4.5 Plasma corticosterone and ACTH levels

Basal and ACTH-induced plasma corticosterone concentrations were measured in 31 mice (C: n=8; B: n=7; G: n=8; GB: n=8) at four months of age.

The basal plasma corticosterone level was more than three-fold increased (P<0.001) in G *vs*. C mice. In contrast, the plasma corticosterone concentration was elevated by only 40% (p=0.117) in GB *vs*. C mice, but was 47% (p<0.001) reduced in GB *vs*. G mice. In B *vs*. C mice, the basal plasma corticosterone level was slightly reduced (by 26%), but the difference between these two groups did not reach level of statistic significance.

The stimulation of corticosterone secretion by ACTH resulted in an approximately three-fold increase of plasma corticosterone levels in every genetic group. Comparable to not stimulated conditions, the stimulated plasma corticosterone level in G *vs*. C mice was three-fold increased (P<0.001), whereas it was significantly lowered in GB *vs*. G mice (by 40%) and slightly reduced in B *vs*. C mice. As described for not stimulated conditions, the stimulated plasma corticosterone concentration of GB mice did not significantly differ from that of controls.
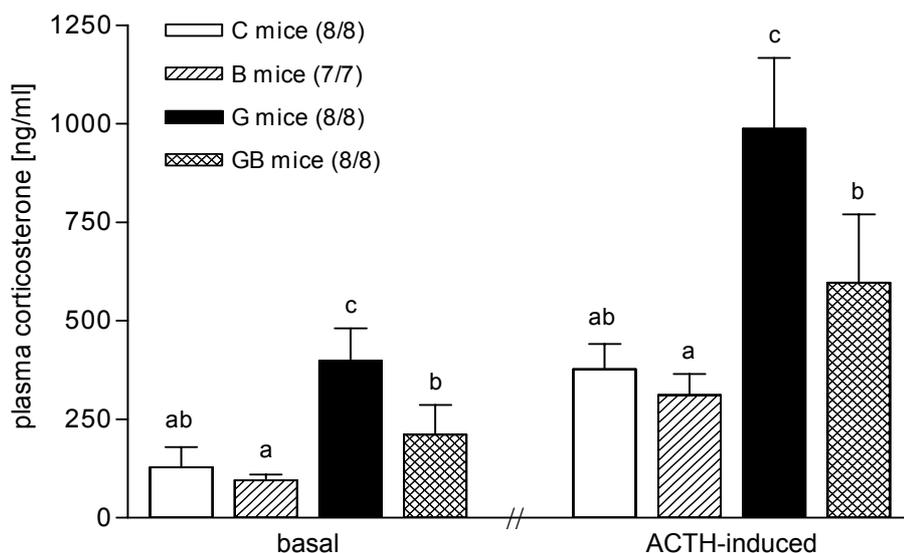

Figure 4.8 Basal and ACTH-induced plasma corticosterone levels. (n/n): number of mice used for basal and ACTH-induced plasma corticosterone levels, respectively. The data are shown as means and SDs. Significant differences (at least p<0.05) between the genetic groups are indicated by different superscripts (a, b, c).

Plasma ACTH levels were determined in the morning in 26 mice (C: n=9; B: n=7; G: n=6; GB: n=4) and in the afternoon in 18 mice (C: n=6; B: n=4; G: n=4; GB: n=4) at four to seven months of age. Additionally, six MT-bGH transgenic mice and six non-transgenic littermate controls were investigated.

The plasma ACTH concentrations were not significantly different between the genetic groups when investigated in the afternoon and were only slightly increased in G and GB *vs.* C and B mice when analyzed in the morning. Only differences between GB *vs.* C and B mice reached level of statistical significance (Fig. 4.9). Plasma ACTH levels of C and B mice were significantly higher in the afternoon than in the morning. This physiological diurnal variation of ACTH secretion was not seen in G and GB mice.

According to the findings in PEPCK-bGH transgenic mice, morning plasma ACTH levels of MT-bGH transgenic mice (91.8 ± 29.0 pg/ml) were not significantly different from these of corresponding controls (74.4 ± 21.1 pg/ml), confirming that GH over-expression does not significantly affect plasma ACTH concentrations.
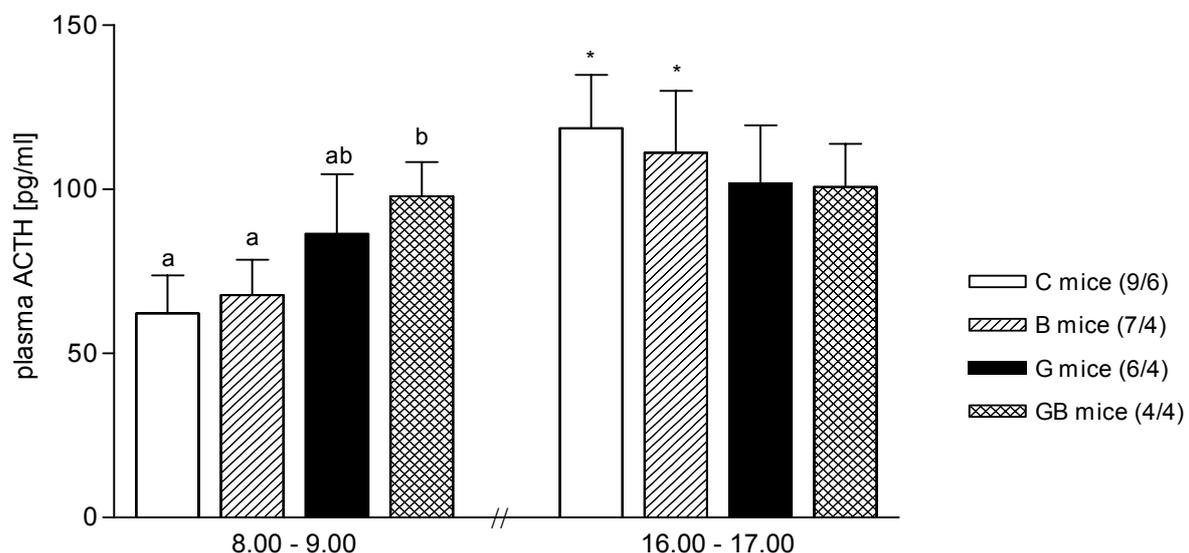

Figure 4.9 Morning and afternoon plasma ACTH levels from mice of the four genetic groups. (n/n): number of animals investigated in the morning and in the afternoon, respectively. The data are shown as means and SDs. Significant differences (at least $p < 0.05$) between the genetic groups are indicated by different superscripts (a, b). Asterisks indicate significant (at least $p < 0.05$) differences between morning and afternoon values within the genetic group.

4.5 Data of the kidneys

4.5.1 Kidney weight

The kidney weight was determined in 28 male mice at 38 days of age (n=7 per genetic group) and in 28 male mice at 75 days of age (C: n=6; B: n=8; G: n=7; GB: n=7) after perfusion fixation.

The kidney weight was markedly increased in 38-day-old G mice (59%; p<0.001) and in 75-day-old G mice (89%; p<0.001), as compared to littermate controls (Fig. 4.10). In 38-day-old GB *vs*. G mice, the kidney weight was reduced to the level of controls (27%; p<0.05). In 75-day-old GB mice, the kidney weight was significantly lower *vs*. G mice, and was significantly higher *vs*. C mice, therefore ranging at an intermediate level between G and C mice.

The kidney weight of B and C mice did not differ at both ages investigated, confirming an effect of IGFBP-2 overexpression on kidney growth in high but not in normal GH/IGF-I conditions.
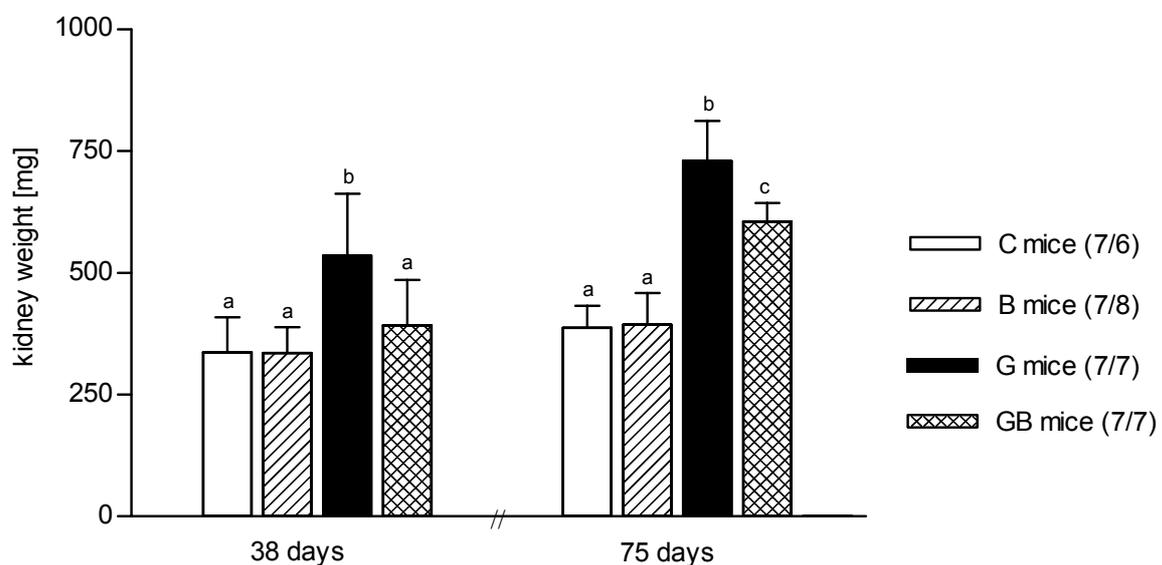

Figure 4.10 Kidney weight of 38- and 75-day-old mice. G *vs*. C mice showed a marked increase in kidney weight. This increase was significantly reduced in GB mice, which were not distinguishable from controls at an age of 38 days. The demonstrated weight of the kidneys represents the sum of the weights of right and left kidney per animal. (n/n): number of mice investigated at an age of 38 and 75 days, respectively. The data are shown as means and SDs. Significant differences (at least p<0.05) between the genetic groups are indicated by different superscripts (a, b, c).

At the age of 38 days, the kidney weight-to-body weight-ratio (relative kidney weight) of the different transgenic mice *vs.* control mice was increased by 24% to 26%, with the differences between G and GB *vs.* C mice being statistically significant (Fig. 4.11). In the 75-day-old group, the relative kidney weight of B *vs.* C mice was significantly elevated (by 18%; p<0.05), but not that of G and GB mice. In 75- *vs.* 38-day-old G and GB mice the relative kidney weight was significantly reduced by 17% and 18%, respectively.
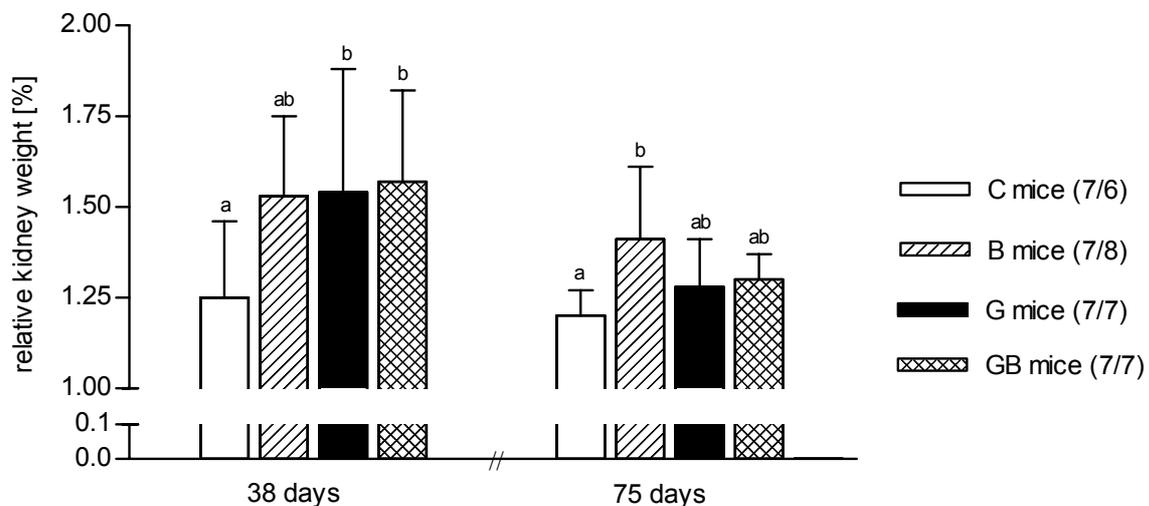
Figure 4.11 Relative kidney weight of 38- and 75-day-old mice. (n/n): number of mice investigated at an age of 38 and 75 days, respectively. The data are shown as means and SDs. Significant differences (at least p<0.05) between the genetic groups are indicated by different superscripts (a, b).

4.5.2 Number of nephrons

The number of nephrons per kidney was determined by analyzing the number of glomeruli in 16 male mice (n=4 per genetic group) at an age of 38 days.

The number of glomeruli in both kidneys per animal was $30.96 \pm 6.09 \times 10^3$ in control mice and was not significantly different compared to that of B mice ($33.96 \pm 3.76 \times 10^3$), G mice ($34.56 \pm 3.08 \times 10^3$), and GB mice ($32.32 \pm 5.80 \times 10^3$). This result excludes effects of expression of the bGH and/or the IGFBP-2 transgene on nephrogenesis.

4.5.3 Fractional volumes and volumes of the renal zones

The fractional volumes and volumes of the renal zones - cortex, outer stripe of medulla (OSM), and inner stripe of medulla together with the inner zone of medulla (ISM/IZM) - were determined in 20 mice (n=5 per genetic group) at an age of 38 days and in 20 mice (n=5 per genetic group) at an age of 75 days.

The volume fractions of the various renal zones did not significantly differ between 38- and 75-day-old C mice (Tables 4.3, 4.4).

In the 38-day-old group, the fractional cortex volume of B and GB *vs*. C and G mice was significantly reduced (Table 4.3). Contrary, the fractional volume of the OSM was slightly increased in B and GB *vs*. C and G mice; the differences between B *vs*. C and G mice reached level of statistical significance. G mice at 38 days of age exhibited no significant changes in the fractional volumes of the renal zones investigated, compared to C mice. No significant difference was detectable in the fractional volume of the ISM/IZM between controls and the different transgenic mice at an age of 38 days.

Table 4.3

genetic group	cortex [%]	OSM [%]	ISM/IZM [%]
C mice (n=5)	70.09^a (1.89)	18.06^a (1.52)	11.85^{ab} (0.65)
B mice (n=5)	67.23^b (1.80)	20.48^{bc} (0.79)	12.29^{ab} (1.34)
G mice (n=5)	70.91^a (1.09)	17.94^a (1.39)	11.15^a (0.41)
GB mice (n=5)	67.90^b (1.82)	19.32^{ac} (0.80)	12.78^b (1.76)

Table 4.3 Fractional volumes of the renal zones - cortex, outer stripe of medulla (OSM), and inner stripe of medulla together with inner zone of medulla (ISM/IZM) - of 38-day-old mice. n=5 mice were analyzed per genetic group. The data were obtained from the average of both separately investigated kidneys per animal, and are shown as means and (SDs). Significant differences (at least $p<0.05$) between the genetic groups are indicated by different superscripts (a, b, c).

At an age of 75 days, controls and the various transgenic mice exhibited a similar fractional cortex volume (Table 4.4). The fractional volume of the OSM was slightly increased in 75-day-old transgenic mice *vs.* C mice; the differences between GB and C mice reached level of statistical significance. Contrary, the fractional volume of the ISM/IZM was significantly decreased in 75-day-old transgenic *vs.* control mice.

Table 4.4

group	cortex [%]	OSM [%]	ISM/IZM [%]
C mice (n=5)	69.76^a (1.25)	19.06^a (0.99)	11.18^a (1.28)
B mice (n=5)	70.01^a (0.74)	20.09^{ab} (0.87)	9.90^b (0.22)
G mice (n=5)	70.57^a (1.30)	20.32^{ab} (1.70)	8.85^b (0.92)
GB mice (n=5)	69.57^a (0.96)	21.12^b (0.85)	9.74^b (0.74)

Table 4.4 Fractional volumes of the renal zones cortex, outer stripe of medulla (OSM), and inner stripe of medulla together with inner zone of medulla (ISM/IZM) of 75-day-old mice. n=5 mice were analyzed per genetic group. The data were obtained from the average of both separately investigated kidneys per animal, and are shown as means and (SDs). Significant differences (at least $p<0.05$) between the genetic groups are indicated by different superscripts (a, b, c).

The absolute volumes of the various renal zones were similar in 38- and 75-day-old C mice (Figs. 4.12, 4.13). The volumes of the various renal zones investigated were equal comparing B and C mice at both ages.

In both age groups, G mice exhibited a marked increase in the volumes of all three renal zones investigated, compared to littermate controls. In G mice, the cortex and the OSM demonstrated the largest relative and absolute volume increase of the renal zones investigated. In 38-day-old G *vs*. C mice, the volumes of cortex and OSM were increased by 53% and 51% (p<0.01), respectively. In the 75-day-old group, the increase of cortex and OSM volume in G *vs*. C mice was 90% (p<0.001) and 101% (p<0.001), respectively. The ISM/IZM relatively and absolutely contributed the least to the renal enlargement of GH transgenic mice.

In 38-day-old GB mice, the volumes of all renal zones investigated were on the level of non-transgenic controls, *i.e.*, the growth stimulation observed in G mice was completely abolished in GB mice overexpressing both bGH and IGFBP-2. The reduction in cortex volume in 38-day-old GB *vs*. G mice was 31% (p<0.01) and in OSM volume was 22% (p<0.05). The reduction was lowest in the ISM/IZM volume (18%) and reached only borderline significance (p=0.055).

In the 75- *vs*. 38-day-old group, the relative growth inhibition of the single renal zones in GB *vs*. G mice was reduced. The cortex was the most markedly reduced renal zone in 75-day-old GB *vs*. G mice (-18%; p<0.01), whereas the volumes of OSM and ISM/IZM were only slightly decreased.

Interestingly, despite the less reduction of the relative volumes of every renal zone in 75-day-old GB *vs*. G mice compared to 38-day-old GB *vs*. G mice, the volume reductions in absolute numbers remained virtually constant.
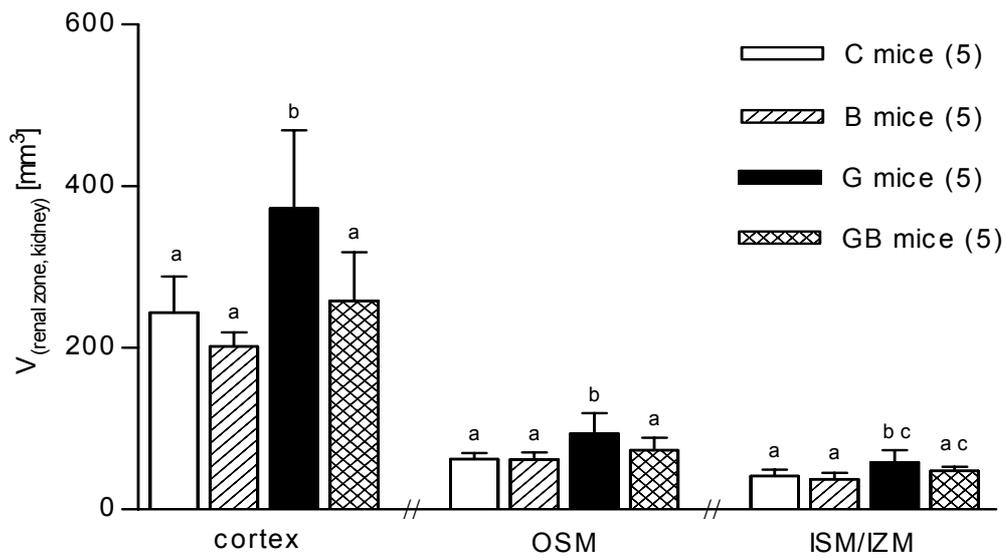
Figure 4.12 Volumes of renal the zones - cortex, outer stripe of medulla (OSM), and inner stripe of medulla together with inner zone of medulla (ISM/IZM) - of 38-day-old mice. (n): number of mice analyzed. The data are presented as the sum of both separately investigated kidneys per mouse, and are shown as means and SDs. Significant differences (at least $p < 0.05$) between the genetic groups are indicated by different superscripts (a, b, c).
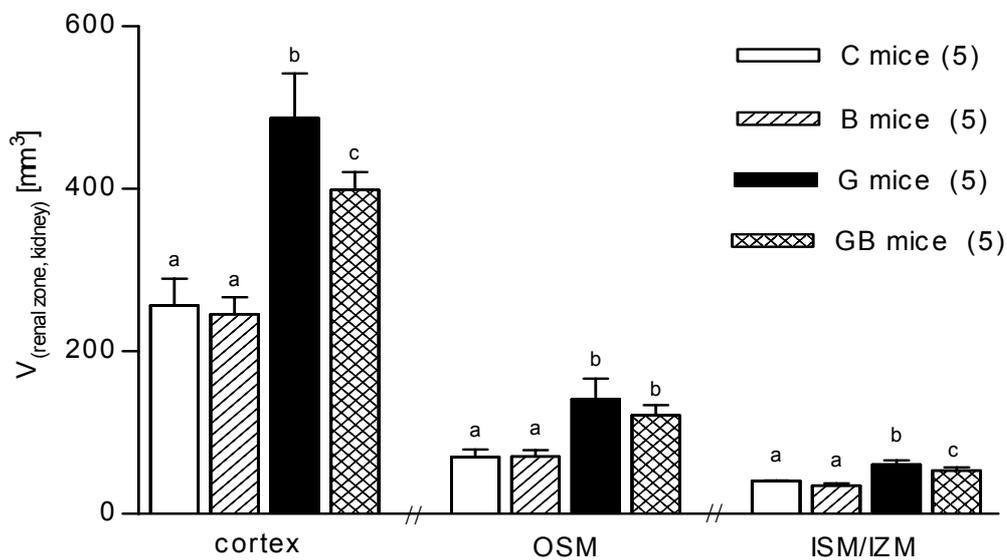

Figure 4.13 Volumes of renal the zones - cortex, outer stripe of medulla (OSM), and inner stripe of medulla together with inner zone of medulla (ISM/IZM) - of 75-day-old mice. (n): number of mice analyzed. The data are presented as the sum of both separately investigated kidneys per mouse, and are shown as means and SDs. Significant differences (at least $p < 0.05$) between the genetic groups are indicated by different superscripts (a, b, c).

4.5.4 Volume fractions and volumes of nephron segments

The fractional volumes and volumes of single nephron segments in the cortex and OSM were determined, namely that of the proximal tubular epithelium (PTE), that of all other tubular epithelia (OTE), and that of miscellaneous structures (MIS), like glomeruli, interstitium, and blood vessels. The kidneys from 20 mice (n=5 per genetic group) at an age of 38 days and 20 mice (n=5 per genetic group) at an age of 75 days were analyzed.

Between C and G mice of both age groups, the fractional volumes of the nephron segments investigated were not significantly different (Tables 4.5, 4.6). In the 38-day-old group, the fractional volume of the PTE in the cortex and OSM ($V_{V(PTE/cortex\&OSM)}$) in B and GB *vs*. C and G mice was reduced, whereas the fractional OTE volume ($V_{V(OTE/cortex\&OSM)}$) in B and GB *vs*. C and G mice was increased. However, only the differences in GB *vs*. C and G mice reached level of statistical significance.

Table 4.5

group	$V_{V(PTE/cortex, OSM)}$ [%]	$V_{V(OTE/cortex, OSM)}$ [%]	$V_{V(MIS/cortex, OSM)}$ [%]
C mice (n=5)	68.5^a (3.0)	22.0^{ab} (2.9)	9.5^a (2.9)
B mice (n=5)	66.3^{ab} (3.5)	24.5^{ac} (2.3)	9.2^a (2.2)
G mice (n=5)	68.6^a (1.9)	20.1^b (1.2)	11.3^a (1.6)
GB mice (n=5)	63.0^b (3.8)	25.6^c (3.7)	11.4^a (3.0)

Table 4.5 Fractional volume of nephron segments in the cortex and the outer stripe of medulla (OSM) of 38-day-old mice. PTE, proximal tubular epithelium; OTE, other tubular epithelia; MIS, miscellaneous structures, like glomeruli, interstitium, and blood vessels. n=5 mice were analyzed per genetic group. The data are presented as the average of both separately investigated kidneys per animal, and are shown as means and (SDs). Significant differences (at least p<0.05) between the genetic groups are indicated by different superscripts (a, b, c).

The results concerning $V_{V(PTE/cortex\&OSM)}$ and $V_{V(OTE/cortex\&OSM)}$ in 75-day-old mice resembled those in 38-day-old mice (Tab. 4.6). In the 75-day-group, $V_{V(PTE/cortex\&OSM)}$ was significantly reduced in both B and GB *vs.* C and G mice, respectively. $V_{V(OTE/cortex\&OSM)}$ in B and GB *vs.* C and G mice were increased, with the differences in B and GB *vs.* G mice being statistically significant.

No significant differences were found in the fractional MIS volume ($V_{V(MIS/cortex, OSM)}$) between the genetic groups at 38 and 75 days of age.

Table 4.6

group	$V_{V(PTE/cortex, OSM)}$ [%]	$V_{V(OTE/cortex, OSM)}$ [%]	$V_{V(MIS/cortex, OSM)}$ [%]
C mice (n=5)	72.2^a (2.8)	18.8^{ab} (1.6)	9.1^a (1.5)
B mice (n=5)	67.6^b (3.0)	21.3^a (2.7)	11.1^a (1.8)
G mice (n=5)	74.2^a (3.6)	16.3^b (2.9)	9.5^a (1.6)
GB mice (n=5)	68.0^b (2.9)	20.6^a (1.5)	11.4^a (3.1)

Table 4.6 Fractional volume of nephron segments in the cortex and the outer stripe of medulla (OSM) of 75-day-old mice. PTE, proximal tubular epithelium; OTE, other tubular epithelia; MIS, miscellaneous structures, like glomeruli, interstitium, and blood vessels. n=5 mice were analyzed per genetic group. The data are presented as the average of both separately investigated kidneys per animal, and are shown as means and (SDs). Significant differences (at least $p<0.05$) between the genetic groups are indicated by different superscripts (a, b).

The absolute volume the various nephron segments investigated in the cortex and OSM, namely that of the PTE ($V_{(PTE, cortex\&OSM)}$), that of the OTE ($V_{(OTE, cortex\&OSM)}$), and that of the MIS ($V_{(MIS, cortex\&OSM)}$) was markedly enlarged in G *vs.* C mice of both age groups (Figs. 4.14, 4.15). In G *vs.* C mice, the PTE demonstrated the greatest relative and absolute volume increase of all nephron segments investigated: the relative increase in $V_{(PTE, cortex\&OSM)}$ ranged from 41% ($p<0.001$) in the 38-day-group to 102% ($p<0.001$) in the 75-day-group.

$V_{(PTE,\ cortex\&OSM)}$ of GB mice at 38 days of age was equal to that of non-transgenic controls, *i.e.*, the growth stimulatory effect on the PTE observed in G mice was completely abolished in GB mice overexpressing both bGH and IGFBP-2. The volumes of the OTE and MIS in the cortex and OSM in GB *vs*. G mice were also reduced to control levels, with the reduction in $V_{(OTE,\ cortex\ \&\ OSM)}$ reaching not the level of statistical significance.

In 75-day-old GB *vs*. G mice, the $V_{(PTE,\ cortex\&OSM)}$ was potently reduced, however, $V_{(PTE,\ cortex\&OSM)}$ of GB mice did not reach the level of controls. Interestingly, the degree of reduction of $V_{(PTE,\ cortex\&OSM)}$ in GB *vs*. G mice in the 38-day-old group (30%; $p<0.001$) was identical to that in 75-day-old mice (30%; $p<0.001$). Contrary, $V_{(OTE,\ cortex\&OSM)}$ and $V_{(MIS,\ cortex\&OSM)}$ of 75-day-old GB *vs*. G mice were not significantly different.
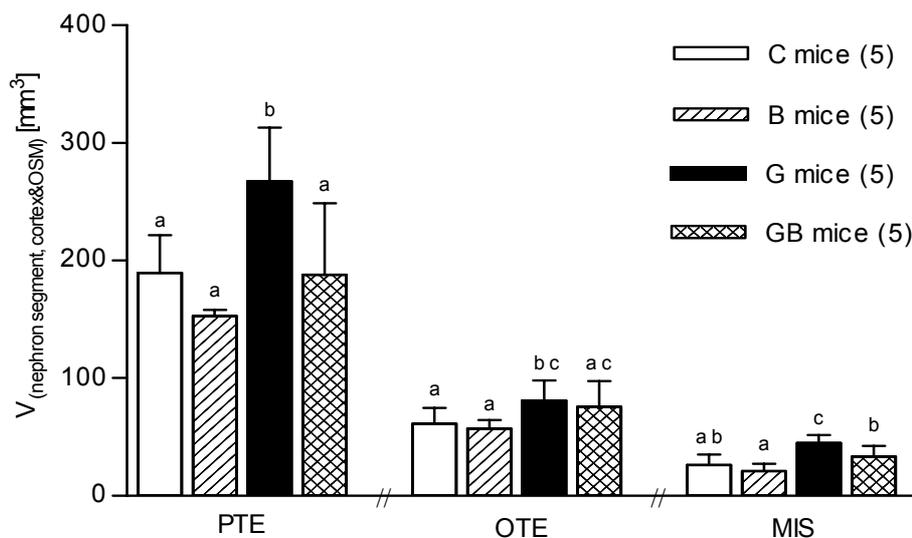

Figure 4.14 Volumes of nephron segments in the cortex and the outer stripe of medulla (OSM) of 38-day-old mice. PTE, proximal tubular epithelium; OTE, other tubular epithelia; MIS, miscellaneous structures, like glomeruli, interstitium, and blood vessels. (n): number of mice analyzed. The data are presented as the sum of both separately investigated kidneys per animal, and are shown as means and SDs. Significant differences (at least $p<0.05$) between the genetic groups are indicated by different superscripts (a, b, c).

These data demonstrate that the increase in $V_{(PTE, cortex \& OSM)}$ in G *vs*. C mice contributes most to the enlargement of renal cortex and OSM, and thereby to the enlargement of the kidney of bGH transgenic mice. Further, as demonstrated in the 75-day-old group, the growth inhibitory effect in the renal cortex and OSM in GB *vs*. G mice is referred exclusively to the proximal tubular epithelium but does not affect other tubular segments.

$V_{(PTE, cortex \& OSM)}$ of B *vs*. C mice were reduced as a tendency in both the 38- (-19%) and 75-day-group (-13%), whereas the volumes of the OTE and MIS in the renal cortex and OSM were virtually identical between B and C mice at both ages investigated.
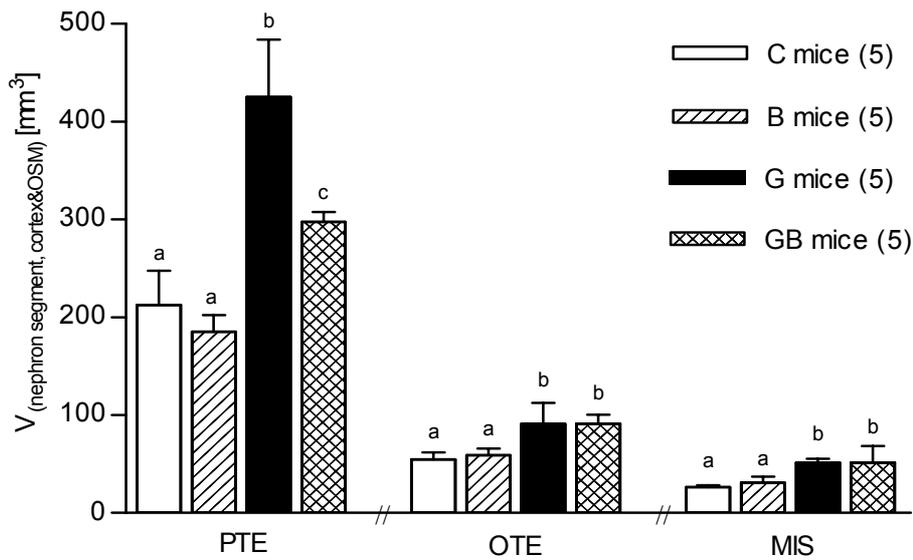

Figure 4.15 Volumes of nephron segments in the cortex and the outer stripe of medulla (OSM) of 75-day-old mice. PTE, proximal tubular epithelium; OTE, other tubular epithelia; MIS, miscellaneous structures, like glomeruli, interstitium, and blood vessels. (n): number of mice analyzed. The data are presented as the sum of both separately investigated kidneys per animal, and are shown as means and SDs. Significant differences (at least $p<0.05$) between the genetic groups are indicated by different superscripts (a, b, c).

4.5.5 Mean volume and total number of PTE cells in the renal cortex

The mean volume ($v_{(PTE\ cells)}$) and the total number of PTE cells ($N_{(PTE\ cells,\ cortex)}$) in the renal cortex was determined in 16 male mice (n=4 per genetic group) at an age of 75 days.

The mean volume of proximal tubular epithelial cells in the cortex did not differ between the four genetic groups (Fig. 4.16 *a*).

In contrast, the total number of cortical PTE cells was nearly doubled (increased by 90%, p<0.001) in G *vs*. C mice (Fig. 4.16 *b*) suggesting that the increase in $V_{(PTE,\ cortex\&OSM)}$ of G mice was exclusively due to PTE cell hyperplasia, but not to PTE cell hypertrophy. In GB *vs*. G mice, the total cortical PTE cell number was markedly reduced by 18% (p<0.005), ranging at an intermediate level between those of G and C mice. The total PTE cell number in B *vs*. C mice was not different.
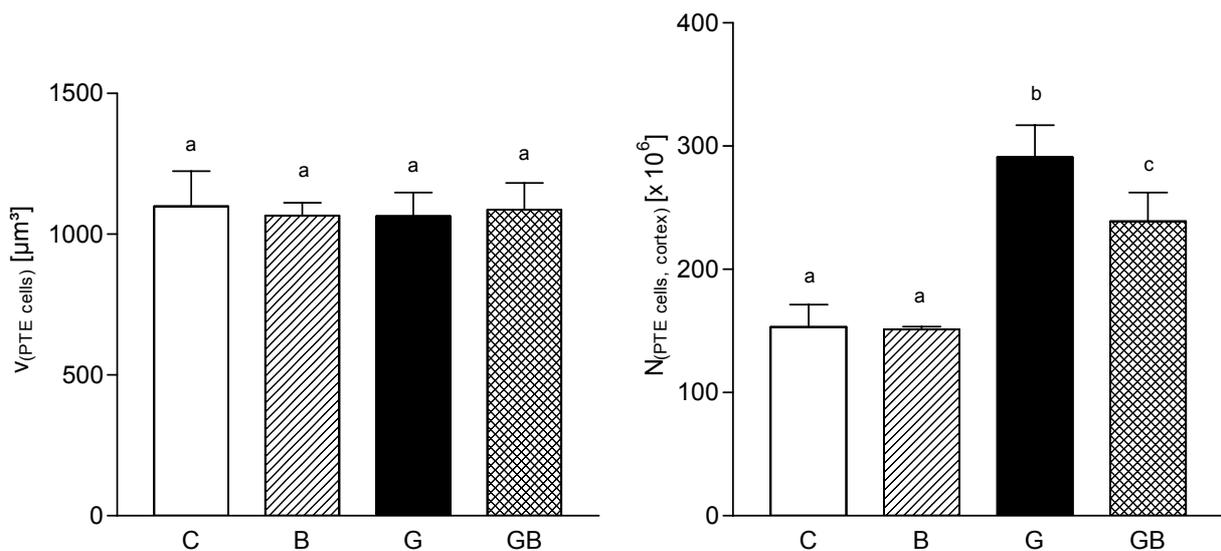

Figure 4.16 *a*   Figure 4.16 *b*

Figure 4.16 Mean volume (*a*) and total number (*b*) of proximal tubular epithelial (PTE) cells. The mean volume of PTE cells did not differ between the four genetic groups. G mice displayed a significant increase in total PTE cell number, which was significantly reduced in GB *vs*. G mice. n=4 animals were investigated per genetic group. The total PTE cell number is the sum of the PTE cell number of both separately investigated kidneys per animal. The data are shown as means and SDs. Significant differences (at least p<0.05) between the genetic groups are indicated by different superscripts (a, b, c, d).

4.5.6 Mean glomerular volume

The mean glomerular volume ($v_{(glom)}$) was determined in 20 mice at 38 days of age (n=5 per genetic group) and in 20 mice at 75 days of age (n=5 per genetic group).

The mean glomerular volume in G and GB *vs*. C mice of both the 38-day-group and the 75-day-group was dramatically increased (Fig. 4.17). bGH transgenic mice exhibited an increase in $v_{(glom)}$ by 82% (p<0.001) at an age of 38 days and by 163% (p<0.001) at an age of 75 days, as compared to littermate controls.

In GB *vs*. G mice, $v_{(glom)}$ was only slightly reduced by 11% (p<0.05) in the 38-day-group and by 9% (p<0.05) in the 75-day-group. In both 38- and 75-day-old B mice, $v_{(glom)}$ did not and significantly differ from that of age-matched controls.
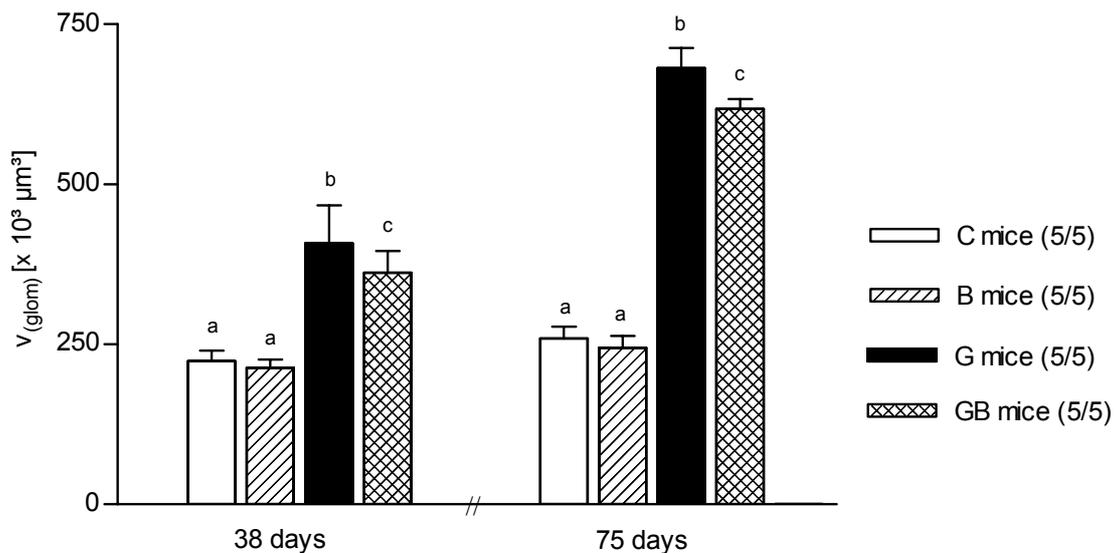

Figure 4.17 Mean glomerular volume of 38- and 75-day-old mice of the four genetic groups. In both age groups, G mice exhibited a dramatic glomerular enlargement, which in GB *vs*. G mice was only slightly reduced. (n/n): number of mice analyzed at an age of 38 days and 75 days, respectively. The data are shown as means and SDs. Significant differences (at least p<0.05) between the genetic groups are indicated by different superscripts (a, b, c).

The comparison of the degree of increase of $v_{(glom)}$ of G and GB *vs*. C mice with the degree of increase of various other parameters, such as body and kidney weight, and $V_{(PTE)}$ of G and GB *vs*. C mice demonstrates an overproportional glomerular growth

through GH overexpression. This discrepancy in glomerular growth and in the growth of other parameters, became even more evident, when relating $v_{(glom)}$ to these parameters (Tables 4.7, 4.8).

The mean glomerular volume-to-body weight-ratio ($v_{(glom)}$/body weight), the mean glomerular volume-to-kidney weight-ratio ($v_{(glom)}$/kidney weight), and the mean glomerular volume-to-PTE volume-ratio ($v_{(glom)}/V_{(PTE)}$) were increased in G mice *vs*. littermate controls at both 38 and 75 days of age. This increase was most pronounced in $v_{(glom)}$/body weight (46%, p<0.001) and $v_{(glom)}/V_{(PTE)}$ (32%, p<0.001) of 75-day-old G *vs*. C mice. These findings confirm an overproportional glomerular growth in G mice.

In 38-day-old GB *vs*. G mice, every ratio investigated was significantly increased. Likewise, in the 75-day-group, every ratio calculated was elevated in GB *vs*. G mice, with $v_{(Glom)}/V_{(PTE)}$ reaching level of statistical significance. In both 38- and 75-day-old GB vs. G mice, $v_{(Glom)}/V_{(PTE)}$ displayed the greatest increase (approximately 26%, p<0.005; respectively). These findings illustrate that the stimulated glomerular growth of G mice was inhibited only by a minor degree in GB mice, as compared to the growth inhibition of various other parameters analysed in this study in GB *vs*. G mice.

Table 4.7

group	$v_{(glom)}$/body weight (x 10^3 µm³/g)	$v_{(glom)}$/kidney weight (x 10^3 µm³/mg)	$v_{(glom)}/V_{(PTE)}$ (x 10^{-6})
C mice (n=5)	8.0^a (0.53)	0.62^a (0.07)	1.23^a (0.07)
B mice (n=5)	9.7^b (0.50)	0.65^a (0.08)	1.41^{ab} (0.02)
G mice (n=5)	11.5^c (1.31)	0.74^a (0.16)	1.59^b (0.24)
GB mice (n=5)	14.5^d (2.34)	0.90^b (0.13)	2.00^c (0.36)

Table 4.7 Mean glomerular volume-to-body weight-ratio ($v_{(glom)}$/body weight), mean glomerular volume-to-kidney weight-ratio ($v_{(glom)}$/kidney weight), and mean glomerular volume-to-PTE volume-ratio ($v_{(glom)}/V_{(PTE)}$) of 38-day-old mice of the four genetic groups. The ratios were calculated from n=5 mice. The data are shown as means and (SDs). Significant differences (at least p<0.05) between the genetic groups are indicated by different superscripts (a, b, c, d).

Table 4.8

group	$v_{(glom)}$/body weight (x 10^3 µm³/g)	$v_{(glom)}$/kidney weight (x 10^3 µm³/mg)	$v_{(glom)}/V_{(PTE)}$ (x 10^{-6})
C mice (n=5)	8.3ᵃ (1.05)	0.69ᵃ (0.08)	1.24ᵃ (0.17)
B mice (n=5)	8.6ᵃ (0.32)	0.60ᵃ (0.09)	1.30ᵃ (0.14)
G mice (n=5)	12.1ᵇ (1.40)	0.96ᵇ (0.10)	1.64ᵇ (0.23)
GB mice (n=5)	13.4ᵇ (1.20)	1.03ᵇ (0.08)	2.07ᶜ (0.07)

Table 4.8 Mean glomerular volume-to-body weight-ratio ($v_{(glom)}$/body weight), mean glomerular volume-to-kidney weight-ratio ($v_{(glom)}$/kidney weight), and mean glomerular volume-to-PTE volume-ratio ($v_{(glom)}/V_{(PTE)}$) of 75-day-old mice of the four genetic groups. The ratios were calculated from n=5 mice. The data are shown as means and (SDs). Significant differences (at least $p<0.05$) between the genetic groups are indicated by different superscripts (a, b, c).

4.5.7 Glomerulosclerosis index

The glomerulosclerosis index (scale 0 - 4) was determined in four mice per genetic group and per age group.

Glomerular lesions were found in both G and GB mice, and were primarily characterized by mesangial expansion and matrix accumulation. No significant differences in the glomerulosclerosis index were found between G and GB mice at both ages investigated. This parameter was slightly increased in 75- *vs*. 38-day-old G and GB mice, however, the increase was not statistically significant (Fig. 4.18 *a*, *b*). Apart from a mild segmental mesangial expansion found in some glomeruli, no glomerular lesions were observed in C and B mice at both ages investigated.
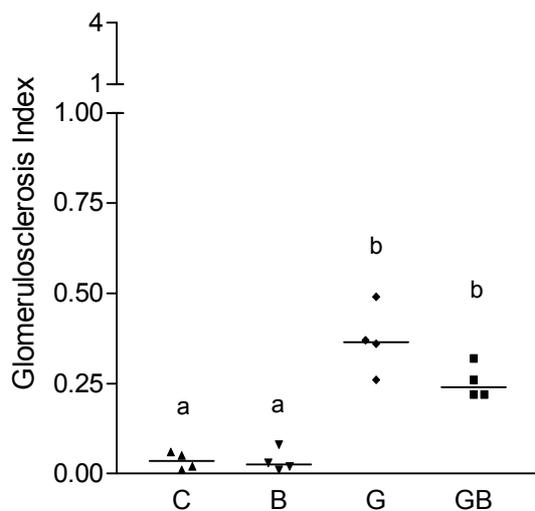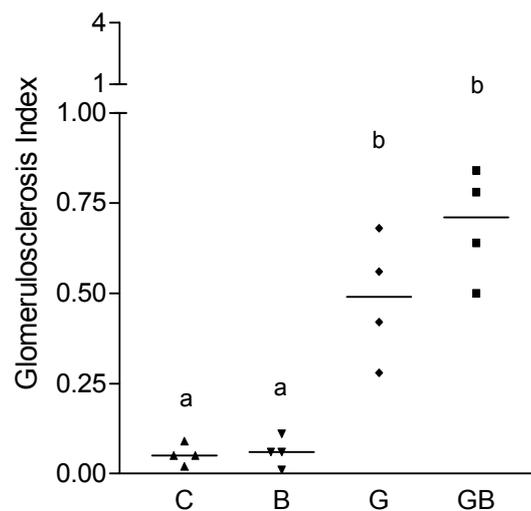

Figure 4.18 *a*   Figure 4.18 *b*

Figure 4.18 *a*, *b* Glomerulosclerosis index of (*a*) 38- and (*b*) 75-day-old mice of the four genetic groups. The degree of glomerular lesions did not differ between G and GB mice. Glomerular changes were negligible in C and B mice. n=4 mice were analyzed per genetic group. The bar indicates the median of every genetic group. Significant differences (at least $p<0.05$) between the genetic groups are indicated by different superscripts (a, b).

4.5.8 Urine protein analysis

4.5.8.1 Pattern of proteinuria

The pattern of proteinuria was determined by SDS-PAGE analysis. Urine samples of 44 mice at the age of 38 days (n=11 per genetic group) and 44 mice at the age of 75 days (C: n=10 ;B: n=12; G: n=11; GB: n=11) were investigated.

C and B mice exhibited identical patterns of proteins excreted in the urine at both ages investigated (Figs 4.19 *a*, *b*). Those mice exhibited a broad band in the region of approximately 18 kDa, which meets the size of major urinary proteins (MUPs) appearing in the urine under physiological conditions particularly in male mice.
Both G and GB mice exhibited bands at approximately 64 kDa meeting the size of murine albumin. The staining intensity of the 64 kDa bands varied from delicate bands of urine samples of 38-day-old G and GB mice to very intensive stained, broad bands of urine samples of 75-day-old G and GB mice. In G and GB *vs.* age-matched C and B mice, the approximately 18 kDa bands were less intensive at both ages investigated.


Alb M C C C B B B G G G GB GB GB   M C C C B B B G G G GB GB GB
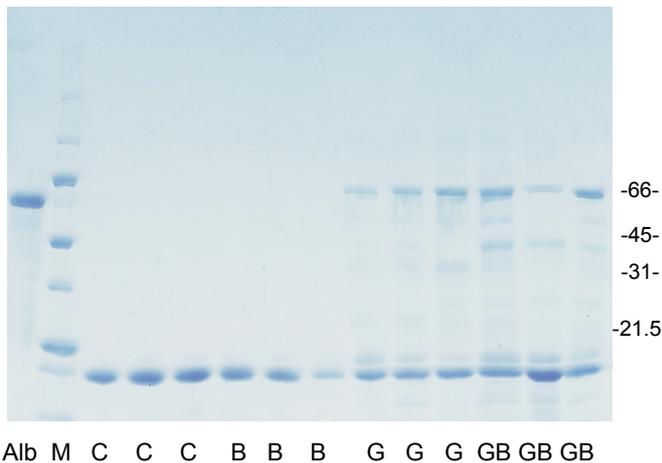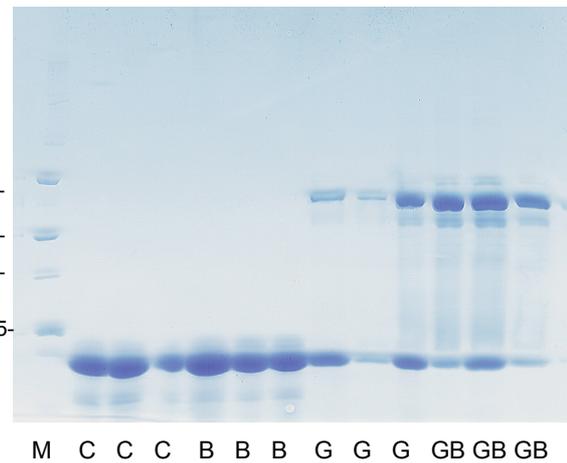
Figure 4.19 *a*   Figure 4.19 *b*

Figure 4.19 SDS-PAGE of urine samples from (*a*) 38- and (*b*) 75-day-old mice of the four genetic groups. Alb, mouse albumin marker; M, Broad range molecular weight standards (Biorad, Ger.) with bands at 66, 45, 31, and 21.5 kDa. Mice of both bGH overexpressing groups exhibited bands at approximately 64 kDa at various intensities, meeting the size of murine albumin and less intensive bands at approximately 18 kDa, meeting the size of major urinary proteins (MUPs).

4.5.8.2 Quantification of albuminuria

The concentration of urinary albumin was measured by ELISA. Additionally, the urinary creatinine concentration was measured by autoanalyzer technique and albumin-creatinine-ratios were calculated. Urine samples of 44 mice (n=11 per genetic group) at the age of 38 days and 44 mice (C: n=10; B: n=12; G: n=11; GB: n=11) at the age of 75 days were analyzed.

At an age of 38 days, G and GB *vs*. C mice exhibited 15- and 23-fold (p<0.001) increased urinary albumin concentrations (Fig. 4.20 *a*), and by 34% and 43% (p<0.005) reduced urinary creatinine concentrations (Table 4.9), respectively. Their albumin-creatinine-ratio was approximately 30-fold elevated (Fig. 4.20 *b*).

In 75- *vs*. 38-day-old G and GB mice, the urinary albumin concentrations were 4.7- and 6.1-fold increased (p<0.005) indicating a more severe albuminuria in the elder bGH overexpressing groups.

In the 75-day-group, G and GB mice demonstrated a 94- and 184-fold (p<0.001) increased urinary albumin concentration (Fig. 4.21 *a*) compared to littermate controls. Within the elder age group, this parameter was significantly increased by 95% in GB *vs*. G mice. A significant increase of 112% was also detectable in the albumin-creatinine-ratio of 75-day-old GB *vs*. G mice (Fig. 4.21 *b*) demonstrating a more severe albuminuria in 75-day-old GB mice than in G mice.

In B *vs*. C mice of both age groups, the urinary albumin and creatinine concentration, and the albumin-creatinine-ratio did not significantly differ, with the exception of a reduced urinary creatinine concentration (by 36%, p<0.005) in 38-day-old B *vs*. C mice.
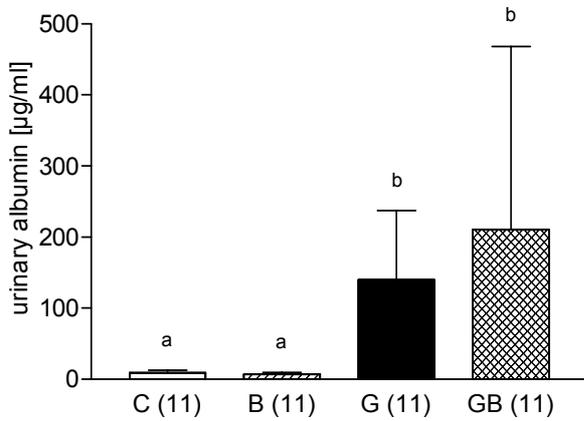
Figure 4.20 *a*
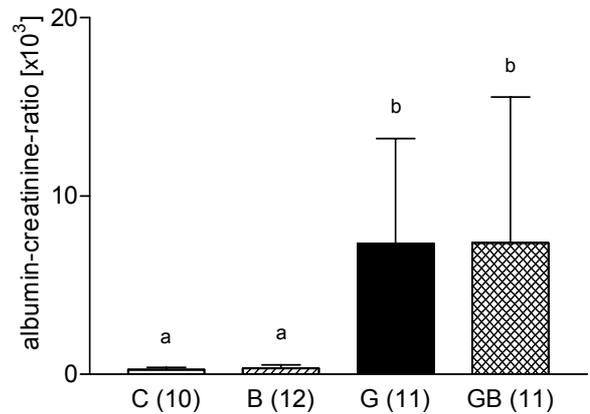
Figure 4.20 *b*

Figure 4.20 Urinary albumin concentration (*a*) and albumin-creatinine-ratio (*b*) of 38-day-old mice of the four genetic groups. G and GB mice exhibited severe albuminuria of a similar extend. (n): number of mice analyzed. The data are shown as means and SDs. Significant differences (at least $p < 0.05$) between the genetic groups are indicated by different superscripts (a, b).
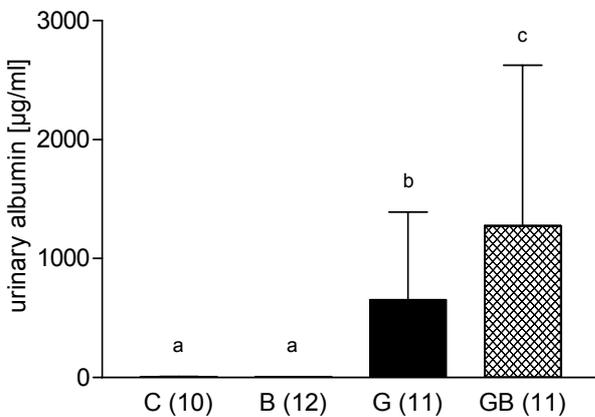
Figure 4.21 *a*
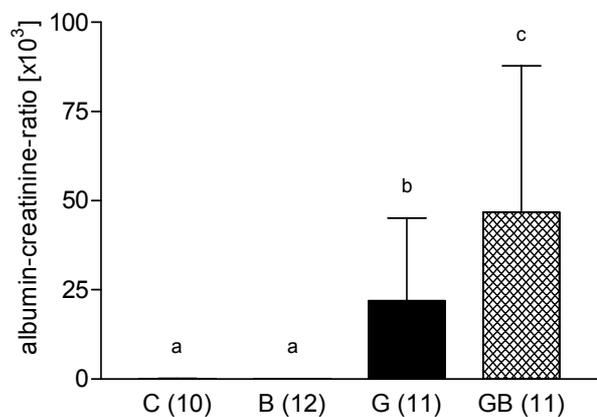
Figure 4.21 *b*

Figure 4.21 Urinary albumin concentration (*a*) and albumin-creatinine-ratio (*b*) of 75-day-old mice of the four genetic groups. G and GB mice exhibited severe albuminuria, which is significantly augmented in GB mice. (n): number of mice analyzed. The data are shown as means and SDs. Significant differences (at least $p < 0.05$) between the genetic groups are indicated by different superscripts (a, b, c).

Table 4.9

group	urinary creatinine concentration [mg/dl]	
	38 days of age	75 days of age
C mice (11/10)	37.9^a (8.7)	50.4^a (19.3)
B mice (11/12)	24.3^b (10.9)	43.5^a (11.1)
G mice (11/11)	21.5^b (8.1)	28.3^b (7.9)
GB mice (11/11)	25.0^b (8.5)	27.6^b (8.2)

Table 4.9 Urinary creatinine concentration of 38- and 75-day-old mice of the four genetic groups. G and GB *vs*. C mice demonstrated reduced urinary creatinine concentrations (n/n): number of mice analyzed at an age of 38 and 75 days, respectively. The data are shown as means and (SDs). Significant differences (at least $p<0.05$) between the genetic groups are indicated by different superscripts (a, b).

4.5.9 Western ligand blot analysis of renal IGFBP-2

Western ligand blot (WLB) analysis was performed of protein extracts from the renal zones - cortex, OSM, and ISM/IZM. The right kidneys of three mice per genetic group at an age of 38 days were investigated.

The apparent size of IGFBP-2 was 32 kDa (Fig. 4.22). The intensity of IGFBP-2 bands was similar between samples of a particular renal zone from mice of the same genetic group. The intensity of the IGFBP-2 bands in both B and GB *vs*. C and G mice in every renal zone was enhanced to a comparable extent. In C and G mice, nearly no [I^{125}]IGF-II binding activity was visible in the cortex, in contrast to the OSM and ISM/IZM, which exhibited endogenous IGFBP-2 abundance.
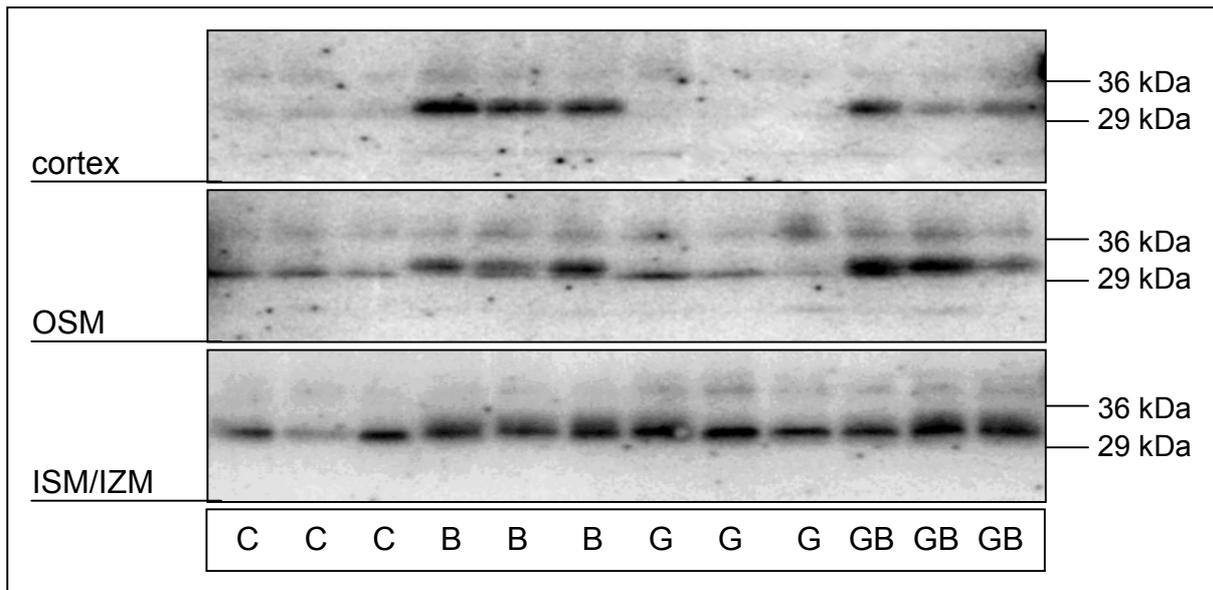

Figure 4.22 Western ligand blot analysis of protein extracts of renal zones of kidneys from 38-day-old mice of the four genetic groups. OSM, outer stripe of medulla; ISM/IZM inner stripe of medulla together with inner zone of medulla. The apparent size of IGFBP-2 was 32 kDa.

The intensity of the fraction of bands between 29 kDa and 36 kDa shown in figure 4.22 was densitometrically determined (Fig. 4.23).

Non-transgenic control mice displayed less intensive IGFBP-2 bands in the cortex, and slightly more intensive IGFBP-2 bands in the OSM and ISM/IZM suggesting the presence of endogenous IGFBP-2 in the renal medulla. The intensity of IGFBP-2 bands of single renal zones in G mice did not significantly differ from that of controls.

Both B and GB *vs*. C mice demonstrated a markedly elevated intensity of IGFBP-2 bands. In the cortex, the intensity of IGFBP-2 bands of B mice was 6.9-fold ($p<0.001$), and of GB mice was 4.4-fold ($p<0.001$) increased, compared to controls. In B and GB *vs*. C mice, the intensity of IGFBP-2 bands in the OSM was 2.4- and 3.3-fold increased ($p<0.01$), and in the ISM/IZM was 2.4- and 2.3-fold increased ($p<0.02$), respectively.
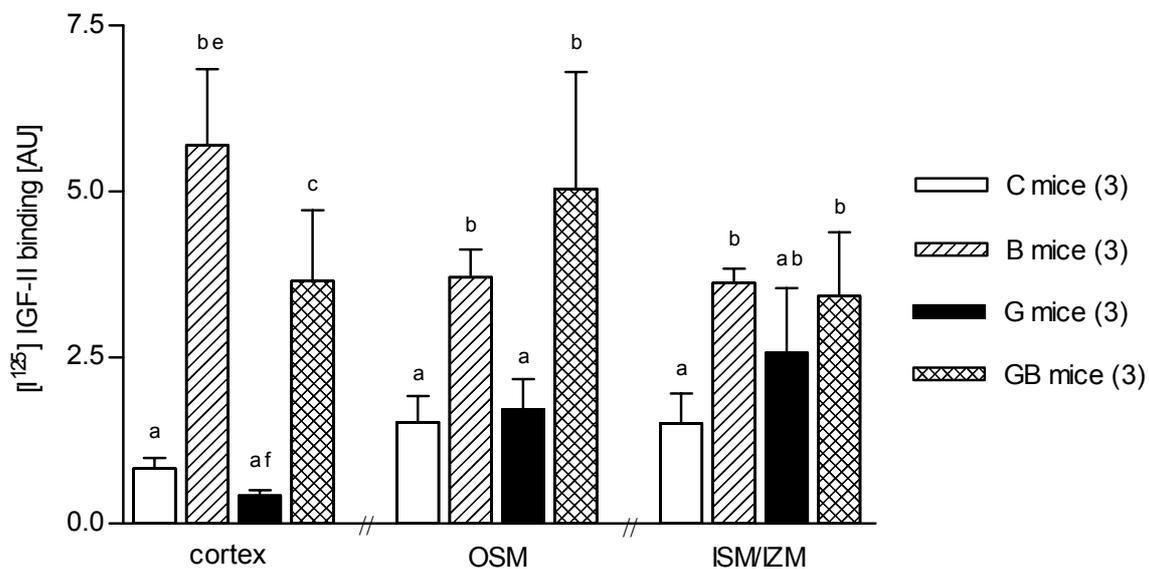
Figure 4.23 Densitometry of IGFBP-2 bands obtained by WLB analysis of different renal zones of mice of the four genetic groups. OSM, outer stripe of medulla; ISM/IZM, inner stripe of medulla together with inner zone of medulla. (n): number of mice analyzed. The data are shown as means and SDs. Significant differences (at least $p<0.05$) within the renal compartment between the genetic groups are indicated by different superscripts (a, b, c). (e) shows a significant difference between cortex and OSM, ISM/IZM of B mice. (f) shows a significant difference between cortex and ISM/IZM of G mice.

4.5.10 Detection IGFBP-2 mRNA and protein in the kidney

Immunohistochemistry and *in situ* hybridization were used to localize IGFBP-2 or IGFBP-2 mRNA, respectively, in the kidneys. Investigations were carried out on subsequent sections of the left kidneys from mice (n=3 per genetic group; 38 days of age) examined by WLB analysis.

Similar staining results were obtained from mice of the same genetic group. IGFBP-2 and IGFBP-2 mRNA were detected by immunohistochemistry (IHC) and *in situ* hybridization (ISH) exclusively in B and GB mice. The staining patterns and intensities were comparable between B and GB mice. The highest staining intensity in both IHC and ISH was found in the renal cortex.

Contrary, C and G mice as well as methodical negative controls did not display any immunohistochemical or *in situ* hybridization staining. (Figs. 24 *a - d*).

Within the glomerulus, podocytes exhibited a strong IGFBP-2 immunostaining that could not be re-identified on subsequent sections that underwent ISH (Figs. 25 *a*, *b*). Other glomerular cells neither showed an IHC signal nor an ISH signal.

A comparable divergence in IHC and ISH signals as seen in podocytes was found in epithelial cells of the parietal layer of the Bowman capsule and in epithelial cells of the pars convoluta of the proximal tubule (Figs. 25 *a*, *b*). These cells displayed an intracellular IGFBP-2 immunostaining that was of granular appearance and was located apically within the epithelial cells. Contrary, no equivalent positive signal on RNA levels was noticeable. The combination of IHC and ISH analysis suggests the cellular presence of IGFBP-2 protein but not its synthesis in podocytes and epithelial cells of the parietal layer of the Bowman capsule and of the pars convoluta of the proximal tubule.

Epithelial cells of the thick ascending limb of Henle´s loop exhibited a slight IGFBP-2 immunostaining located in the cytoplasm. The intensity of the immunostaining varied between single cells. A slight, positive signal with comparable localization was detectable by *in situ* hybridization (Figs. 27 *a - d*).

The distal tubule epithelia showed the most intensive staining in both IHC and ISH, suggesting a strong expression of transgene encoded IGFBP-2 and local presence of IGFBP-2 protein within these structures (Figs. 26 *a*, *b*).
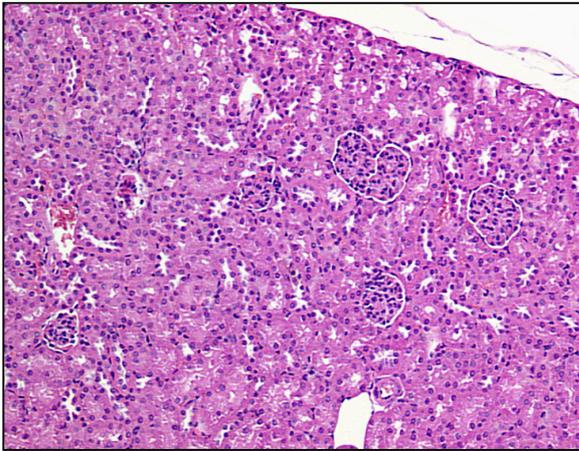
Fig. 4.24 *a*: Overview of the renal cortex

B mouse; H&E staining; original magnification 125 x
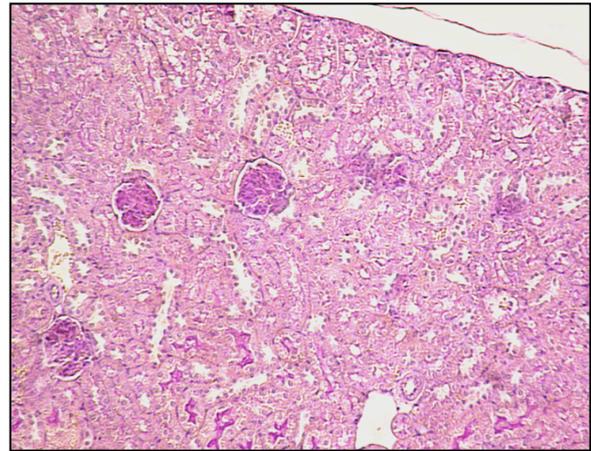
Fig. 4.24 *b*: Overview of the renal cortex

B mouse; PAS staining; original magnification 125 x
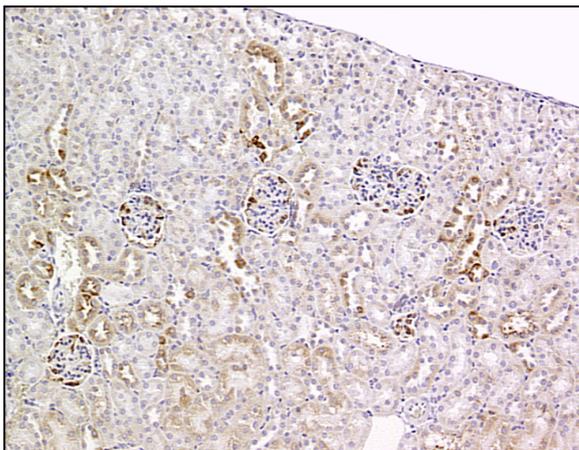
Fig. 4. 24 *c*: Overview of the renal cortex

B mouse; IHC IGFBP-2, counterstaining with hemalaun; original magnification 125 x
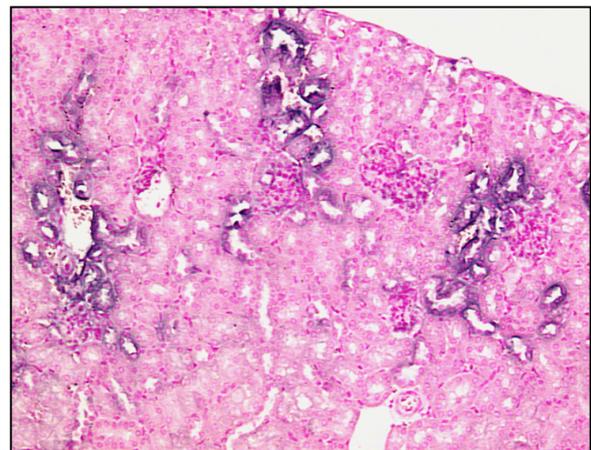
Fig. 4.24 *d*: Overview of the renal cortex

B mouse; ISH IGFBP-2 mRNA; counterstaining with Nuclear fast red; original magnif. 125 x

Figure 4.24 *a* - *d*: Overview of the renal cortex. Four subsequent sections of a kidney from a 38-day-old IGFBP-2 transgenic (B) mouse were differentially stained. IGFBP-2 overexpression in B and GB mice do not reveal any morphological changes in the kidneys (*a, b*). Note the pronounced IGFBP-2 immunostaining (*c*) of tubular structures, which can be re-identified in the section analyzed by ISH (*d*). Further, a strong punctual signal is detectable in glomeruli of the IHC stained section, whereas no corresponding signal is noticeable on the ISH stained section.
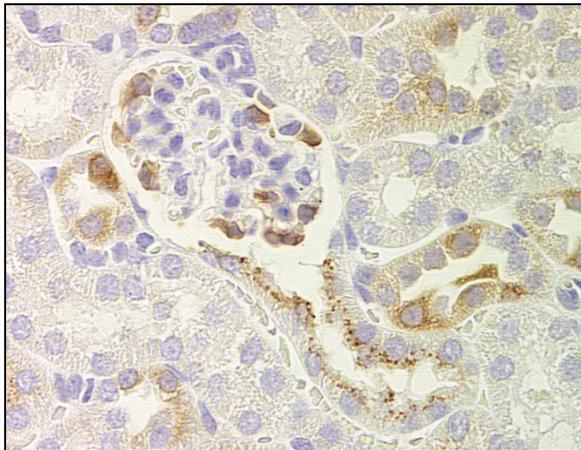
Fig. 4.25 *a*: Glomerulus and beginning
pars convoluta of the proximal tubule

B mouse; IHC IGFBP-2; counterstaining with
hemalaun; original magnification 400 x
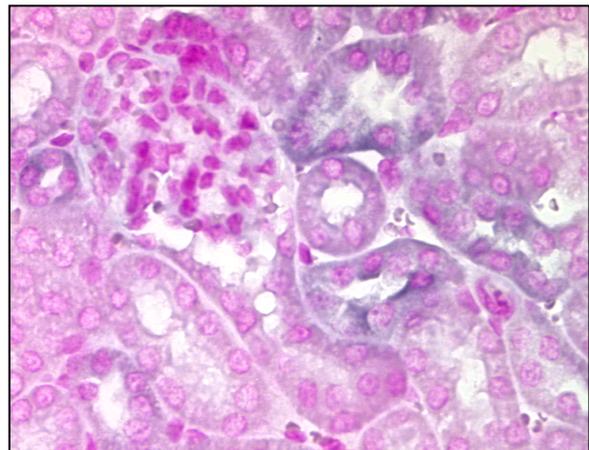
Fig. 4.25 *b*: Glomerulus and beginning
pars convoluta of the proximal tubule

B mouse; ISH IGFBP-2 mRNA; counterstaining
with Nuclear fast red; original magnif. 400 x

Figure 4.25 *a*, *b*: Glomerulus and beginning pars convoluta of the proximal tubule.
Two subsequent sections of the kidney from a 38-day-old IGFBP-2 transgenic (B) mouse are shown.
Note the intensive IGFBP-2 immunostaining of podocytes, epithelial cells of the parietal layer of the
Bowman capsule, and of the proximal tubule. The IHC staining of the epithelial cells of the parietal
layer of the Bowman capsule and PTE cells is of granular appearance and intracellular located, with
distinct apical distribution (*a*). No corresponding signal is noticeable by ISH (*b*).
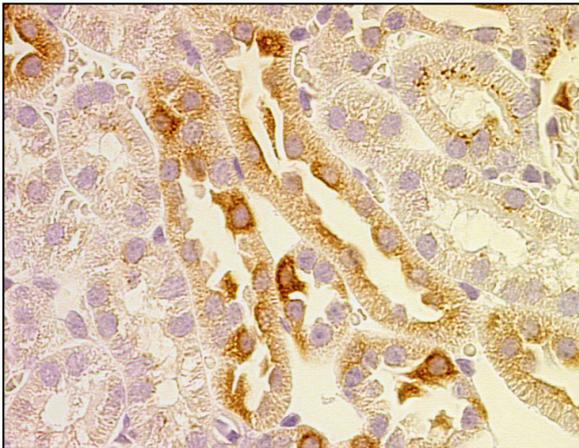
Fig. 4.26 *a*: Distal tubules in the renal cortex

B mouse; IHC IGFBP-2; counterstaining with hemalaun; original magnification 400 x
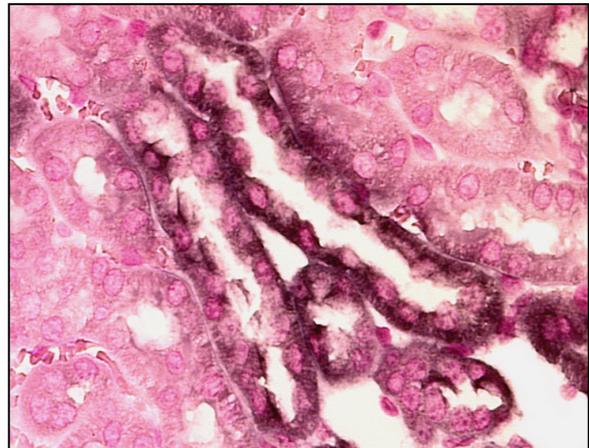
Fig. 4.26 *b*: Distal tubules in the renal cortex

B mouse; ISH IGFBP-2 mRNA; counterstaining with Nuclear fast red; original magnif. 400 x

Figure 4.26 *a*, *b*: Distal tubules in the renal cortex. Two subsequent sections of the kidney from a 38-day-old IGFBP-2 transgenic (B) mouse are shown. Distal tubules in the renal cortex exhibit both a strong IHC and ISH staining for IGFBP-2 and IGFBP-2 mRNA, respectively. Note the discrepancy in IHC and ISH staining of the proximal tubule in the top right-hand corner.
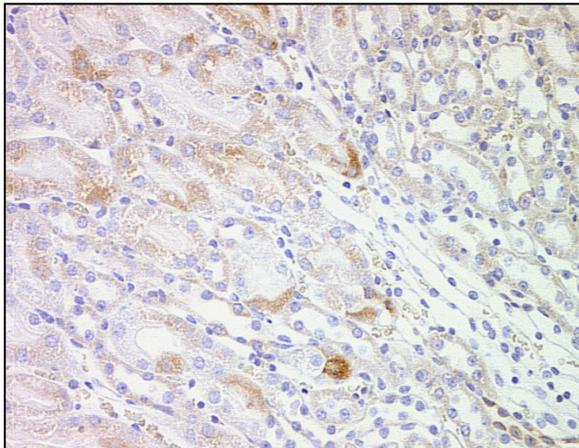
Fig. 4.27 *a*: Overview of borderline bet-
ween outer and inner stripe of medulla

B mouse; IHC IGFBP-2; counterstaining with
hemalaun; original magnification 250 x
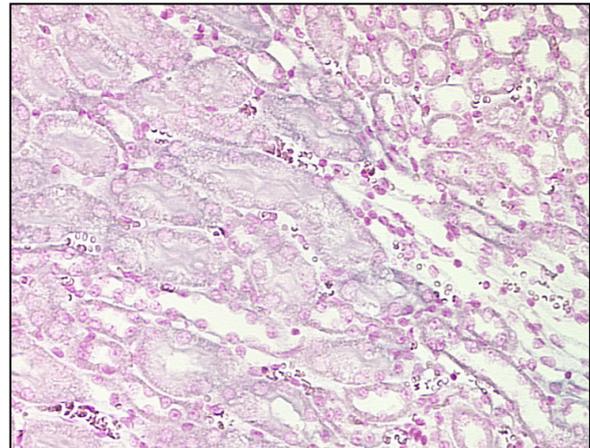
Fig. 4.27 *b*: Overview of borderline bet-
ween outer and inner stripe of medulla

B mouse; ISH IGFBP-2 mRNA; counterstaining
with Nuclear fast red; original magnif. 250 x
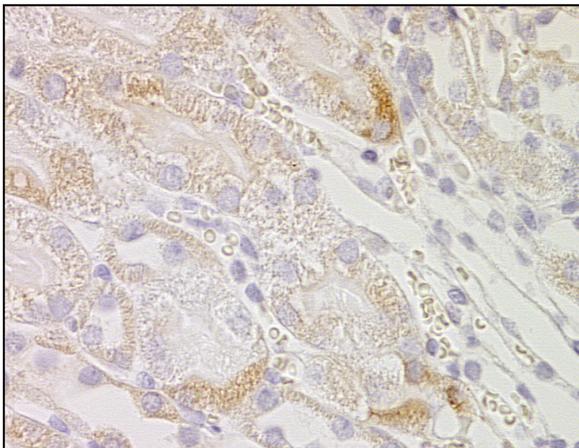
Fig. 4.27 *c*: Borderline between outer
and inner stripe of medulla in detail

B mouse; IHC IGFBP-2; counterstaining with
hemalaun; original magnification 400 x
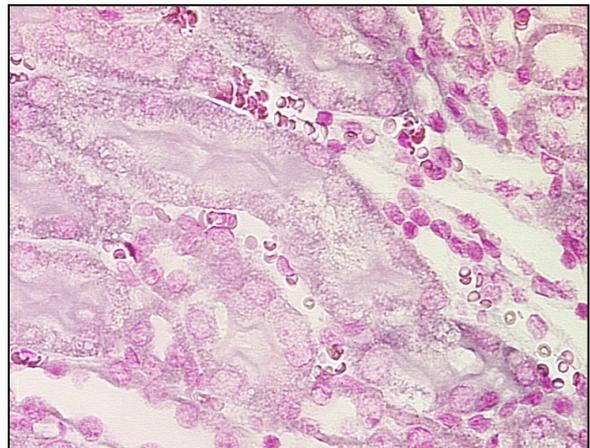
Fig. 4.27 *d*: Borderline between outer
and inner stripe of medulla in detail

B mouse; ISH IGFBP-2 mRNA; counterstaining
with Nuclear fast red; original magnif. 400 x

**Figure 4.27 *a* - *d*: Borderline between outer and inner stripe of medulla in an
overview (*a*, *b*) and in detail (*c*, *d*).** Two subsequent sections of the kidney of a 38-day-old
IGFBP-2 transgenic mouse are shown. Epithelial cells of the thick ascending limb of Henle´s loop
exhibit a slight, diffuse intracellular distributed signal in both IHC and ISH analyses. Single cells
display a more pronounced immuno- and ISH-staining.

5 Discussion

5.1 General aspects

The present study analyzed effects of IGFBP-2 overexpression on both normal and GH/IGF-I-stimulated growth and function of the adrenal glands and kidneys in transgenic mice. For that purpose, hemizygous PEPCK-bGH and hemizygous CMV-mIGFBP-2 transgenic mice were crossed and the resulting four different genetic groups of offspring (non-transgenic controls (C), mIGFBP-2 transgenic (B), bGH transgenic (G), and double transgenic (GB) mice) were examined at different ages.

The overexpression of bGH in G mice caused a significant increase in body weight, whereas overexpression of IGFBP-2 led to decreased body weights in B *vs*. C and in GB *vs*. G mice of both age groups (38 and 75 days of age). The results of the present study concerning body weight and circulating levels of IGF-I and IGFBP-2 of mice of the four different genetic groups resembled those recently published by Hoeflich *et al*. [7]. Confirming preceding data, the growth inhibitory effect of elevated IGFBP-2 was more pronounced under high than under normal GH/IGF-I conditions. In 38-day-old GB mice, the GH-induced body growth stimulation was abolished.

Serum levels of bGH correspond to 2 µg/ml in both G and GB mice [7]. Circulating endogenous IGF-I levels in both bGH overexpressing groups included in this study were found to be similarly elevated. This indicates that phenotypical differences between G and GB mice were not due to altered bGH expression or differences in systemic IGF-I levels by overexpression of IGFBP-2 in GB mice. Likewise, serum IGFBP-2 levels of both IGFBP-2 overexpressing groups were similarly elevated confirming previous data [7]. Contrary, serum IGFBP-2 levels of G *vs*. C mice were significantly decreased in the present study, while they were found to be only slightly lowered in a previous experiment [7]. In humans, GH treatment also leads to reduced IGFBP-2 serum levels, which are linked with a significant decrease in liver IGFBP-2 mRNA levels [117]. Thus, the reduced IGFBP-2 serum levels in bGH transgenic mice probably resulted from reduced hepatic endogenous IGFBP-2 expression. Further discussed regulators of IGFBP-2 are IGF-II and insulin. However, since serum IGFBP-2 levels are positively correlated with IGF-II levels [129,298], but IGF-II levels

were found to be slightly elevated in PEPCK-bGH transgenic mice [37], a regulatory effect of IGF-II on IGFBP-2 serum levels is not comprehensible in G mice. High insulin levels are known to be negatively correlated to serum IGFBP-2 levels [72,299]. Since GH transgenic mice were reported to be hyperinsulinemic [14], reduced IGFBP-2 levels of G mice might be secondary to bGH-induced elevation of insulin levels.

5.2 Clinical-chemical findings

GH is known to affect clinical-chemical serum parameters. However, the consequences of elevated IGFBP-2 levels on clinical-chemical serum parameters were unclear so far.

Serum creatinine and urea represent kidney relevant serum parameters. Serum creatinine levels of 38- and 75-day-old G *vs*. C mice were significantly elevated. This finding is in contrast to reports from 7- and 19-week-old MT-bGH and 7- and 14-week-old PEPCK-bGH transgenic mice characterized by unchanged serum creatinine levels [85,229]. Serum creatinine almost exclusively originates from muscle metabolism and its production has been shown to be proportional to muscle mass [300]. Since G mice of the present study were of relatively young age, glomerular alterations correspond to initial stage changes of glomerulosclerosis. An increase in serum creatinine values due to impaired kidney function is observed after kidney function is reduced by more than 50% [79]. Thus, elevation of serum creatinine in G mice of the present study probably resulted from increased muscle metabolism rather than from impaired renal excretion. However, serum creatinine is regarded as a quite insensitive parameter to characterize glomerular changes [301,302].

Serum creatinine levels were not influenced by overexpression of IGFBP-2 in B *vs*. C and GB *vs*. G mice, with exception of a slight reduction of this serum parameter in 75-day-old GB *vs*. G mice. This reduction possibly reflected reduced creatinine production in GB *vs*. G mice, due to their lowered muscle mass.

Serum urea levels were unchanged in mice of the four genetic groups at an age of 38 days, whereas this parameter was significantly decreased in G and GB *vs*. C and B mice in the elder (75-day-old) collective of the present study. Serum urea levels of G mice analyzed in this study are in line with findings from seven-week-old MT-bGH transgenic mice, which exhibited serum urea levels not different from those of controls, and from 14-week-old PEPCK-bGH transgenic mice, which displayed

reduced serum urea levels compared to those of control animals [229]. The decrease of serum urea levels of GH transgenic mice is attributed to the anabolic effect of GH [303]. However, a 2-fold increase of serum urea levels was found in MT-hGH transgenic mice at the end of their life-span, caused by marked catabolism and declining kidney function [79]. Overexpression of IGFBP-2 in B *vs*. C and GB *vs*. G mice did not influence serum urea levels.

Serum levels of phosphate are known to be linked to those of GH [304]. Thus, increased serum phosphate levels are found in growing children and in adults with active gigantism or acromegaly [305]. GH-treated dogs also show increased serum phosphate levels [306]. Likewise, 38- *vs*. 75-day-old C mice and 75-day-old G *vs*. C mice of the present study exhibited elevated serum phosphate levels. However, since serum GH levels were not determined in mice of this study, and age-related changes of serum GH levels in mice of the strain used are not known yet, a correlation between elevated serum phosphate levels and serum GH levels can only be speculated. Elevated serum phosphate levels in high GH states are - at least partially - due to reduced renal phosphate excretion. Since IGF-I, but not GH, has been shown to be able to specifically stimulate phosphate transport in isolated perfused rabbit proximal tubules, the GH-induced reduction in renal phosphate excretion is suggested to be IGF-I-mediated [210]. Accordingly, IGF-I-treatment increases renal tubular phosphate reabsorption in humans and rats [307]. *In vitro*, IGF-I stimulates phosphate absorption in murine PTE cells and this effect is not affected by IGFBP-2 [308]. Accordingly, IGFBP-2 overexpression in B *vs*. C and GB *vs*. G mice did not reduce serum phosphate levels in the 38-day-group. In the 75-day-group, serum phosphate levels of B and G mice were slightly, and of GB mice were significantly increased as compared to controls implicating an additional effect of both bGH and IGFBP-2 overexpression on serum phosphate levels. Since IGF-I also promotes the shift of phosphate from the serum mainly into muscle and bone tissue, possibly by stimulation of sodium-phosphate co-transport [304], the increased serum phosphate levels of 75-day-old B *vs*. C and GB *vs*. G mice might reflect an IGFBP-2-induced inhibition of this IGF-I effect.

Serum calcium levels were elevated in mice of both bGH overexpressing groups. Similarly, hypercalcemia was found to be a frequent feature in acromegalic patients. After successful treatment, serum calcium values normalized in a number of those patients [305]. In the rat, elevated GH levels also cause an increase of serum calcium

levels [309]. Controversial reports exist about a linkage between GH excess and secondary hyperparathyroidism due to parathyroid hyperplasia [305,310].

Serum sodium levels were not different between the four genetic groups. In contrast, serum chloride was slightly lowered (~5%) in G and GB *vs.* C and B mice of both age groups, probably due to altered renal excretion [311]. A sodium as well as fluid retentive effect of high GH levels is well established in several GH transgenic mouse strains [229,312], and in rats and humans [313]. GH transgenic mice demonstrate increased plasma volumes, absolute and relative to body weight [314], and reduced hematocrit values [229,312]. Thus, the sodium concentrations in the serum of G and eventually of GB mice in the present study likely remained unchanged because of secondary hypervolemia. As shown in PEPCK-bGH transgenic mice, serum and cardiac atria levels of the atrial natriuretic peptide (ANP), an endogenous regulator of volume homeostasis, are increased, compared to non-transgenic controls. The authors, therefore, suggest an influence of the ANP on the effect of GH in fluid retention [312]. Further, in acromegalic patients, an increased renal tubular sodium-potassium-ATPase activity has been found to be responsible for the anti-natriuretic effect of GH [313].

Serum potassium levels were inconsistently affected by bGH and/or IGFBP-2 over-expression in the 38- and 75-day-old group implicating a certain influence of the age on this parameter. IGF-I has been demonstrated to decrease serum potassium levels [315], most likely by promoting the cellular up-take of potassium [316,317]. Thus, the slightly increased serum potassium levels in GB *vs.* G mice of both age groups might derive from an IGFBP-2-induced inhibition of that IGF-I effect.

The serum concentrations of total proteins were elevated in bGH overexpressing mice of both age groups despite progressive renal protein loss. This result is in line with previous findings in several GH transgenic mouse strains and is regarded as a result of increased hepatic protein synthesis [79,229]. Overexpression of IGFBP-2 in B *vs.* C and GB *vs.* G mice had no significant influence on this parameter.

The lipid status of mice of the four genetic groups was characterized by a significant elevation of serum cholesterol levels of G and GB *vs.* C and B mice. Serum triglyceride levels in G mice were reduced, which is in line with previous findings in MT-hGH transgenic mice [79]. Likewise, 7-week-old MT-bGH transgenic mice demonstrate increased serum cholesterol and reduced triglyceride levels [229]. IGFBP-2 overexpres-

sion in B *vs*. C and GB *vs*. G mice had no significant influence on serum cholesterol and triglyceride concentrations.

5.3 Effects of bGH and/or IGFBP-2 transgene expression on the adrenal gland

This study used the enlarged and corticosterone hypersecreting adrenal glands of PEPCK-bGH transgenic mice as a model to characterize components of growth in terms of hyperplasia and hypertrophy, and to evaluate potential modulatory effects of IGFBP-2 on growth characteristics and function of the adrenal cortex.

PEPCK-bGH transgenic mice, an established model for studying long-term consequences of elevated GH, exhibited markedly increased adrenal weights, which is in line with previous findings [16]. In contrast, the adrenal glands of GH-deficient Snell dwarf mice are several times smaller than those of normal mice [318]. bGH transgenic mice display systemically elevated bGH and IGF-I levels. Since the adrenal gland expresses both the GHR [160,161] and IGF-IR [319], basically both bGH and IGF-I may be reasonable for effects on adrenal growth promotion in that model. However, several lines of evidence indicate that adrenocortical enlargement and increased corticosterone secretion in G mice were most likely caused by increased levels of IGF-I: *1)* In cultured HAC, hGH does not stimulate basal or ACTH-stimulated cortisol secretion [162], whereas the IGFs show mitogenic and steroidogenic effects on fetal and adult adrenocortical cells. Moreover, IGF-I analogues with reduced affinity for IGFBPs even more potently stimulate steroidogenesis than normal IGF-I [163]. *2) In vivo*, infusion of IGF-I into guinea pigs increases the fractional weight of the adrenal glands, and again, this effect is more pronounced with long R^3 IGF-I, an analogue with reduced affinity for IGFBPs [178]. *3)* Overexpression of IGF-II in transgenic mice causes adrenal enlargement and enhanced steroidogenesis [8]. *4)* Both adrenal IGF-I expression and circulating IGF-I levels were significantly elevated in bGH transgenic (G and GB) mice [159]. *5)* The elevation of plasma corticosterone levels in different GH transgenic mouse strains correlates largely with serum IGF-I levels rather than with circulating GH levels [16]. *6)* IGFBP-2, a presumed inhibitor of IGF actions in various human and rodent cell culture models and *in vivo* [7,72], strongly reduced adrenal growth and abolished corticosterone secretion in the context of high GH and IGF-I levels in GB mice. Contrary, in normal growth conditions, IGFBP-2 overexpression in

B *vs*. C mice reduced adrenal weight only as a tendency. Adrenal IGFBP-2 mRNA and protein levels were similarly elevated in B and GB mice [159].

IGFBP-2 is assumed to inhibit IGF actions [7,72]. Nevertheless, an influence of elevated IGFBP-2 on GH effects or a GH/IGF-I independent growth inhibitory effect of IGFBP-2 cannot be excluded [9]. For instance, IGFBP-2 has been shown to increase GHR mRNA expression and binding of GH to its receptor in rat osteosarcoma cells [320]. In contrast, no significant differences in the levels of GHR mRNA and IGF-IR mRNA abundance in the adrenal glands of mice of the four genetic groups were observed [159].

The extent of growth inhibition by IGFBP-2 excess in GB *vs*. G mice varies between different organs with the adrenal gland being overproportionally reduced in weight [7]. The adrenal gland was the organ with the greatest relative weight reduction (-22%, -37%, respectively) in GB *vs*. G mice at an age of 75 days (present study) and of four months in a previous study. The fact that even the relative adrenal weight was as a tendency smaller in GB than in G mice at four months of age points to a specific effect of IGFBP-2 on adrenal growth especially in the context of GH excess [159].

Using state-of-the-art stereological methods, the growth manipulating effects of bGH and/or IGFBP-2 overexpression on adrenal structures and cells was determined. The volume fractions of cortex and medulla, ($V_{V(cortex/adrenal\ gland)}$ and $V_{V(medulla/adrenal\ gland)}$), were not different between the four genetic groups. This finding is consistent with the presence of IGF-IR in both zones [186,321]. As a consequence, G mice exhibited increased absolute volumes of adrenal cortex and medulla. Contrary, IGFBP-2 excess inhibited both adrenocortical and -medullary growth, and the degree of growth inhibition was greater in the context of GH/IGF-I excess than in animals with normal GH and IGF-I levels (C mice).

The absolute volume of the zona fasciculata ($V_{(zona\ fasc.,\ cortex)}$) was markedly increased through GH overexpression in G mice, due to both hypertrophy (44% increase in mean cell volume) and hyperplasia (50% increase in cell number) of zona fasciculata cells. Contrary, overexpression of IGFBP-2 in GB mice significantly reduced $V_{(zona\ fasc.,\ cortex)}$. Interestingly, on cellular level IGFBP-2 inhibited only the hypertrophic action of GH on zona fasciculata cells, whereas cellular hyperplasia was unaffected.

These data show for the first time that even with saturating amounts of GH and IGF-I, IGFBP-2 is capable of limiting cell growth and maximum cell size.

The adrenocortical phenotype in GB mice resembles that in IGF-II transgenic mice. Like GB mice, IGF-II transgenic mice exhibit an increased volume of the adrenal cortex, which is exclusively due to hyperplasia (50% increase in cell number) of zona fasciculata cells, whereas the cell volume remains unchanged. Instead of increased IGF-I levels, IGF-II transgenic mice demonstrate two- to three-fold elevated serum IGF-II levels, adrenal IGF-II transgene expression, and increased IGFBP-2 serum levels [8,129]. This comparison suggests that on the one hand, both IGFs act similarly in the context of high IGFBP-2 levels in regulating growth of zona fasciculata cells, implicating the activation of the same receptor, namely the IGF-IR [44,45]. On the other hand, this comparison implicates that GH seems to have no direct effect on adrenocortical growth, which is also underlined by *in vitro* findings [162].

The molecular mechanisms underlying the specific hypertrophy-inhibiting effect of IGFBP-2 on adrenocortical zona fasciculata cells remain unclear. If this effect were independent of GH or IGF-I, one would expect a decrease in cell volume also in B *vs.* C mice, which was not the case. On the other hand, IGFBP-2 could specifically block an increase in cell size rather than decrease normal-sized cells. If the effect of IGFBP-2 were GH/IGF-I dependent, it remains unclear why only the hypertrophic actions of GH/IGF-I excess were blocked. Since much evidence indicates that cellular size and proliferation is regulated by independent signaling pathways [71,322,323], one can speculate, that IGFBP-2 specifically targets signal transduction pathways downstream of the IGF-I receptor. A possible candidate, involved in growth of zona fasciculata cells is the 3-phosphoinositide-dependent protein kinase-1 (PDK1). PDK1 functions as a master kinase and plays a key role in regulating the activity of a group of insulin and IGF-stimulated protein kinases [324,325]. Mice that possess PDK1 hypomorphic alleles and express only ~10% of the normal level of PDK1, exhibit reduced adrenal gland volumes. Morphometric analysis revealed that the volume of zona fasciculata cells of those mice was reduced by 45%, whereas the cell number was unchanged [326].

Analysis of plasma corticosterone levels in mice of the four genetic groups revealed that the changes in adrenal weight were paralleled by their capacity to secrete gluco-corticoids. Both basal and ACTH-induced plasma corticosterone levels were marked-ly increased in G mice, and this effect was significantly reduced by coexpression of IGFBP-2 in GB mice. Since the number of adrenocortical cells was not different between G and GB mice, corticosterone hypersecretion seems to depend on cell size rather than on cell number.

Basal plasma corticosterone levels of C mice included in the present study were higher than those observed in an earlier experiment [8]. In contrast to the previous experiment, blood samples of the present study were taken in the afternoon, the last third of the light period, where the highest levels of circulating corticosterone are measured in mice [327]. The sampling time and/or different genetic backgrounds might be responsible for the differences in plasma corticosterone levels observed.

Plasma ACTH levels of C and B mice were significantly higher in the afternoon than in the morning. This physiological diurnal variation of ACTH secretion was not seen in G and GB mice. In both G and GB mice, ACTH levels were normal or only slightly elevated. This finding is in contrast to a previous report, in which three-fold increased morning plasma ACTH levels were measured in male mice of one PEPCK-bGH transgenic strain [15]. To further characterize effects of GH excess on plasma ACTH levels, MT-bGH transgenic mice were investigated in the present study. Their plasma ACTH levels also were not significantly different from these of non-transgenic litter-mate controls. Furthermore, PEPCK-bGH transgenic mice maintained on an NMRI outbred background do not show significantly different morning plasma ACTH levels, if compared to non-transgenic controls [328]. Therefore, it is unlikely that the trophic effects of GH on the adrenal gland are mediated *via* increased ACTH levels. Interestingly, plasma ACTH levels in GH transgenic mice were not reduced in spite of markedly increased plasma corticosterone concentrations suggesting a disturbed feedback regulation of ACTH secretion [329].

5.4 Effects of bGH and/or IGFBP-2 transgene expression on the kidney

Stimulation of kidney growth through bGH overexpression in G mice is in line with previous findings [14]. Coexpression of the CMV-IGFBP-2 transgene in GB mice markedly inhibited bGH-associated renal hypertrophy, while IGFBP-2 excess under normal growth conditions had no effect on renal growth. The results in the present study concerning renal growth modulation by IGFBP-2 overexpression are consistent with these of previous studies using the same collective of mice, and confirm the close involvement of the GH/IGF-axis in renal growth regulation [7].

The renal enlargement observed in GH transgenic mice is likely to be mediated mainly by IGF-I rather than by GH for several reasons. *1)* Both IGF-I transgenic mice, which are characterized by lowered serum GH levels, and GH transgenic mice exhibit elevated serum IGF-I levels and renal hypertrophy [85,86]. *2)* Similar renal growth effects can be achieved by administration of IGF-I or GH to normal [255,330] or GH deficient rats [237]. *3)* GH deficiency is linked to reduced circulating and renal IGF-I levels and reduced renal mass [200]. *4)* Markedly reduced serum IGF-I levels in mice, lacking hepatic *Igf1* gene expression, are associated with reduced kidney growth in spite of elevated GH levels [41,42]. *5)* Overexpression of IGFBP-2, a presumed inhibitor of IGF-I action, causes a marked inhibition of renal growth in GB *vs*. G mice [7].

The differences in renal weight of mice of the four genetic groups included in this study were not attributable to changed numbers of nephrons. Concerning G mice, this result was expected, as MT-bGH transgenic mice also do not exhibit changed nephron numbers [229], despite the earlier expression of the MT promoter (at embryonic day 13 [331], whereas the PEPCK promoter is expressed from birth on-wards [81]). As perinatal commenced IGFBP-1 overexpression in mice is reported to be associated with reduced nephron numbers, this parameter needed to be assessed in the present study. Even normal (non-transgenic) mice born from IGFBP-1 transgenic mothers have reduced nephron numbers due to prenatally reduced IGF-I levels [243]. In the present study, neither bGH nor IGFBP-2 transgene expression influenced the nephron numbers, and the nephron number in the kidneys of mice born from IGFBP-2 transgenic mothers was not different from those born from wild-type mothers in previous studies [229].

The present study analyzed the renal sites of action of bGH and IGFBP-2 excess on suborgan and cellular level using quantitative-stereological methods. The volume fractions of the renal zones did not or only slightly differ between the four genetic groups. Unchanged or slightly changed cortical and medullar volume fractions have also been observed in adult rats with renal hypertrophy due to STZ-induced diabetes mellitus, or due to unilateral nephrectomy [332]. Renal hypertrophy in these models is known to be associated with elevated renal IGF-I immunoreactivity [194].

The renal hypertrophy observed in G mice of the present study was due to an increase of the absolute volumes of all renal zones. However, the enlarged cortex and OSM relatively and absolutely contributed most to bGH-induced renal hypertrophy of G mice of both ages (38- and 75-day-old). The enlargement of the cortex and OSM was mainly due to an increase of the proximal tubular epithelium (PTE). As shown in 75-day-old G mice, the increase of the cortical PTE was exclusively caused by PTE cell hyperplasia (90% increase in total cell number), whereas the mean volume of PTE cells was not affected.

As proximal tubular epithelia express both the GHR and IGF-IR, principally both direct and indirect - *via* IGF-I - effects of GH may be responsible for the increase in total PTE cell number. However, the PTE cell hyperplasia most likely reflects an IGF-I mediated effect of GH rather than a direct GH effect for several reasons. *1) In vivo*, renal cellular hyperplasia in rats can be achieved by administration of both GH and IGF-I [255]. *2)* GH binding results in activation of phospholipase C in PTE cells, however, no direct growth promoting effect on PTE cells has been demonstrated for GH [18,333]. *3) In vitro*, IGF-I is a strong mitogen for PTE cells and promotes proliferation of PTE cells of various species [249-252] *via* activation of the IGF-I receptor [250,253]. *4)* IGFBP-2, a presumed inhibitor of IGF actions markedly reduced the absolute volume of PTE in the cortex and OSM as well as the total number of PTE cells in the cortex in GH/IGF-I excess conditions (see below), but not in a normal GH/IGF-I background.

IGFBP-2 transgene coexpression markedly inhibited the total volume of PTE in both 38- and 75-day-old GB *vs*. G mice, further, in 75-day-old GB *vs*. G mice significantly reduced the total number of cortical PTE cells (18% decrease in total cell number), while the mean volume of cortical PTE cells was unaffected. This finding is in line

with a study demonstrating that IGFBP-2 together with IGFBP-4 and -5 is capable to inhibit the mitogenic activity of IGF-I in cultured rabbit PTE cells [252].

The molecular pathways, by which IGF-I and IGFBP-2 act on hyperplasia of PTE cells remain speculative so far. As shown in rabbit PTE cells, IGF-I binding causes phosphorylation of the IGF-IR tyrosine kinase and a dose-dependent increase in PTE cell number [334]. Several signal transduction pathways that promote cell growth and survival lay downstream of the IGF receptor tyrosine kinase [254]. Protein synthesis represents a requirement for cellular growth. IGF-I induces protein synthesis in murine PTE cells, which is dependent on the activation of the PI (3) K/ Akt pathway and ERK1/2-type MAP kinase pathway [335]. Furthermore, IGF-I has an anti-apoptotic effect on PTE cells, as shown in a rat cell culture study. This anti-apoptotic effect of IGF-I is mediated by PI (3) K/ Akt dependent BAD phosphorylation [254]. The most likely mechanism, by which IGFPB-2 acts on GH-induced hyperplasia of PTE cells is by interfering with IGF-I, in that way sequestering IGF-I from the IGF-IR and thereby inhibiting its effects. Several *in vitro* studies support the concept of an IGF-dependent growth-inhibitory effect of IGFBP-2 [9]. Especially in PTE cells, IGFBP-2 together with IGFBP-4 and -5 inhibits IGF-I-induced cell proliferation [252].

Remarkably, the renal zonal composition and the cellular growth investigated in this study were not different between B and C mice, indicating a modulatory effect of IGFBP-2 overexpression on the growth of renal structures only in stimulated growth conditions. Further investigations will be required in order to determine the molecular pathways of IGFBP-2 actions in PTE cells, and to address, whether IGFBP-2 affects IGF-I-induced proliferation or survival of PTE cells, or both.

The effects of IGFBP-2 overexpression were in coincidence with a 4.4-fold increase of IGFBP-2 binding activity in the cortex in GB *vs*. C mice. Remarkably, IGFBP-2 mRNA was not detected in PTE cells of GB mice, as demonstrated by *in situ* hybridization. Therefore, a systemic effect of high IGFBP-2 on growth of the PTE cells is assumed. Consistent with this assumption, PTE cells of B and GB mice showed a strong granular IGFBP-2 immunostaining using IHC, implicating tubular absorption and intracellular granular storage of ultrafiltrated IGFBP-2. No IGFBP-2 expression was detectable in PTE cells in C mice, which is in line with previous findings [212]. However, Lindenbergh-Kortleve *et al*. [212] detected predominant IGFBP-2 expression in the thin limbs of Henle's Loop of the mature kidney using *in situ* hybridization,

which was not observed in this study. Conflicting data concerning renal IGFBP-2 expression also derive from Northern blot analyses. IGFBP-2 mRNA was found in the kidneys of 28-day-old BALB/c mice [336], whereas no renal endogenous IGFBP-2 expression was found by Northern blot hybridization in C mice in a previous study [152]. The IGFBP expression pattern is known to be developmentally influenced [18,65]. If there are also strain specific differences in IGFBP expression, which could explain the divergent findings, remain to be elucidated.

In human patients and experimental animals with an increased permeability of the glomerular filtration barrier, *e.g.*, in the nephrotic syndrome, ultrafiltration of the smaller (45 kDa) IGF-IGFBP complexes raises and a larger amount of IGF-I is excreted in the urine [337]. This has led to the thesis that the increased tubular cell exposure to filtrated IGF-I may contribute to the tubulointerstitial disease that develops in most heavy proteinuric states [223]. As intact IGFBP-3 levels are decreased in the serum of individuals suffering from chronic renal failure (CRF), but IGFBP-2 levels are elevated [74,266], due to an increased hepatic IGFBP-2 synthesis [269], IGF-I shifts toward the smaller IGF-IGFBP-2 binary complex, which is more readily filtered than the larger ternary complex [337]. In nephrotic rats, IGF-I is ultra-filtrated predominantly in conjunction with IGFBP-2 and is present in proximal tubular fluid at 1.35 nM. The ultrafiltrated IGF-I has been shown to increase proliferation of cultured proximal tubular cells [220].

Cystogenesis in humans and experimental animals is associated with hyperplasia of tubular epithelia [338]. Acquired cystic kidney disease (ACKD) is the result of cyst formation in the failing kidney and displays a serious complication in longstanding CRF [338,339].

The findings of the present study demonstrate that high IGFBP-2 levels in GB mice are capable of inhibiting proximal tubular epithelial growth. The tubulocystic alterations occurring in GH transgenic mice represent a model for human ACKD [17]. In order to in depth characterize the relevance of elevated serum IGFBP-2 levels on renal tubular cyst formation, studies should address growth-modulating effects of IGFBP-2 on the proximal tubular epithelium in older GH transgenic mice.

In humans with multicystic renal dysplasia, the kidneys are characterized by a strong IGFBP-2 mRNA expression and IGFBP-2 immunoreactivity, both limited exclusively

to cyst epithelia [13]. Thus, the proposed growth promoting effect of IGFBP-2 in multicystic renal dysplasia seems to be in contrast to the anti-proliferative effect of high IGFBP-2 levels on PTE cells observed in this study. However, the effects of IGFBP-2 overexpression of both studies cannot be directly compared, as in the human study, fetal and early postnatal organs were analyzed, whereas in this study, juvenile-adult and adult kidneys were examined. Thus, potential development-specific effects of components of the GH/IGF-axis cannot be excluded and might be responsible for the different outcome of high IGFBP-2 levels in proximal tubules [18,65]. Further, in human multicystic renal dysplasia, the cyst epithelia were demonstrated to be dedifferentiated and may be better suited to proliferation [13]. Contrary, in mice of this study, no signs of dedifferentiation of PTE cells were observed.

GH overexpression in mice is known to be associated with the development of pro-gressive glomerular hypertrophy, which is overproportional as a function of either body or kidney weight, and associated with the development of glomerulosclerosis [79,85,229]. The present findings concerning glomerular alterations in G mice are consistent with those of previous studies. In contrast to its substantial growth inhibitory potency concerning the proximal tubular epithelium, IGFBP-2 overexpression in both 38- and 75-day-old GB *vs*. G mice reduced GH-induced glomerular enlargement only to a minor degree (~10%). The failure of IGFBP-2 in limiting glomerular growth became even more evident, when the glomerular volume was related to either body- or kidney weight, or total PTE volume. Thus, IGFBP-2 excess dissociates the effects of high GH/IGF-I levels on growth of renal structures, namely on that of the PTE and of glomeruli. Contrary, under normal growth conditions, IGFBP-2 overexpression had no significant effect on glomerular parameters investigated in this study.

Manifest glomerulosclerosis including hyalinosis, capillary obliteration and synechia formation was rarely observed in the GH overexpressing animals of this study, due to the young age of the mice investigated. Thus, the increase in the glomerulosclerosis-index of G as well as of GB mice was above all due to mesangial matrix accumulation. An accumulation of mesangial matrix was also confirmed by immunohistochemistry, which demonstrated mesangial accumulation of type IV collagen, laminin, and fibronectin of similar extend in both G and GB mice of the present study (Fisch, T. M., Wolf, E., Wanke, R., unpublished data). The

glomerulosclerosis-index of G and GB mice was not significantly different. This finding was not unexpected, since glomerular hypertrophy, as a key event in formation of progressive glomerulosclerosis [227,229], was not severely affected by IGFBP-2 coexpression in GB *vs*. G mice.

Interestingly, the degree of inhibition of GH/IGF-I-induced glomerular hypertrophy in GB *vs*. G mice (~10%) through overexpression of IGFBP-2, a presumed inhibitor of IGF-I actions, ranges in the same magnitude as the degree of stimulation of glomerular growth (~30%) through IGF-I overexpression in seven-week-old MT-IGF-I transgenic mice [85]. This implies that elevated levels of IGF-I would only marginally contribute to glomerular hypertrophy. However, a true statement about the contributions of GH and IGF-I to glomerular hypertrophy (and subsequent sclerosis) from a comparison of these models is not allowed for several reasons, such as different patterns of transgene-derived and/or endogenous IGF-I and/or GH expression in IGF-I *vs*. GH transgenic mice, or various side effects of the expression of the transgenes that cannot be assessed completely [72]. For example, IGF-I overexpression in transgenic mice is associated with an inhibited expression of endogenous GH and IGF-I [126]. *In vitro* studies show that high IGF-I levels stimulate IGFBP-2 secretion by murine mesangial cells, maybe to protect themselves from excessive IGF-I stimulation [12], which may also occur *in vivo*. IGF-I is known to stimulate mesangial cell proliferation and matrix production [340,341], which are characteristics of GH-induced glomerular hypertrophy and sclerosis [229]. Contrary, high GH levels are known to reduce endogenous IGFBP-2 levels [117,118], thereby probably exposing mesangial cells to disproportionate stimulation through IGF-I. Such an effect was demonstrated *in vitro* for high levels of glucose, which reduced IGFBP-2 synthesis of mesangial cells, in the presence or absence of elevated IGF-I levels [12]. In the present study, no IGFBP-2 mRNA or IGFBP-2 could be detected by *in situ* hybridization or by immunohistochemistry, respectively, within mesangial cells of mice of the four genetic groups investigated. Within the glomerulus, IGFBP-2 immunoreactivity was found only in podocytes of B and GB mice and was most likely attributable to absorption of filtrated IGFBP-2.

The results of urine protein analysis were in line with the alterations of glomerular morphology. Both G and GB mice displayed selective glomerular proteinuria. IGFBP-2 overexpression in B *vs*. C and GB *vs*. G mice did not alter the pattern of

proteinuria. Severe albuminuria in GH transgenic mice is attributed to glomerular changes leading to an increased glomerular filtration of albumin [85,229]. The age-related increase in urinary albumin excretion in G and GB mice reflects the progression of glomerular lesions. In 75-day-old GB mice, the urinary albumin concentration and urinary albumin/creatinine-ratio was significantly elevated when compared to G mice. This fact may be explained by a lowered capacity of tubular protein reabsorption due to the markedly reduced total volume of the proximal tubular epithelia in GB *vs*. G mice. C and B mice displayed a physiologic microalbuminuria.

Urine of bGH overexpressing mice displayed reduced concentrations of major urinary proteins (MUPs), which is a characteristic finding in GH transgenic mice [229]. Normal MUP synthesis requires a pulsatile GH secretion, whereas constant high GH levels cause a reduction in hepatic synthesis of MUPs [342,343]. MUPs are liver synthesized pheromone-binding proteins, which are physiologically excreted and play complex roles in chemosensory signaling among rodents [344].

In conclusion, the collective of mice used in this study represents a valuable model for unraveling the roles of components of the GH/IGF-axis in growth regulation *in vivo*. The findings of the present study demonstrate that excess of GH/IGF-I results in renal and adrenal enlargement *via* cellular hyperplasia or cellular hyperplasia linked to hypertrophy indicating a cell type-dependent growth response. Likewise, high IGFBP-2 levels modulate cellular growth in a cell type-specific fashion. Demonstrating a clear-cut effect, IGFBP-2 exclusively inhibited GH/IGF-I-induced hypertrophy but not hyperplasia of adrenal zona fasciculata cells. In contrast, high IGFBP-2 levels inhibited GH/IGF-I-induced hyperplasia of PTE cells without affecting PTE cell size. This selective modulation of cellular growth parameters represents an important new facet in the spectrum of IGFBP-2 actions.

As shown in this study, transgenic overexpression strategies can be elegantly used to characterize the potential of individual genes involved in the regulation of growth. Nevertheless, the current IGFBP overexpression models are limited, as they have been established on different genetic backgrounds, with different expression vectors and copy numbers that have been integrated randomly into the genome. Thus, it cannot be excluded that some of the observed phenotypic alterations are related to strain-specific factors. Strategies for future studies should aim to target the respective

transgene to a specific locus in the genome, avoiding position effects that may markedly influence the activity of a transgene [5]. Furthermore, the analysis of polygenic models resulting from phenotypic selection may be interesting for understanding the physiology of IGFBPs and their interactions with other biological systems involved in growth regulation.

6 Summary

Effects of insulin-like growth factor-binding protein-2 (IGFBP-2) overexpression on adrenal and renal growth processes and functions: findings in transgenic mouse models

The growth hormone (GH)/insulin-like growth factor- (IGF-) axis plays a crucial role in adrenal and renal growth and function and is intimately involved in the pathogenesis of various diseases of the adrenal gland and kidney. The functions of IGF binding proteins (IGFBPs) have been studied extensively *in vitro*, revealing IGF-dependent and also IGF-independent effects on cell growth, differentiation, and survival. In contrast, the biological relevance of IGFBPs *in vivo* is only partially understood. IGFBP-2 is the second most abundant IGFBP in the circulation and acts as a growth inhibitor *in vivo* in mice.

This study investigates the effects of IGFBP-2 on growth and function of the adrenal gland and the kidney under normal and GH/IGF-I stimulated growth conditions. For that purpose, hemizygous cytomegalovirus (CMV)-promoter murine (m) IGFBP-2 transgenic mice were crossed with hemizygous phosphoenolpyruvate carboxykinase (PEPCK)-promoter bovine (b) GH transgenic mice, generating four genetic groups of offsping: mice carrying both transgenes (GB), a single mIGFBP-2 (B) or bGH transgene (G), and non-transgenic controls (C). The kidneys and adrenal glands of male individuals at the age of 38 and 75 days were analyzed, using qualitative morphological and quantitative-stereological methods. In addition, *in situ* hybridization, immunohistochemistry and Western ligand blot analysis of the kidney were performed. The investigations further included the measurement of various serum and urine parameters.

The absolute weight of the adrenal glands was significantly increased in 75-day-old G *vs*. C and B mice. This adrenal enlargement was found to involve both hypertrophy (44% increase in mean cell volume) and hyperplasia (50% increase in cell number) of zona fasciculata cells. IGFBP-2 overexpression in GB mice significantly reduced bGH-induced adrenal enlargement. bGH-induced hypertrophy of zona fasciculata cells was completely abolished in GB mice, whereas hyperplasia was not affected. Basal and ACTH-induced plasma corticosterone levels of four-month-old G mice, but

not of GB mice, were 2- to 3-fold increased as compared to C mice. Plasma ACTH levels were similar in all groups.

The absolute kidney weight was significantly increased in 38- and 75-day-old G *vs*. C and B mice. This renal enlargement was found to be mainly due to stimulated growth of the cortex and the outer stripe of the medulla. The increased volume of these two renal zones was primarily the consequence of an increased volume of the proximal tubular epithelium (PTE). Determination of the mean volume and total number of cortical PTE cells in 75-day-old G mice revealed that this increase was exclusively due to PTE cell hyperplasia (90% increase in cell number), whereas the mean PTE cell volume was unaffected. Comparing the findings of GB mice with those of G mice revealed that overexpression of IGFBP-2 significantly reduced renal enlargement and total PTE volume in both age groups. bGH-induced hyperplasia of PTE cells was selectively inhibited in 75-day-old GB mice without affecting cell size. Glomerular hypertrophy observed in G mice was only slightly reduced by coexpression of IGFBP-2 in GB mice and glomerular damage was not affected.

The results of the present study demonstrate that overexpression of IGFBP-2 modulates cellular growth in a cell type-specific fashion *in vivo*. The findings represent an important new facet in the spectrum of IGFBP-2 actions. Therefore the transgenic mice included in this study are considered as valuable models for unraveling the mechanisms involved in regulation of cell size and cell number.

7 Zusammenfassung

Effekte einer Überexpression des insulin-like growth factor Bindungsproteins-2 (IGFBP-2) auf adrenale und renale Wachstumsprozesse und Funktionen: An transgenen Mausmodellen erhobene Befunde

Das Wachstumshormon (growth hormone; GH)/insulin-like growth factor- (IGF-) System ist maßgeblich an der Regulation adrenaler und renaler Wachstumsprozesse beteiligt und spielt eine wesentliche Rolle in der Pathogenese verschiedener Erkrankungen der Nebenniere und Niere. Die Funktion der IGF Bindungsproteine (IGFBPs) wurde intensiv *in vitro* untersucht. Dabei zeigten sich sowohl IGF-abhängige als auch IGF-unabhängige Effekte auf das Wachstum, die Differenzierung und das Überleben von Zellen. Die biologische Relevanz der IGFBPs *in vivo* ist dagegen bislang weitgehend ungeklärt. IGFBP-2 ist das in der Zirkulation am zweit-häufigsten vorkommende IGFBP und erwies sich in Untersuchungen an Mäusen als Wachstumsinhibitor.

Ziel dieser Studie war es, die Effekte von IGFBP-2 auf das Wachstum und die Funktion der Nebenniere und der Niere unter normalen und GH/IGF-I stimulierten Wachstumsbedingungen zu untersuchen. Zu diesem Zweck wurden Mäuse, die murines (m) IGFBP-2 unter der Kontrolle des Cytomegalievirus (CMV)-Promotors exprimieren, mit Mäusen gekreuzt, die bovines (b) GH unter der Kontrolle des Phosphoenolpyruvatkarboxykinase (PEPCK)-Promotors exprimieren. Aus dieser Anpaarung resultierende Nachkommen gehörten vier genetischen Gruppen an: doppelt transgene Mäuse (GB), einfach mIGFBP-2 (B) oder bGH transgene (G) Mäuse, und nicht-transgene Kontrolltiere (C). Die Nieren und Nebennieren wurden mittels qualitativer morphologischer und quantitativ-stereologischer Methoden untersucht. Die Nieren wurden zusätzlich mittels *in situ* Hybridisierung, Immun-histochemie und Western Ligandenblot analysiert. Weiterhin wurden verschiedene Serum- und Urinparameter bestimmt.

Das absolute Gewicht der Nebennieren von 75 Tage alten G Mäusen war im Vergleich zu C und B Mäusen signifikant erhöht. Das erhöhte Nebennierenvolumen beinhaltete sowohl eine Hypertrophie (44% Zunahme der Zellzahl) als auch eine Hyperplasie (50% Zunahme des mittleren Zellvolumens) von Zona fasciculata Zellen.

Die Überexpression von IGFBP-2 führte bei GB Mäusen im Vergleich zu G Mäusen zu einer signifikanten Reduktion des Nebennierenvolumens. Die GH-induzierte Hypertrophie der Zona fasciculata Zellen wurde vollständig gehemmt, wohingegen die Hyperplasie nicht beeinflusst war. Basale und ACTH-induzierte Plasmakortikosteronspiegel von vier Monate alten G Mäusen, nicht jedoch die von GB Mäusen, waren im Vergleich zu C Mäusen 2- bis 3-fach erhöht. Die Plasma ACTH Spiegel der vier genetischen Gruppen waren nicht signifikant verschieden.

Das Nierengewicht war bei 38 und 75 Tage alten G Mäusen im Vergleich zu C und B Mäusen signifikant erhöht. Diese Erhöhung des Nierengewichts resultierte überwiegend aus einer Stimulation des Wachstums des Kortex und des Außenstreifens der Medulla. Die Vergrößerung dieser beiden Zonen beruhte vornehmlich auf der Zunahme des Volumens des proximalen Tubulusepithels (PTE). Die Bestimmung des mittleren Volumens und der absoluten Anzahl von PTE-Zellen ergab, dass der Anstieg des Volumens des PTE in G versus C Mäusen ausschließlich durch eine Hyperplasie der PTE Zellen verursacht war (90% Anstieg der Zellzahl), während das mittlere PTE-Zellvolumen nicht beeinflusst war. Ein Vergleich der an GB und G Mäusen erhobenen Befunde zeigte, dass die Überexpression von IGFBP-2 in beiden Altersgruppen zu einer signifikanten Reduktion des Nierengewichts und des Volumens des PTE führte. Die bGH-induzierte Hyperplasie der PTE Zellen 75 Tage alter G Mäuse war durch IGFBP-2 Überexpression in GB Tieren selektiv gehemmt, wohingegen das mittlere Volumen der PTE Zellen unbeeinflusst blieb. Die bei G Mäusen beobachtete glomeruläre Hypertrophie wurde durch die Koexpression von IGFBP-2 nur geringgradig reduziert und der glomeruläre Schädigungsgrad wurde nicht beeinflußt.

Die Befunde der vorliegenden Studie demonstrieren eine durch Überexpression von IGFBP-2 bedingte Zelltyp-spezifische Modulation von zellulärem Wachstum. Die Ergebnisse stellen einen wesentlichen, neuen Aspekt in der Wirkungsweise von IGFBP-2 dar. Die in dieser Studie verwendeten transgenen Mäuse werden daher als wertvolle Modelle angesehen, um die an der Regulation von Zellgröße und -zahl beteiligten Mechanismen zu entschlüsseln.

8 References

1. Le Roith, D., Bondy, C., Yakar, S., Liu, J. L. & Butler, A. The somatomedin hypothesis: 2001. *Endocr Rev* **22**, 53-74. (2001).
2. Jones, J. I. & Clemmons, D. R. Insulin-like growth factors and their binding proteins: biological actions. *Endocr Rev* **16**, 3-34. (1995).
3. Rosenzweig, S. A. What's new in the IGF-binding proteins? *Growth Horm IGF Res* **14**, 329-36 (2004).
4. Rajaram, S., Baylink, D. J. & Mohan, S. Insulin-like growth factor-binding proteins in serum and other biological fluids: regulation and functions. *Endocr Rev* **18**, 801-31. (1997).
5. Wolf, E., Schneider, M. R., Zhou, R., Fisch, T. M., Herbach, N., Dahlhoff, M., Wanke, R., Hoeflich, A. Functional consequences of IGFBP excess - lessons from transgenic mice. *Pediatr Nephrol* (*in press*).
6. Hoeflich, A. Funktionelle Analyse von IGFBP-2 in vitro und in vivo. *Habilitationsschrift. University of Munich* (2001).
7. Hoeflich, A., Nedbal, S., Blum, W. F., Erhard, M., Lahm, H., Brem, G., Kolb, H. J., Wanke, R. & Wolf, E. Growth inhibition in giant growth hormone transgenic mice by overexpression of insulin-like growth factor-binding protein-2. *Endocrinology* **142**, 1889-98. (2001).
8. Weber, M. M., Fottner, C., Schmidt, P., Brodowski, K. M., Gittner, K., Lahm, H., Engelhardt, D. & Wolf, E. Postnatal overexpression of insulin-like growth factor II in transgenic mice is associated with adrenocortical hyperplasia and enhanced steroidogenesis. *Endocrinology* **140**, 1537-43. (1999).
9. Hoeflich, A., Reisinger, R., Lahm, H., Kiess, W., Blum, W. F., Kolb, H. J., Weber, M. M. & Wolf, E. Insulin-like growth factor-binding protein 2 in tumorigenesis: protector or promoter? *Cancer Res* **61**, 8601-10. (2001).
10. Hoeflich, A., Fettscher, O., Lahm, H., Blum, W. F., Kolb, H. J., Engelhardt, D., Wolf, E. & Weber, M. M. Overexpression of insulin-like growth factor-binding protein-2 results in increased tumorigenic potential in Y-1 adrenocortical tumor cells. *Cancer Res* **60**, 834-8. (2000).
11. Tonshoff, B., Blum, W. F., Wingen, A. M. & Mehls, O. Serum insulin-like growth factors (IGFs) and IGF binding proteins 1, 2, and 3 in children with chronic renal failure: relationship to height and glomerular filtration rate. The European Study Group for Nutritional Treatment of Chronic Renal Failure in Childhood. *J Clin Endocrinol Metab* **80**, 2684-91. (1995).
12. Horney, M. J., Shirley, D. W., Kurtz, D. T. & Rosenzweig, S. A. Elevated glucose increases mesangial cell sensitivity to insulin-like growth factor I. *Am J Physiol* **274**, F1045-53. (1998).
13. Matsell, D. G., Bennett, T., Goodyer, P., Goodyer, C. & Han, V. K. The pathogenesis of multicystic dysplastic kidney disease: insights from the study of fetal kidneys. *Lab Invest* **74**, 883-93 (1996).
14. Wanke, R., Wolf, E., Brem, G., Hermanns, W. Physiology and pathology of growth - studies in GH transgenic mice. *J Anim Breed Genet* **113**, 445-456 (1996).
15. Cecim, M., Alvarez-Sanz, M., Van de Kar, L., Milton, S. & Bartke, A. Increased plasma corticosterone levels in bovine growth hormone (bGH) transgenic mice: effects of ACTH, GH and IGF-I on in vitro adrenal corticosterone production. *Transgenic Res* **5**, 187-92. (1996).

16. Cecim, M., Ghosh, P. K., Esquifino, A. I., Begam, T., Wagner, T. E., Yun, J. S. & Bartke, A. Elevated corticosterone levels in transgenic mice expressing human or bovine growth hormone genes. *Neuroendocrinology* **53**, 313-6. (1991).

17. Wolf, E. W., R. Growth hormone overproduction in transgenic mice: Phenotypic alterations and deduced animal models. In: *Welfare aspects of transgenic animals* (van Zutphen, L. F. M., van der Meer, M., edts.) Springer Verlag, Berlin. (1997).

18. Feld, S. & Hirschberg, R. Growth hormone, the insulin-like growth factor system, and the kidney. *Endocr Rev* **17**, 423-80. (1996).

19. Kopchick, J. J. & Andry, J. M. Growth hormone (GH), GH receptor, and signal transduction. *Mol Genet Metab* **71**, 293-314 (2000).

20. Robinson, I. C. The growth hormone secretory pattern: a response to neuroendocrine signals. *Acta Paediatr Scand Suppl* **372**, 70-8; discussion 79-80 (1991).

21. Clark, R. G., Carlsson, L. M. & Robinson, I. C. Growth hormone secretory profiles in conscious female rats. *J Endocrinol* **114**, 399-407 (1987).

22. Chene, N., Martal, J., de la Llosa, P. & Charrier, J. Growth hormones. II. Structure-function relationships. *Reprod Nutr Dev* **29**, 1-25 (1989).

23. Muller, E. E., Locatelli, V. & Cocchi, D. Neuroendocrine control of growth hormone secretion. *Physiol Rev* **79**, 511-607 (1999).

24. Tuggle, C. K. & Trenkle, A. Control of growth hormone synthesis. *Domest Anim Endocrinol* **13**, 1-33 (1996).

25. Scacchi, M., Ida Pincelli, A. & Cavagnini, F. Nutritional status in the neuroendocrine control of growth hormone secretion: the model of anorexia nervosa. *Front Neuroendocrinol* **24**, 200-24 (2003).

26. Bermann, M., Jaffe, C. A., Tsai, W., DeMott-Friberg, R. & Barkan, A. L. Negative feedback regulation of pulsatile growth hormone secretion by insulin-like growth factor I. Involvement of hypothalamic somatostatin. *J Clin Invest* **94**, 138-45 (1994).

27. Zhang, Y., Jiang, J., Kopchick, J. J. & Frank, S. J. Disulfide linkage of growth hormone (GH) receptors (GHR) reflects GH-induced GHR dimerization. Association of JAK2 with the GHR is enhanced by receptor dimerization. *J Biol Chem* **274**, 33072-84 (1999).

28. Martinez, V., Balbin, M., Ordonez, F. A., Rodriguez, J., Garcia, E., Medina, A. & Santos, F. Hepatic expression of growth hormone receptor/binding protein and insulin-like growth factor I genes in uremic rats. Influence of nutritional deficit. *Growth Horm IGF Res* **9**, 61-8 (1999).

29. Shuto, Y., Nakano, T., Sanno, N., Domoto, H., Sugihara, H. & Wakabayashi, I. Reduced growth hormone receptor messenger ribonucleic acid in an aged man with chronic malnutrition and growth hormone resistance. *J Clin Endocrinol Metab* **84**, 2320-3 (1999).

30. Bennett, P. A., Levy, A., Carmignac, D. F., Robinson, I. C. & Lightman, S. L. Differential regulation of the growth hormone receptor gene: effects of dexamethasone and estradiol. *Endocrinology* **137**, 3891-6 (1996).

31. Meinhardt, U., Eble, A., Besson, A., Strasburger, C. J., Sraer, J. D. & Mullis, P. E. Regulation of growth-hormone-receptor gene expression by growth hormone and pegvisomant in human mesangial cells. *Kidney Int* **64**, 421-30 (2003).

32. Dastot, F., Duquesnoy, P., Sobrier, M. L., Goossens, M. & Amselem, S. Evolutionary divergence of the truncated growth hormone receptor isoform in its ability to generate a soluble growth hormone binding protein. *Mol Cell Endocrinol* **137**, 79-84 (1998).

33. Baumann, G., Amburn, K. & Shaw, M. A. The circulating growth hormone (GH)-binding protein complex: a major constituent of plasma GH in man. *Endocrinology* **122**, 976-84 (1988).

34. Hokken-Koelega, A. C., Hackeng, W. H., Stijnen, T., Wit, J. M., de Muinck Keizer-Schrama, S. M. & Drop, S. L. Twenty-four-hour plasma growth hormone (GH) profiles, urinary GH excretion, and plasma insulin-like growth factor-I and -II levels in prepubertal children with chronic renal insufficiency and severe growth retardation. *J Clin Endocrinol Metab* **71**, 688-95 (1990).

35. Iida, K., Del Rincon, J. P., Kim, D. S., Itoh, E., Nass, R., Coschigano, K. T., Kopchick, J. J. & Thorner, M. O. Tissue-specific regulation of growth hormone (GH) receptor and insulin-like growth factor-I gene expression in the pituitary and liver of GH deficient (lit/lit) mice and transgenic mice that overexpress bGH or a bGH antagonist. *Endocrinology* (2004).

36. Chen, N. Y., Chen, W. Y. & Kopchick, J. J. Liver and kidney growth hormone (GH) receptors are regulated differently in diabetic GH and GH antagonist transgenic mice. *Endocrinology* **138**, 1988-94 (1997).

37. Nedbal, S. Effects and interactions of growth hormone (GH) and insulin-like growth factor-binding protein-2 (IGFBP-2) in transgenic mice. Thesis, University of Munich. (2001).

38. Blundell, T. L. & Humbel, R. E. Hormone families: pancreatic hormones and homologous growth factors. *Nature* **287**, 781-7 (1980).

39. Ohlsson, C., Sjogren, K., Jansson, J. O. & Isaksson, O. G. The relative importance of endocrine versus autocrine/paracrine insulin- like growth factor-I in the regulation of body growth. *Pediatr Nephrol* **14**, 541-3. (2000).

40. Dupont, J. & Holzenberger, M. Biology of insulin-like growth factors in development. *Birth Defects Res Part C Embryo Today* **69**, 257-71 (2003).

41. Yakar, S., Liu, J. L., Stannard, B., Butler, A., Accili, D., Sauer, B. & LeRoith, D. Normal growth and development in the absence of hepatic insulin-like growth factor I. *Proc Natl Acad Sci U S A* **96**, 7324-9. (1999).

42. Sjogren, K., Liu, J. L., Blad, K., Skrtic, S., Vidal, O., Wallenius, V., LeRoith, D., Tornell, J., Isaksson, O. G., Jansson, J. O. & Ohlsson, C. Liver-derived insulin-like growth factor I (IGF-I) is the principal source of IGF-I in blood but is not required for postnatal body growth in mice. *Proc Natl Acad Sci U S A* **96**, 7088-92. (1999).

43. Daughaday, W. H. Growth hormone axis overview--somatomedin hypothesis. *Pediatr Nephrol* **14**, 537-40. (2000).

44. Baxter, R. C. Insulin-like growth factor (IGF)-binding proteins: interactions with IGFs and intrinsic bioactivities. *Am J Physiol Endocrinol Metab* **278**, E967-76 (2000).

45. Pantaleon, M., Jericho, H., Rabnott, G. & Kaye, P. L. The role of insulin-like growth factor II and its receptor in mouse preimplantation development. *Reprod Fertil Dev* **15**, 37-45 (2003).

46. DaCosta, S. A., Schumaker, L. M. & Ellis, M. J. Mannose 6-phosphate/insulin-like growth factor 2 receptor, a bona fide tumor suppressor gene or just a promising candidate? *J Mammary Gland Biol Neoplasia* **5**, 85-94 (2000).

47. LeRoith, D., Werner, H., Beitner-Johnson, D. & Roberts, C. T., Jr. Molecular and cellular aspects of the insulin-like growth factor I receptor. *Endocr Rev* **16**, 143-63 (1995).

48. De Meyts, P., Wallach, B., Christoffersen, C. T., Urso, B., Gronskov, K., Latus, L. J., Yakushiji, F., Ilondo, M. M. & Shymko, R. M. The insulin-like growth factor-I receptor. Structure, ligand-binding mechanism and signal transduction. *Horm Res* **42**, 152-69 (1994).

49. Czech, M. P. Signal transmission by the insulin-like growth factors. *Cell* **59**, 235-8 (1989).

50. Tollefsen, S. E., Stoszek, R. M. & Thompson, K. Interaction of the alpha beta dimers of the insulin-like growth factor I receptor is required for receptor autophosphorylation. *Biochemistry* **30**, 48-54 (1991).

51. Mulroney, S. E., Haramati, A., Werner, H., Bondy, C., Roberts, C. T., Jr. & LeRoith, D. Altered expression of insulin-like growth factor-I (IGF-I) and IGF receptor genes after unilateral nephrectomy in immature rats. *Endocrinology* **130**, 249-56 (1992).

52. Werner, H., Shen-Orr, Z., Stannard, B., Burguera, B., Roberts, C. T., Jr. & LeRoith, D. Experimental diabetes increases insulinlike growth factor I and II receptor concentration and gene expression in kidney. *Diabetes* **39**, 1490-7 (1990).

53. Ludwig, T., Eggenschwiler, J., Fisher, P., D'Ercole, A. J., Davenport, M. L. & Efstratiadis, A. Mouse mutants lacking the type 2 IGF receptor (IGF2R) are rescued from perinatal lethality in Igf2 and Igf1r null backgrounds. *Dev Biol* **177**, 517-35 (1996).

54. Nissley, S. P., Kiess, W., Sklar, M., M. The insulin-like growth factor II/mannose-6-phosphate receptor: In: LeRoith, D. (eds.) Insulin-like growth factors: Cellular and Molecular Aspects. CRC Press, Boca Raton. 111-150 (1991).

55. Funk, B., Kessler, U., Eisenmenger, W., Hansmann, A., Kolb, H. J. & Kiess, W. Expression of the insulin-like growth factor-II/mannose-6-phosphate receptor in multiple human tissues during fetal life and early infancy. *J Clin Endocrinol Metab* **75**, 424-31 (1992).

56. Pfuender, M., Sauerwein, H., Funk, B., Kessler, U., Barenton, B., Schwarz, H. P., Hoeflich, A. & Kiess, W. The insulin-like growth factor-II/mannose-6-phosphate receptor is present in fetal bovine tissues throughout gestation. *Domest Anim Endocrinol* **12**, 317-24 (1995).

57. Sklar, M. M., Thomas, C. L., Municchi, G., Roberts, C. T., Jr., LeRoith, D., Kiess, W. & Nissley, P. Developmental expression of rat insulin-like growth factor-II/mannose 6-phosphate receptor messenger ribonucleic acid. *Endocrinology* **130**, 3484-91 (1992).

58. Kim, H. S., Nagalla, S. R., Oh, Y., Wilson, E., Roberts, C. T., Jr. & Rosenfeld, R. G. Identification of a family of low-affinity insulin-like growth factor binding proteins (IGFBPs): characterization of connective tissue growth factor as a member of the IGFBP superfamily. *Proc Natl Acad Sci U S A* **94**, 12981-6. (1997).

59. Hwa, V., Oh, Y. & Rosenfeld, R. G. The insulin-like growth factor-binding protein (IGFBP) superfamily. *Endocr Rev* **20**, 761-87. (1999).

60. Rosenfeld, R. G., Hwa, V., Wilson, L., Lopez-Bermejo, A., Buckway, C., Burren, C., Choi, W. K., Devi, G., Ingermann, A., Graham, D., Minniti, G.,

Spagnoli, A. & Oh, Y. The insulin-like growth factor binding protein superfamily: new perspectives. *Pediatrics* **104**, 1018-21. (1999).

61. Baxter, R. C., Binoux, M., Clemmons, D. R., Conover, C., Drop, S. L., Holly, J. M., Mohan, S., Oh, Y. & Rosenfeld, R. G. Recommendations for nomenclature of the insulin-like growth factor binding protein (IGFBP) superfamily. *Growth Horm IGF Res* **8**, 273-4 (1998).

62. Ferry, R. J., Jr., Cerri, R. W. & Cohen, P. Insulin-like growth factor binding proteins: new proteins, new functions. *Horm Res* **51**, 53-67 (1999).

63. Boisclair, Y. R., Rhoads, R. P., Ueki, I., Wang, J. & Ooi, G. T. The acid-labile subunit (ALS) of the 150 kDa IGF-binding protein complex: an important but forgotten component of the circulating IGF system. *J Endocrinol* **170**, 63-70. (2001).

64. Twigg, S. M. & Baxter, R. C. Insulin-like growth factor (IGF)-binding protein 5 forms an alternative ternary complex with IGFs and the acid-labile subunit. *J Biol Chem* **273**, 6074-9 (1998).

65. Firth, S. M. & Baxter, R. C. Cellular actions of the insulin-like growth factor binding proteins. *Endocr Rev* **23**, 824-54 (2002).

66. Guler, H. P., Zapf, J., Schmid, C. & Froesch, E. R. Insulin-like growth factors I and II in healthy man. Estimations of half-lives and production rates. *Acta Endocrinol (Copenh)* **121**, 753-8 (1989).

67. Hodgkinson, S. C., Davis, S. R., Moore, L. G., Henderson, H. V. & Gluckman, P. D. Metabolic clearance of insulin-like growth factor-II in sheep. *J Endocrinol* **123**, 461-8 (1989).

68. Hoeflich, A., Reisinger, R., Schuett, B. S., Elmlinger, M. W., Russo, V. C., Vargas, G. A., Jehle, P. M., Lahm, H., Renner-Muller, I. & Wolf, E. Peri/nuclear localization of intact insulin-like growth factor binding protein-2 and a distinct carboxyl-terminal IGFBP-2 fragment in vivo. *Biochem Biophys Res Commun* **324**, 705-10 (2004).

69. Clemmons, D. R. Role of insulin-like growth factor binding proteins in controlling IGF actions. *Mol Cell Endocrinol* **140**, 19-24. (1998).

70. Rajah, R., Katz, L., Nunn, S., Solberg, P., Beers, T., Cohen, P. Insulin-like growth factor binding protein proteases: Functional regulators of cell growth. *Prog Growth Factor Res* **6**, 273-284 (1996).

71. Conlon, I. & Raff, M. Size control in animal development. *Cell* **96**, 235-44. (1999).

72. Wolf, E., Lahm, H., Wu, M., Wanke, R. & Hoeflich, A. Effects of IGFBP-2 overexpression in vitro and in vivo. *Pediatr Nephrol* **14**, 572-8. (2000).

73. Weber, M. M., Fottner, C. & Wolf, E. The role of the insulin-like growth factor system in adrenocortical tumourigenesis. *Eur J Clin Invest* **30 Suppl 3**, 69-75. (2000).

74. Tonshoff, B., Blum, W. F. & Mehls, O. Serum insulin-like growth factors and their binding proteins in children with end-stage renal disease. *Pediatr Nephrol* **10**, 269-74. (1996).

75. Lupu, F., Terwilliger, J. D., Lee, K., Segre, G. V. & Efstratiadis, A. Roles of growth hormone and insulin-like growth factor 1 in mouse postnatal growth. *Dev Biol* **229**, 141-62 (2001).

76. Schneider, M. R., Lahm, H., Wu, M., Hoeflich, A. & Wolf, E. Transgenic mouse models for studying the functions of insulin-like growth factor-binding proteins. *Faseb J* **14**, 629-40. (2000).

77. Murphy, L. J. & Silha, J. V. Unexpected and unexplained phenotypes in transgenic models. *Growth Horm IGF Res* **10**, 233-5 (2000).

78. Palmiter, R. D., Brinster, R. L., Hammer, R. E., Trumbauer, M. E., Rosenfeld, M. G., Birnberg, N. C. & Evans, R. M. Dramatic growth of mice that develop from eggs microinjected with metallothionein-growth hormone fusion genes. *Nature* **300**, 611-5. (1982).

79. Brem, G., Wanke, R., Wolf, E., Buchmuller, T., Muller, M., Brenig, B. & Hermanns, W. Multiple consequences of human growth hormone expression in transgenic mice. *Mol Biol Med* **6**, 531-47. (1989).

80. Palmiter, R. D., Norstedt, G., Gelinas, R. E., Hammer, R. E. & Brinster, R. L. Metallothionein-human GH fusion genes stimulate growth of mice. *Science* **222**, 809-14 (1983).

81. McGrane, M. M., de Vente, J., Yun, J., Bloom, J., Park, E., Wynshaw-Boris, A., Wagner, T., Rottman, F. M. & Hanson, R. W. Tissue-specific expression and dietary regulation of a chimeric phosphoenolpyruvate carboxykinase/bovine growth hormone gene in transgenic mice. *J Biol Chem* **263**, 11443-51. (1988).

82. Wanke, R., Hermanns, W., Folger, S., Wolf, E. & Brem, G. Accelerated growth and visceral lesions in transgenic mice expressing foreign genes of the growth hormone family: an overview. *Pediatr Nephrol* **5**, 513-21. (1991).

83. Kopchick, J. J., Bellush, L. L. & Coschigano, K. T. Transgenic models of growth hormone action. *Annu Rev Nutr* **19**, 437-61 (1999).

84. Quaife, C. J., Mathews, L. S., Pinkert, C. A., Hammer, R. E., Brinster, R. L. & Palmiter, R. D. Histopathology associated with elevated levels of growth hormone and insulin-like growth factor I in transgenic mice. *Endocrinology* **124**, 40-8. (1989).

85. Doi, T., Striker, L. J., Gibson, C. C., Agodoa, L. Y., Brinster, R. L. & Striker, G. E. Glomerular lesions in mice transgenic for growth hormone and insulinlike growth factor-I. I. Relationship between increased glomerular size and mesangial sclerosis. *Am J Pathol* **137**, 541-52. (1990).

86. Wanke, R., Wolf, E., Hermanns, W., Folger, S., Buchmuller, T. & Brem, G. The GH-transgenic mouse as an experimental model for growth research: clinical and pathological studies. *Horm Res* **37**, 74-87. (1992).

87. Wanke, R., Hermanns, W., Wolf, E. & Brem, G. Wachstum und Organpathologie bei exzessiver Wachstumshormonproduktion am Beispiel der mMT I-hGH-transgenen Maus. *Verh Dtsch Ges Pathol* **74**, 510 (1990).

88. Wolf, E., Rapp, K. & Brem, G. Expression of metallothionein-human growth hormone fusion genes in transgenic mice results in disproportionate skeletal gigantism. *Growth Dev Aging* **55**, 117-27. (1991).

89. Shea, B. T., Hammer, R. E. & Brinster, R. L. Growth allometry of the organs in giant transgenic mice. *Endocrinology* **121**, 1924-30. (1987).

90. Wanke, R., Folger, S., Hermanns, W., Wolf, E., Schams, D. & Brem, G. Induktion neoplastischer und nicht-neoplastischer Leberveränderungen durch Wachstumshormon-Überproduktion bei bGH-transgenen Mäusen. *Verh Dtsch Ges Pathol* **75**, 312 (1991).

91. Wanke, R., Milz, S., Rieger, N., Ogiolda, L., Renner-Muller, I., Brem, G., Hermanns, W. & Wolf, E. Overgrowth of skin in growth hormone transgenic mice depends on the presence of male gonads. *J Invest Dermatol* **113**, 967-71. (1999).

92. Wolf, E., Kahnt, E., Ehrlein, J., Hermanns, W., Brem, G. & Wanke, R. Effects of long-term elevated serum levels of growth hormone on life expectancy of mice: lessons from transgenic animal models. *Mech Ageing Dev* **68**, 71-87. (1993).

93. Bartke, A., Brown-Borg, H., Mattison, J., Kinney, B., Hauck, S. & Wright, C. Prolonged longevity of hypopituitary dwarf mice. *Exp Gerontol* **36**, 21-8 (2001).

94. Longo, V. D. & Finch, C. E. Evolutionary medicine: from dwarf model systems to healthy centenarians? *Science* **299**, 1342-6 (2003).

95. Snell, G. D. Dwarf, a new Mendelian recessive character of the house mouse. *Proc Natl Acad Sci U S A* **15**, 733-734 (1929).

96. Li, S., Crenshaw, E. B., 3rd, Rawson, E. J., Simmons, D. M., Swanson, L. W. & Rosenfeld, M. G. Dwarf locus mutants lacking three pituitary cell types result from mutations in the POU-domain gene pit-1. *Nature* **347**, 528-33 (1990).

97. Sornson, M. W., Wu, W., Dasen, J. S., Flynn, S. E., Norman, D. J., O'Connell, S. M., Gukovsky, I., Carriere, C., Ryan, A. K., Miller, A. P., Zuo, L., Gleiberman, A. S., Andersen, B., Beamer, W. G. & Rosenfeld, M. G. Pituitary lineage determination by the Prophet of Pit-1 homeodomain factor defective in Ames dwarfism. *Nature* **384**, 327-33 (1996).

98. Eicher, E. M. & Beamer, W. G. Inherited ateliotic dwarfism in mice. Characteristics of the mutation, little, on chromosome 6. *J Hered* **67**, 87-91 (1976).

99. Zhou, Y., Xu, B. C., Maheshwari, H. G., He, L., Reed, M., Lozykowski, M., Okada, S., Cataldo, L., Coschigamo, K., Wagner, T. E., Baumann, G. & Kopchick, J. J. A mammalian model for Laron syndrome produced by targeted disruption of the mouse growth hormone receptor/binding protein gene (the Laron mouse). *Proc Natl Acad Sci U S A* **94**, 13215-20 (1997).

100. Fowden, A. L. Endocrine regulation of fetal growth. *Reprod Fertil Dev* **7**, 351-63 (1995).

101. Garcia-Aragon, J., Lobie, P. E., Muscat, G. E., Gobius, K. S., Norstedt, G. & Waters, M. J. Prenatal expression of the growth hormone (GH) receptor/binding protein in the rat: a role for GH in embryonic and fetal development? *Development* **114**, 869-76 (1992).

102. Pantaleon, M., Whiteside, E. J., Harvey, M. B., Barnard, R. T., Waters, M. J. & Kaye, P. L. Functional growth hormone (GH) receptors and GH are expressed by preimplantation mouse embryos: a role for GH in early embryogenesis? *Proc Natl Acad Sci U S A* **94**, 5125-30 (1997).

103. Salmon, W. D., Jr. & Daughaday, W. H. A hormonally controlled serum factor which stimulates sulfate incorporation by cartilage in vitro. *J Lab Clin Med* **49**, 825-36 (1957).

104. Mathews, L. S., Norstedt, G. & Palmiter, R. D. Regulation of insulin-like growth factor I gene expression by growth hormone. *Proc Natl Acad Sci U S A* **83**, 9343-7 (1986).

105. Newman, C. B. Medical therapy for acromegaly. *Endocrinol Metab Clin North Am* **28**, 171-90 (1999).

106. Colao, A., Ferone, D., Marzullo, P. & Lombardi, G. Systemic complications of acromegaly: epidemiology, pathogenesis, and management. *Endocr Rev* **25**, 102-52 (2004).

107. Toogood, A. A. Growth hormone (GH) status and body composition in normal ageing and in elderly adults with GH deficiency. *Horm Res* **60**, 105-11 (2003).

108. Okada, S. & Kopchick, J. J. Biological effects of growth hormone and its antagonist. *Trends Mol Med* **7**, 126-32 (2001).

109. Yoshizato, H., Fujikawa, T., Soya, H., Tanaka, M. & Nakashima, K. The growth hormone (GH) gene is expressed in the lateral hypothalamus: enhancement by GH-releasing hormone and repression by restraint stress. *Endocrinology* **139**, 2545-51 (1998).

110. Sonksen, P. H., Salomon, F. & Cuneo, R. Metabolic effects of hypopituitarism and acromegaly. *Horm Res* **36 Suppl 1**, 27-31 (1991).

111. Ganda, O. P. S., D. C. Growth hormone, acromegaly, and diabetes. *Diabetes Rev* **1**, 286-300 (1993).

112. Valera, A., Rodriguez-Gil, J. E., Yun, J. S., McGrane, M. M., Hanson, R. W. & Bosch, F. Glucose metabolism in transgenic mice containing a chimeric P-enolpyruvate carboxykinase/bovine growth hormone gene. *Faseb J* **7**, 791-800 (1993).

113. Costa, C., Solanes, G., Visa, J. & Bosch, F. Transgenic rabbits overexpressing growth hormone develop acromegaly and diabetes mellitus. *Faseb J* **12**, 1455-60 (1998).

114. Lee, P. D., Durham, S. K., Martinez, V., Vasconez, O., Powell, D. R. & Guevara-Aguirre, J. Kinetics of insulin-like growth factor (IGF) and IGF-binding protein responses to a single dose of growth hormone. *J Clin Endocrinol Metab* **82**, 2266-74 (1997).

115. Scanes, C. G. D., W. H. Growth hormone action: Growth. *In* "Growth Hormone" (S. Harvey, C. G. Scanes, and W. H. Daughaday, eds.). CRC Press, Boca Raton, FL., 351-370 (1995).

116. Olivecrona, H., Hilding, A., Ekstrom, C., Barle, H., Nyberg, B., Moller, C., Delhanty, P. J., Baxter, R. C., Angelin, B., Ekstrom, T. J. & Tally, M. Acute and short-term effects of growth hormone on insulin-like growth factors and their binding proteins: serum levels and hepatic messenger ribonucleic acid responses in humans. *J Clin Endocrinol Metab* **84**, 553-60 (1999).

117. Olivecrona, H., Hilding, A., Ekstrom, C., Barle, H., Nyberg, B., Moller, C., Delhanty, P. J., Baxter, R. C., Angelin, B., Ekstrom, T. J. & Tally, M. Acute and short-term effects of growth hormone on insulin-like growth factors and their binding proteins: serum levels and hepatic messenger ribonucleic acid responses in humans. *J Clin Endocrinol Metab* **84**, 553-60. (1999).

118. Donahue, L. R. & Beamer, W. G. Growth hormone deficiency in 'little' mice results in aberrant body composition, reduced insulin-like growth factor-I and insulin-like growth factor-binding protein-3 (IGFBP-3), but does not affect IGFBP-2, -1 or -4. *J Endocrinol* **136**, 91-104. (1993).

119. Camacho-Hubner, C., Clemmons, D. R. & D'Ercole, A. J. Regulation of insulin-like growth factor (IGF) binding proteins in transgenic mice with altered expression of growth hormone and IGF-I. *Endocrinology* **129**, 1201-6. (1991).

120. Lemmey, A. B., Glassford, J., Flick-Smith, H. C., Holly, J. M. & Pell, J. M. Differential regulation of tissue insulin-like growth factor-binding protein (IGFBP)-3, IGF-I and IGF type 1 receptor mRNA levels, and serum IGF-I and IGFBP concentrations by growth hormone and IGF-I. *J Endocrinol* **154**, 319-28 (1997).

121. Lewitt, M. S., Saunders, H., Phuyal, J. L. & Baxter, R. C. Complex formation by human insulin-like growth factor-binding protein-3 and human acid-labile subunit in growth hormone-deficient rats. *Endocrinology* **134**, 2404-9 (1994).

122. Rosenfeld, R. G., Rosenbloom, A. L. & Guevara-Aguirre, J. Growth hormone (GH) insensitivity due to primary GH receptor deficiency. *Endocr Rev* **15**, 369-90 (1994).

123. List, E. O., Coschigano, K. T. & Kopchick, J. J. Growth hormone receptor/binding protein (GHR/BP) knockout mice: a 3-year update. *Mol Genet Metab* **73**, 1-10 (2001).

124. Kopchick, J. J. & Laron, Z. Is the Laron mouse an accurate model of Laron syndrome? *Mol Genet Metab* **68**, 232-6 (1999).

125. Laron, Z., Avitur, Y., Klinger, B. Insulin resistance in Laron syndrome (primary insulin-like growth factor-I [IGF-I] deficiency) and effect of IGF-I replacement therapy. *J Pediatr Endocrinol Metab* **10**, 105-115 (1997).

126. Mathews, L. S., Hammer, R. E., Behringer, R. R., D'Ercole, A. J., Bell, G. I., Brinster, R. L. & Palmiter, R. D. Growth enhancement of transgenic mice expressing human insulin-like growth factor I. *Endocrinology* **123**, 2827-33 (1988).

127. Doi, T., Striker, L. J., Quaife, C., Conti, F. G., Palmiter, R., Behringer, R., Brinster, R. & Striker, G. E. Progressive glomerulosclerosis develops in transgenic mice chronically expressing growth hormone and growth hormone releasing factor but not in those expressing insulinlike growth factor-1. *Am J Pathol* **131**, 398-403. (1988).

128. Wolf, E., Hoeflich, A. & Lahm, H. What is the function of IGF-II in postnatal life? Answers from transgenic mouse models. *Growth Horm IGF Res* **8**, 185-93. (1998).

129. Wolf, E., Kramer, R., Blum, W. F., Foll, J. & Brem, G. Consequences of postnatally elevated insulin-like growth factor-II in transgenic mice: endocrine changes and effects on body and organ growth. *Endocrinology* **135**, 1877-86. (1994).

130. Wilson, D. M., Thomas, J. A., Hamm, T. E., Jr., Wyche, J., Hintz, R. L. & Rosenfeld, R. G. Transplantation of insulin-like growth factor-II-secreting tumors into nude rodents. *Endocrinology* **120**, 1896-901 (1987).

131. Koea, J. B., Breier, B. H., Shaw, J. H. & Gluckman, P. D. A possible role for IGE-II: evidence in sheep for in vivo regulation of IGF-I mediated protein anabolism. *Endocrinology* **130**, 2423-5 (1992).

132. Baker, J., Liu, J. P., Robertson, E. J. & Efstratiadis, A. Role of insulin-like growth factors in embryonic and postnatal growth. *Cell* **75**, 73-82 (1993).

133. DeChiara, T. M., Efstratiadis, A. & Robertson, E. J. A growth-deficiency phenotype in heterozygous mice carrying an insulin-like growth factor II gene disrupted by targeting. *Nature* **345**, 78-80 (1990).

134. Powell-Braxton, L., Hollingshead, P., Warburton, C., Dowd, M., Pitts-Meek, S., Dalton, D., Gillett, N. & Stewart, T. A. IGF-I is required for normal embryonic growth in mice. *Genes Dev* **7**, 2609-17 (1993).

135. Liu, J. P., Baker, J., Perkins, A. S., Robertson, E. J. & Efstratiadis, A. Mice carrying null mutations of the genes encoding insulin-like growth factor I (Igf-1) and type 1 IGF receptor (Igf1r). *Cell* **75**, 59-72 (1993).

136. Woods, K. A., Camacho-Hubner, C., Savage, M. O. & Clark, A. J. Intrauterine growth retardation and postnatal growth failure associated with deletion of the insulin-like growth factor I gene. *N Engl J Med* **335**, 1363-7 (1996).

137. Efstratiadis, A. Genetics of mouse growth. *Int J Dev Biol* **42**, 955-76 (1998).

138. Sauer, B. Inducible gene targeting in mice using the Cre/lox system. *Methods* **14**, 381-92 (1998).

139. Yakar, S., Liu, J. L., Fernandez, A. M., Wu, Y., Schally, A. V., Frystyk, J., Chernausek, S. D., Mejia, W. & Le Roith, D. Liver-specific igf-1 gene deletion leads to muscle insulin insensitivity. *Diabetes* **50**, 1110-8 (2001).

140. Yakar, S., Setser, J., Zhao, H., Stannard, B., Haluzik, M., Glatt, V., Bouxsein, M. L., Kopchick, J. J. & LeRoith, D. Inhibition of growth hormone action improves insulin sensitivity in liver IGF-1-deficient mice. *J Clin Invest* **113**, 96-105 (2004).

141. Holzenberger, M., Leneuve, P., Hamard, G., Ducos, B., Perin, L., Binoux, M. & Le Bouc, Y. A targeted partial invalidation of the insulin-like growth factor I receptor gene in mice causes a postnatal growth deficit. *Endocrinology* **141**, 2557-66 (2000).

142. Holzenberger, M., Dupont, J., Ducos, B., Leneuve, P., Geloen, A., Even, P. C., Cervera, P. & Le Bouc, Y. IGF-1 receptor regulates lifespan and resistance to oxidative stress in mice. *Nature* **421**, 182-7 (2003).

143. Lau, M. M., Stewart, C. E., Liu, Z., Bhatt, H., Rotwein, P. & Stewart, C. L. Loss of the imprinted IGF2/cation-independent mannose 6-phosphate receptor results in fetal overgrowth and perinatal lethality. *Genes Dev* **8**, 2953-63 (1994).

144. Wang, Z. Q., Fung, M. R., Barlow, D. P. & Wagner, E. F. Regulation of embryonic growth and lysosomal targeting by the imprinted Igf2/Mpr gene. *Nature* **372**, 464-7 (1994).

145. Pintar, J. E., Cerro, J. A. & Wood, T. L. Genetic approaches to the function of insulin-like growth factor- binding proteins during rodent development. *Horm Res* **45**, 172-7 (1996).

146. Pintar, J., Schuller, A., Bradshaw, S., Cerro, J., and Grewal, A. Genetic disruption of IGF binding proteins. In *Molecular Mechanisms to Regulate the Activities of Insulin-like Growth Factors* (Takano, K., Hizuka, N., and Takahashi, S.-I., eds.) Elsevier Science, Amsterdam, The Netherlands. 65-70 (1998).

147. Zhou, R., Flaswinkel, H., Schneider, M. R., Lahm, H., Hoeflich, A., Wanke, R. & Wolf, E. Insulin-like growth factor-binding protein-4 inhibits growth of the thymus in transgenic mice. *J Mol Endocrinol* **32**, 349-64 (2004).

148. Mazerbourg, S., Callebaut, I., Zapf, J., Mohan, S., Overgaard, M. & Monget, P. Up date on IGFBP-4: regulation of IGFBP-4 levels and functions, in vitro and in vivo. *Growth Horm IGF Res* **14**, 71-84 (2004).

149. Devlin, R. D., Du, Z., Buccilli, V., Jorgetti, V. & Canalis, E. Transgenic mice overexpressing insulin-like growth factor binding protein-5 display transiently decreased osteoblastic function and osteopenia. *Endocrinology* **143**, 3955-62 (2002).

150. Tonner, E., Barber, M. C., Allan, G. J., Beattie, J., Webster, J., Whitelaw, C. B. & Flint, D. J. Insulin-like growth factor binding protein-5 (IGFBP-5) induces premature cell death in the mammary glands of transgenic mice. *Development* **129**, 4547-57 (2002).

151. Bienvenu, G., Seurin, D., Grellier, P., Froment, P., Baudrimont, M., Monget, P., Le Bouc, Y. & Babajko, S. Insulin-like growth factor binding protein-6 transgenic mice: postnatal growth, brain development, and reproduction abnormalities. *Endocrinology* **145**, 2412-20 (2004).

152. Hoeflich, A., Wu, M., Mohan, S., Foll, J., Wanke, R., Froehlich, T., Arnold, G. J., Lahm, H., Kolb, H. J. & Wolf, E. Overexpression of insulin-like growth

factor-binding protein-2 in transgenic mice reduces postnatal body weight gain. *Endocrinology* **140**, 5488-96. (1999).

153. Hoeflich, A., Schmidt, P., Foll, J., Rottmann, O., Weber, M. M., Kolb, H. J., Pirchner, F. & Wolf, E. Altered growth of mice divergently selected for body weight is associated with complex changes in the growth hormone/insulin-like growth factor system. *Growth Horm IGF Res* **8**, 113-23 (1998).

154. Mesiano, S. & Jaffe, R. B. Developmental and functional biology of the primate fetal adrenal cortex. *Endocr Rev* **18**, 378-403 (1997).

155. Sillence, M. N. & Etherton, T. D. Chronic effects of recombinant porcine growth hormone on adrenal weight and activity in pigs. *J Anim Sci* **67**, 1740-3 (1989).

156. Coyne, M. D., Alpert, L. C., Harter, K. C. & Nunez, A. Effect of the growth hormone-secreting tumor StW5 on pituitary and adrenal gland function in rats. *Horm Res* **14**, 36-46 (1981).

157. Lewinski, A., Bartke, A., Esquifino, A., Sewerynek, E. & Steger, R. W. Adrenal catecholamine content: effects of congenital GH, PRL and TSH deficiency and of hormone replacement therapy in the male mouse. *Exp Clin Endocrinol* **87**, 176-82 (1986).

158. Merola, B., Rossi, E., Colao, A., Cataldi, M., Longobardi, S., Schettini, G. & Lombardi, G. Effect of a short-term treatment with recombinant growth hormone (GH) on adrenal responsiveness to corticotrophin stimulation in children affected by isolated GH deficiency. *J Clin Endocrinol Metab* **74**, 1210-4 (1992).

159. Hoeflich, A., Weber, M. M., Fisch, T., Nedbal, S., Fottner, C., Elmlinger, M. W., Wanke, R. & Wolf, E. Insulin-like growth factor binding protein 2 (IGFBP-2) separates hypertrophic and hyperplastic effects of growth hormone (GH)/IGF-I excess on adrenocortical cells in vivo. *Faseb J* **16**, 1721-31. (2002).

160. Tiong, T. S. & Herington, A. C. Tissue distribution, characterization, and regulation of messenger ribonucleic acid for growth hormone receptor and serum binding protein in the rat. *Endocrinology* **129**, 1628-34 (1991).

161. Mercado, M., DaVila, N., McLeod, J. F. & Baumann, G. Distribution of growth hormone receptor messenger ribonucleic acid containing and lacking exon 3 in human tissues. *J Clin Endocrinol Metab* **78**, 731-5 (1994).

162. Michl, P., Engelhardt, D., Oberneder, R. & Weber, M. M. Growth hormone has no direct effect on human adrenal steroid and insulin-like growth factor-binding protein secretion. *Endocr Res* **25**, 281-93 (1999).

163. l'Allemand, D., Penhoat, A., Lebrethon, M. C., Ardevol, R., Baehr, V., Oelkers, W. & Saez, J. M. Insulin-like growth factors enhance steroidogenic enzyme and corticotropin receptor messenger ribonucleic acid levels and corticotropin steroidogenic responsiveness in cultured human adrenocortical cells. *J Clin Endocrinol Metab* **81**, 3892-7 (1996).

164. l'Allemand, D., Penhoat, A., Blum, W. & Saez, J. M. Is there a local IGF-system in human adrenocortical cells? *Mol Cell Endocrinol* **140**, 169-73 (1998).

165. Ilvesmaki, V., Blum, W. F. & Voutilainen, R. Insulin-like growth factor-II in human fetal adrenals: regulation by ACTH, protein kinase C and growth factors. *J Endocrinol* **137**, 533-42 (1993).

166. Coulter, C. L., Goldsmith, P. C., Mesiano, S., Voytek, C. C., Martin, M. C., Han, V. K. & Jaffe, R. B. Functional maturation of the primate fetal adrenal in

vivo: I. Role of insulin-like growth factors (IGFs), IGF-I receptor, and IGF binding proteins in growth regulation. *Endocrinology* **137**, 4487-98 (1996).

167. Han, V. K., Lu, F., Bassett, N., Yang, K. P., Delhanty, P. J. & Challis, J. R. Insulin-like growth factor-II (IGF-II) messenger ribonucleic acid is expressed in steroidogenic cells of the developing ovine adrenal gland: evidence of an autocrine/paracrine role for IGF-II. *Endocrinology* **131**, 3100-9 (1992).

168. Rotwein, P., Pollock, K. M., Watson, M. & Milbrandt, J. D. Insulin-like growth factor gene expression during rat embryonic development. *Endocrinology* **121**, 2141-4 (1987).

169. Mesiano, S., Mellon, S. H. & Jaffe, R. B. Mitogenic action, regulation, and localization of insulin-like growth factors in the human fetal adrenal gland. *J Clin Endocrinol Metab* **76**, 968-76 (1993).

170. McNulty, W. P., Novy, M. J. & Walsh, S. W. Fetal and postnatal development of the adrenal glands in Macaca mulatta. *Biol Reprod* **25**, 1079-89 (1981).

171. van Dijk, J. P., Tanswell, A. K. & Challis, J. R. Insulin-like growth factor (IGF)-II and insulin, but not IGF-I, are mitogenic for fetal rat adrenal cells in vitro. *J Endocrinol* **119**, 509-16 (1988).

172. Mesiano, S., Katz, S. L., Lee, J. Y. & Jaffe, R. B. Insulin-like growth factors augment steroid production and expression of steroidogenic enzymes in human fetal adrenal cortical cells: implications for adrenal androgen regulation. *J Clin Endocrinol Metab* **82**, 1390-6 (1997).

173. Mesiano, S. & Jaffe, R. B. Interaction of insulin-like growth factor-II and estradiol directs steroidogenesis in the human fetal adrenal toward dehydroepiandrosterone sulfate production. *J Clin Endocrinol Metab* **77**, 754-8 (1993).

174. Fottner, C., Engelhardt, D. & Weber, M. M. Regulation of steroidogenesis by insulin-like growth factors (IGFs) in adult human adrenocortical cells: IGF-I and, more potently, IGF-II preferentially enhance androgen biosynthesis through interaction with the IGF-I receptor and IGF-binding proteins. *J Endocrinol* **158**, 409-17. (1998).

175. Ilvesmaki, V., Blum, W. F. & Voutilainen, R. Insulin-like growth factor binding proteins in the human adrenal gland. *Mol Cell Endocrinol* **97**, 71-9 (1993).

176. l'Allemand, D., Penhoat, A., Blum, W. & Saez, J. M. Is there a local IGF-system in human adrenocortical cells? *Mol Cell Endocrinol* **140**, 169-73. (1998).

177. Penhoat, A., Leduque, P., Jaillard, C., Chatelain, P. G., Dubois, P. M. & Saez, J. M. ACTH and angiotensin II regulation of insulin-like growth factor-I and its binding proteins in cultured bovine adrenal cells. *J Mol Endocrinol* **7**, 223-32. (1991).

178. Conlon, M. A., Tomas, F. M., Owens, P. C., Wallace, J. C., Howarth, G. S. & Ballard, F. J. Long R3 insulin-like growth factor-I (IGF-I) infusion stimulates organ growth but reduces plasma IGF-I, IGF-II and IGF binding protein concentrations in the guinea pig. *J Endocrinol* **146**, 247-53. (1995).

179. Le Roy, C., Li, J. Y., Stocco, D. M., Langlois, D. & Saez, J. M. Regulation by adrenocorticotropin (ACTH), angiotensin II, transforming growth factor-beta, and insulin-like growth factor I of bovine adrenal cell steroidogenic capacity and expression of ACTH receptor, steroidogenic acute regulatory protein, cytochrome P450c17, and 3beta-hydroxysteroid dehydrogenase. *Endocrinology* **141**, 1599-607 (2000).

180. Weber, M. M., Simmler, P., Fottner, C. & Engelhardt, D. Insulin-like growth factor II (IGF-II) is more potent than IGF-I in stimulating cortisol secretion from cultured bovine adrenocortical cells: interaction with the IGF-I receptor and IGF-binding proteins. *Endocrinology* **136**, 3714-20. (1995).

181. Stocco, D. M. & Clark, B. J. Role of the steroidogenic acute regulatory protein (StAR) in steroidogenesis. *Biochem Pharmacol* **51**, 197-205 (1996).

182. Nicol, M. R., Wang, H., Ivell, R., Morley, S. D., Walker, S. W. & Mason, J. I. The expression of steroidogenic acute regulatory protein (StAR) in bovine adrenocortical cells. *Endocr Res* **24**, 565-9 (1998).

183. Fujii, H., Iida, S., Tsugawa, M., Gomi, M., Moriwaki, K. & Tarui, S. Inhibitory effect of somatomedin C/insulin-like growth factor I on adrenocorticotropin- or forskolin-induced steroidogenesis in isolated rat adrenocortical cells. *Endocrinology* **126**, 26-30 (1990).

184. Leboulleux, S., Gaston, V., Boulle, N., Le Bouc, Y. & Gicquel, C. Loss of heterozygosity at the mannose 6-phosphate/insulin-like growth factor 2 receptor locus: a frequent but late event in adrenocortical tumorigenesis. *Eur J Endocrinol* **144**, 163-8 (2001).

185. Penhoat, A., Rainey, W. E., Viard, I. & Saez, J. M. Regulation of adrenal cell-differentiated functions by growth factors. *Horm Res* **42**, 39-43 (1994).

186. Weber, M. M., Auernhammer, C. J., Kiess, W. & Engelhardt, D. Insulin-like growth factor receptors in normal and tumorous adult human adrenocortical glands. *Eur J Endocrinol* **136**, 296-303 (1997).

187. Penhoat, A., Naville, D., Jaillard, C., Chatelain, P. G. & Saez, J. M. Hormonal regulation of insulin-like growth factor I secretion by bovine adrenal cells. *J Biol Chem* **264**, 6858-62 (1989).

188. Fottner, C., Engelhardt, D., Elmlinger, M. W. & Weber, M. M. Identification and characterization of insulin-like growth factor (IGF)- binding protein expression and secretion by adult human adrenocortical cells: differential regulation by IGFs and adrenocorticotropin. *J Endocrinol* **168**, 465-74. (2001).

189. Fottner, C., Engelhardt, D. & Weber, M. M. Characterization of insulin-like growth factor binding proteins (IGFBPs) secreted by bovine adrenocortical cells in primary culture: regulation by insulin-like growth factors (IGFs) and adrenocorticotropin (ACTH). *Horm Metab Res* **31**, 203-8 (1999).

190. Fottner, C., Spöttl, G., Engelhardt, D., Weber, M. M. The divergent effect of insulin-like growth factor binding protein (IGFBP)-1 on the steroidogenic effect of IGF-I and IGF-II in bovine adrenocortical cells is not due to its phosphorylation status. *Growth Horm IGF Res* **13**, 219 (2003).

191. Boulle, N., Logie, A., Gicquel, C., Perin, L. & Le Bouc, Y. Increased levels of insulin-like growth factor II (IGF-II) and IGF- binding protein-2 are associated with malignancy in sporadic adrenocortical tumors. *J Clin Endocrinol Metab* **83**, 1713-20. (1998).

192. Boulle, N., Baudin, E., Gicquel, C., Logie, A., Bertherat, J., Penfornis, A., Bertagna, X., Luton, J. P., Schlumberger, M. & Le Bouc, Y. Evaluation of plasma insulin-like growth factor binding protein-2 as a marker for adrenocortical tumors. *Eur J Endocrinol* **144**, 29-36 (2001).

193. Zumkeller, W. & Schofield, P. N. The role of insulin-like growth factors and IGF-binding proteins in the physiological and pathological processes of the kidney. *Virchows Arch B Cell Pathol Incl Mol Pathol* **62**, 207-20 (1992).

194. Hirschberg, R. & Adler, S. Insulin-like growth factor system and the kidney: physiology, pathophysiology, and therapeutic implications. *Am J Kidney Dis* **31**, 901-19. (1998).

195. Chin, E. & Bondy, C. Insulin-like growth factor system gene expression in the human kidney. *J Clin Endocrinol Metab* **75**, 962-8 (1992).

196. Chin, E., Zhou, J. & Bondy, C. A. Renal growth hormone receptor gene expression: relationship to renal insulin-like growth factor system. *Endocrinology* **131**, 3061-6 (1992).

197. Rogers, S. A., Karl, I. E. & Hammerman, M. R. Growth hormone directly stimulates gluconeogenesis in canine renal proximal tubule. *Am J Physiol* **257**, E751-6 (1989).

198. Chin, E., Zhou, J., Dai, J., Baxter, R. C. & Bondy, C. A. Cellular localization and regulation of gene expression for components of the insulin-like growth factor ternary binding protein complex. *Endocrinology* **134**, 2498-504 (1994).

199. Esposito, C., Liu, Z. H., Striker, G. E., Phillips, C., Chen, N. Y., Chen, W. Y., Kopchick, J. J. & Striker, L. J. Inhibition of diabetic nephropathy by a GH antagonist: a molecular analysis. *Kidney Int* **50**, 506-14. (1996).

200. Chin, E., Zhou, J. & Bondy, C. Anatomical relationships in the patterns of insulin-like growth factor (IGF)-I, IGF binding protein-1, and IGF-I receptor gene expression in the rat kidney. *Endocrinology* **130**, 3237-45 (1992).

201. Abboud, H. E. Growth factors and the mesangium. *J Am Soc Nephrol* **2**, S185-9 (1992).

202. Conti, F. G., Striker, L. J., Elliot, S. J., Andreani, D. & Striker, G. E. Synthesis and release of insulinlike growth factor I by mesangial cells in culture. *Am J Physiol* **255**, F1214-9 (1988).

203. Matejka, G. L., Eriksson, P. S., Carlsson, B. & Jennische, E. Distribution of IGF-I mRNA and IGF-I binding sites in the rat kidney. *Histochemistry* **97**, 173-80 (1992).

204. Kobayashi, S., Clemmons, D. R. & Venkatachalam, M. A. Colocalization of insulin-like growth factor-binding protein with insulin-like growth factor I. *Am J Physiol* **261**, F22-8 (1991).

205. Chin, E., Michels, K. & Bondy, C. A. Partition of insulin-like growth factor (IGF)-binding sites between the IGF-I and IGF-II receptors and IGF-binding proteins in the human kidney. *J Clin Endocrinol Metab* **78**, 156-64 (1994).

206. Evan, A. P., Henry, D. P., Connors, B. A., Summerlin, P. & Lee, W. H. Analysis of insulin-like growth factors (IGF)-I, and -II, type II IGF receptor and IGF-binding protein-2 mRNA and peptide levels in normal and nephrectomized rat kidney. *Kidney Int* **48**, 1517-29 (1995).

207. Valentino, K. L., Pham, H., Ocrant, I. & Rosenfeld, R. G. Distribution of insulin-like growth factor II receptor immunoreactivity in rat tissues. *Endocrinology* **122**, 2753-63 (1988).

208. Cui, S., Flyvbjerg, A., Nielsen, S., Kiess, W. & Christensen, E. I. IGF-II/Man-6-P receptors in rat kidney: apical localization in proximal tubule cells. *Kidney Int* **43**, 796-807 (1993).

209. Flyvbjerg, A., Nielsen, S., Sheikh, M. I., Jacobsen, C., Orskov, H. & Christensen, E. I. Luminal and basolateral uptake and receptor binding of IGF-I in rabbit renal proximal tubules. *Am J Physiol* **265**, F624-33 (1993).

210. Quigley, R. & Baum, M. Effects of growth hormone and insulin-like growth factor I on rabbit proximal convoluted tubule transport. *J Clin Invest* **88**, 368-74 (1991).

211. Price, G. J., Berka, J. L., Edmondson, S. R., Werther, G. A. & Bach, L. A. Localization of mRNAs for insulin-like growth factor binding proteins 1 to 6 in rat kidney. *Kidney Int* **48**, 402-11. (1995).

212. Lindenbergh-Kortleve, D. J., Rosato, R. R., van Neck, J. W., Nauta, J., van Kleffens, M., Groffen, C., Zwarthoff, E. C. & Drop, S. L. Gene expression of the insulin-like growth factor system during mouse kidney development. *Mol Cell Endocrinol* **132**, 81-91. (1997).

213. Rabkin, R., Brody, M., Lu, L. H., Chan, C., Shaheen, A. M. & Gillett, N. Expression of the genes encoding the rat renal insulin-like growth factor-I system. *J Am Soc Nephrol* **6**, 1511-8 (1995).

214. Hise, M. K., Mantzouris, N. M., Lahn, J. S., Sheikh, M. S., Shao, Z. M. & Fontana, J. A. IGF binding protein 5 and IGF-I receptor regulation in hypophysectomized rat kidneys. *Am J Physiol* **266**, F147-54 (1994).

215. Albini, C. H., Quattrin, T., Vandlen, R. L. & MacGillivray, M. H. Quantitation of urinary growth hormone in children with normal and abnormal growth. *Pediatr Res* **23**, 89-92 (1988).

216. Maack, T. & Park, C. H. Endocytosis and lysosomal hydrolysis of proteins in proximal tubules. *Methods Enzymol* **191**, 340-54 (1990).

217. Haffner, D., Schaefer, F., Girard, J., Ritz, E. & Mehls, O. Metabolic clearance of recombinant human growth hormone in health and chronic renal failure. *J Clin Invest* **93**, 1163-71 (1994).

218. Johnson, V. & Maack, T. Renal extraction, filtration, absorption, and catabolism of growth hormone. *Am J Physiol* **233**, F185-96 (1977).

219. Johannsson, G. & Ahlmen, J. End-stage renal disease: endocrine aspects of treatment. *Growth Horm IGF Res* **13 Suppl A**, S94-S101 (2003).

220. Hirschberg, R. Bioactivity of glomerular ultrafiltrate during heavy proteinuria may contribute to renal tubulo-interstitial lesions: evidence for a role for insulin-like growth factor I. *J Clin Invest* **98**, 116-24 (1996).

221. Rabkin, R., Fervenza, F., Maidment, H., Ike, J., Jamison, R., Hintz, R., Bukar, J., Arcila, P., Gesundheit, N. IGF-I pharmacokinetics in chronic renal failure. *J Am Soc Nephrol* **5**, 340 (1994).

222. Frystyk, J., Ivarsen, P., Skjaerbaek, C., Flyvbjerg, A., Pedersen, E. B. & Orskov, H. Serum-free insulin-like growth factor I correlates with clearance in patients with chronic renal failure. *Kidney Int* **56**, 2076-84. (1999).

223. Wang, S. N., LaPage, J. & Hirschberg, R. Role of glomerular ultrafiltration of growth factors in progressive interstitial fibrosis in diabetic nephropathy. *Kidney Int* **57**, 1002-14 (2000).

224. Tang, S., Lai, K. N., Chan, T. M., Lan, H. Y., Ho, S. K. & Sacks, S. H. Transferrin but not albumin mediates stimulation of complement C3 biosynthesis in human proximal tubular epithelial cells. *Am J Kidney Dis* **37**, 94-103 (2001).

225. Burton, C. J., Bevington, A., Harris, K. P. & Walls, J. Growth of proximal tubular cells in the presence of albumin and proteinuric urine. *Exp Nephrol* **2**, 345-50 (1994).

226. Jacot, T. A., Striker, G. E., Stetler-Stevenson, M. & Striker, L. J. Mesangial cells from transgenic mice with progressive glomerulosclerosis exhibit stable, phenotypic changes including undetectable MMP-9 and increased type IV collagen. *Lab Invest* **75**, 791-9 (1996).

227. Wanke, R., Wolf, E., Brem, G. & Hermanns, W. Role of podocyte damage in the pathogenesis of glomerulosclerosis and tubulointerstitial lesions: findings

in the growth hormone transgenic mouse model of progressive nephropathy. *Verh Dtsch Ges Pathol* **85**, 250-6 (2001).

228. Rastaldi, M. P., Armelloni, S., Berra, S., Li, M., Pesaresi, M., Poczewski, H., Langer, B., Kerjaschki, D., Henger, A., Blattner, S. M., Kretzler, M., Wanke, R. & D'Amico, G. Glomerular podocytes possess the synaptic vesicle molecule Rab3A and its specific effector rabphilin-3a. *Am J Pathol* **163**, 889-99 (2003).

229. Wanke, R. Zur Morpho- und Pathogenese der progressiven Glomerulosklerose. Habilitationsschrift, University of Munich. (1996).

230. Marshall, S. M., Flyvbjerg, A., Jorgensen, K. D., Weeke, J. & Orskov, H. Effects of growth hormone and thyroxine on kidney insulin-like growth factor-I and renal growth in hypophysectomized rats. *J Endocrinol* **136**, 399-406 (1993).

231. Kawaguchi, H., Itoh, K., Mori, H., Hayashi, Y. & Makino, S. Renal pathology in rats bearing tumour-secreting growth hormone. *Pediatr Nephrol* **5**, 533-8 (1991).

232. Molon-Noblot, S., Laroque, P., Prahalada, S., Stabinski, L. G., Peter, C. P., Duprat, P. & van Zwieten, M. J. Morphological changes in the kidney of dogs chronically exposed to exogenous growth hormone. *Toxicol Pathol* **28**, 510-7 (2000).

233. Dullaart, R. P., Meijer, S., Marbach, P. & Sluiter, W. J. Effect of a somatostatin analogue, octreotide, on renal haemodynamics and albuminuria in acromegalic patients. *Eur J Clin Invest* **22**, 494-502 (1992).

234. Ogle, G. D., Rosenberg, A. R. & Kainer, G. Renal effects of growth hormone. I. Renal function and kidney growth. *Pediatr Nephrol* **6**, 394-8 (1992).

235. Gershberg, H., Heinemann, H. O. & Stumpf, H. H. Renal function studies and autopsy report in a patient with gigantism and acromegaly. *J Clin Endocrinol Metab* **17**, 377-85 (1957).

236. Takai, M., Izumino, K., Oda, Y., Terada, Y., Inoue, H. & Takata, M. Focal segmental glomerulosclerosis associated with acromegaly. *Clin Nephrol* **56**, 75-7 (2001).

237. Hirschberg, R. Effects of growth hormone and IGF-I on glomerular ultrafiltration in growth hormone-deficient rats. *Regul Pept* **48**, 241-50 (1993).

238. Goya, R. G., Castelletto, L. & Sosa, Y. E. Plasma levels of growth hormone correlate with the severity of pathologic changes in the renal structure of aging rats. *Lab Invest* **64**, 29-34 (1991).

239. Yoshida, H., Mitarai, T., Kitamura, M., Suzuki, T., Ishikawa, H., Fogo, A. & Sakai, O. The effect of selective growth hormone defect in the progression of glomerulosclerosis. *Am J Kidney Dis* **23**, 302-12 (1994).

240. Flyvbjerg, A., Frystyk, J., Thorlacius-Ussing, O. & Orskov, H. Somatostatin analogue administration prevents increase in kidney somatomedin C and initial renal growth in diabetic and uninephrectomized rats. *Diabetologia* **32**, 261-5 (1989).

241. Flyvbjerg, A., Bennett, W. F., Rasch, R., van Neck, J. W., Groffen, C. A., Kopchick, J. J. & Scarlett, J. A. Compensatory renal growth in uninephrectomized adult mice is growth hormone dependent. *Kidney Int* **56**, 2048-54. (1999).

242. Liu, Z. Z., Kumar, A., Wallner, E. I., Wada, J., Carone, F. A. & Kanwar, Y. S. Trophic effect of insulin-like growth factor-I on metanephric development: relationship to proteoglycans. *Eur J Cell Biol* **65**, 378-91 (1994).

243. Doublier, S., Amri, K., Seurin, D., Moreau, E., Merlet-Benichou, C., Striker, G. E. & Gilbert, T. Overexpression of human insulin-like growth factor binding protein-1 in the mouse leads to nephron deficit. *Pediatr Res* **49**, 660-6. (2001).

244. Rogers, S. A., Powell-Braxton, L. & Hammerman, M. R. Insulin-like growth factor I regulates renal development in rodents. *Dev Genet* **24**, 293-8 (1999).

245. Baud, L., Fouqueray, B., Bellocq, A., Doublier, S. & Dumoulin, A. Growth hormone and somatostatin in glomerular injury. *J Nephrol* **12**, 18-23. (1999).

246. Johnson, D. W., Saunders, H. J., Brew, B. K., Ganesan, A., Baxter, R. C., Poronnik, P., Cook, D. I., Gyory, A. Z., Field, M. J. & Pollock, C. A. Human renal fibroblasts modulate proximal tubule cell growth and transport via the IGF-I axis. *Kidney Int* **52**, 1486-96 (1997).

247. O'Shea, M., Miller, S. B. & Hammerman, M. R. Insulin-like growth factor I and the kidney. *Semin Nephrol* **13**, 96-108 (1993).

248. Norman, J. T., Fine, L. G. Renal Growth and Hypertrophy in: *Textbook of Nephrology.* S. G. Massry & R. J. Glassock (Eds.), Baltimore; Williams&Wilkins. 146-158 (1995).

249. Cheung, C. W., Vesey, D. A., Nicol, D. L. & Johnson, D. W. The roles of IGF-I and IGFBP-3 in the regulation of proximal tubule, and renal cell carcinoma cell proliferation. *Kidney Int* **65**, 1272-9 (2004).

250. Blazer-Yost, B. L., Watanabe, M., Haverty, T. P. & Ziyadeh, F. N. Role of insulin and IGF1 receptors in proliferation of cultured renal proximal tubule cells. *Biochim Biophys Acta* **1133**, 329-35 (1992).

251. Zhang, G. H., Ichimura, T., Wallin, A., Kan, M. & Stevens, J. L. Regulation of rat proximal tubule epithelial cell growth by fibroblast growth factors, insulin-like growth factor-1 and transforming growth factor-beta, and analysis of fibroblast growth factors in rat kidney. *J Cell Physiol* **148**, 295-305 (1991).

252. Yap, J., Tsao, T., Fawcett, J., Fielder, P. J., Keller, G. A. & Rabkin, R. Effect of insulin-like growth factor binding proteins on the response of proximal tubular cells to insulin-like growth factor-I. *Kidney Int* **52**, 1216-23. (1997).

253. Gansler, T., Hsu, W. C., Gramling, T. S., Robinson, K. A., Buse, M. G., Blocker, N., Roy, L., Green, S., Garvin, A. J. & Sens, D. A. Growth factor binding and bioactivity in human kidney epithelial cell cultures. *In Vitro Cell Dev Biol* **26**, 285-90 (1990).

254. Kiley, S. C., Thornhill, B. A., Tang, S. S., Ingelfinger, J. R. & Chevalier, R. L. Growth factor-mediated phosphorylation of proapoptotic BAD reduces tubule cell death in vitro and in vivo. *Kidney Int* **63**, 33-42 (2003).

255. Mehls, O., Irzynjec, T., Ritz, E., Eden, S., Kovacs, G., Klaus, G., Floege, J. & Mall, G. Effects of rhGH and rhIGF-1 on renal growth and morphology. *Kidney Int* **44**, 1251-8 (1993).

256. Wolf, G. & Neilson, E. G. Cellular biology of tubulointerstitial growth. *Curr Top Pathol* **88**, 69-97 (1995).

257. Liu, B. & Preisig, P. A. Compensatory renal hypertrophy is mediated by a cell cycle-dependent mechanism. *Kidney Int* **62**, 1650-8 (2002).

258. Preisig, P. What makes cells grow larger and how do they do it? Renal hypertrophy revisited. *Exp Nephrol* **7**, 273-83 (1999).

259. Doi, T., Striker, L. J., Elliot, S. J., Conti, F. G. & Striker, G. E. Insulinlike growth factor-1 is a progression factor for human mesangial cells. *Am J Pathol* **134**, 395-404. (1989).

260. Feld, S. M., Hirschberg, R., Artishevsky, A., Nast, C. & Adler, S. G. Insulin-like growth factor I induces mesangial proliferation and increases mRNA and secretion of collagen. *Kidney Int* **48**, 45-51 (1995).

261. Mooney, A., Jobson, T., Bacon, R., Kitamura, M. & Savill, J. Cytokines promote glomerular mesangial cell survival in vitro by stimulus-dependent inhibition of apoptosis. *J Immunol* **159**, 3949-60 (1997).

262. Conti, F. G., Striker, L. J., Lesniak, M. A., MacKay, K., Roth, J. & Striker, G. E. Studies on binding and mitogenic effect of insulin and insulin-like growth factor I in glomerular mesangial cells. *Endocrinology* **122**, 2788-95. (1988).

263. Gooch, J. L., Tang, Y., Ricono, J. M. & Abboud, H. E. Insulin-like growth factor-I induces renal cell hypertrophy via a calcineurin-dependent mechanism. *J Biol Chem* **276**, 42492-500. (2001).

264. Doublier, S., Seurin, D., Fouqueray, B., Verpont, M. C., Callard, P., Striker, L. J., Striker, G. E., Binoux, M. & Baud, L. Glomerulosclerosis in mice transgenic for human insulin-like growth factor-binding protein-1. *Kidney Int* **57**, 2299-307. (2000).

265. Gay, E., Seurin, D., Babajko, S., Doublier, S., Cazillis, M. & Binoux, M. Liver-specific expression of human insulin-like growth factor binding protein-1 in transgenic mice: repercussions on reproduction, ante- and perinatal mortality and postnatal growth. *Endocrinology* **138**, 2937-47. (1997).

266. Houang, M., Cabrol, S., Perin, L., Ducos, B., Bensman, A. & Le Bouc, Y. Insulin-like growth factor-I (IGF-I), insulin-like growth factor binding proteins (IGFBP) and insulin-like growth factor type I receptor in children with various status of chronic renal failure. *Growth Horm IGF Res* **10**, 332-41. (2000).

267. Powell, D. R., Liu, F., Baker, B. K., Hinzt, R. L., Kale, A., Suwanichkul, A. & Durham, S. K. Effect of chronic renal failure and growth hormone therapy on the insulin-like growth factors and their binding proteins. *Pediatr Nephrol* **14**, 579-83. (2000).

268. Hirschberg, R. & Kaysen, G. A. Insulin-like growth factor I and its binding proteins in the experimental nephrotic syndrome. *Endocrinology* **136**, 1565-71. (1995).

269. Tonshoff, B., Powell, D. R., Zhao, D., Durham, S. K., Coleman, M. E., Domene, H. M., Blum, W. F., Baxter, R. C., Moore, L. C. & Kaskel, F. J. Decreased hepatic insulin-like growth factor (IGF)-I and increased IGF binding protein-1 and -2 gene expression in experimental uremia. *Endocrinology* **138**, 938-46. (1997).

270. Ulinski, T., Mohan, S., Kiepe, D., Blum, W. F., Wingen, A. M., Mehls, O. & Tonshoff, B. Serum insulin-like growth factor binding protein (IGFBP)-4 and IGFBP-5 in children with chronic renal failure: relationship to growth and glomerular filtration rate. The European Study Group for Nutritional Treatment of Chronic Renal Failure in Childhood. German Study Group for Growth Hormone Treatment in Chronic Renal Failure. *Pediatr Nephrol* **14**, 589-97. (2000).

271. Tonshoff, B., Veldhuis, J. D., Heinrich, U. & Mehls, O. Deconvolution analysis of spontaneous nocturnal growth hormone secretion in prepubertal children with preterminal chronic renal failure and with end-stage renal disease. *Pediatr Res* **37**, 86-93. (1995).

272. Kapila, P., Jones, J. & Rees, L. Effect of chronic renal failure and prednisolone on the growth hormone-insulin-like growth factor axis. *Pediatr Nephrol* **16**, 1099-104 (2001).

273. Fukuda, I., Hizuka, N., Okubo, Y., Takano, K., Asakawa-Yasumoto, K., Shizume, K., Demura, H., Kimata, N., Ishikawa, N. & Toma, H. Changes in serum insulin-like growth factor binding protein-2, -3, and - 6 levels in patients with chronic renal failure following renal transplantation. *Growth Horm IGF Res* **8**, 481-6. (1998).

274. Bernstein, J., Gilbert-Barness, E. Congenital malformations of the kidney. *In: Renal Pathology* (edt. Tisher, C. C., Brenner, B. M), JB Lippincott Company, Philadelphia. 1278-1308 (1989).

275. Bang, P. Valid measurements of total IGF concentrations in biological fluids: recommendations from the 3rd International Symposium on Insulin-like Growth Factors. *Eur J Endocrinol* **132**, 338-9 (1995).

276. Blum, W. F. & Breier, B. H. Radioimmunoassays for IGFs and IGFBPs. *Growth Regul* **4 Suppl 1**, 11-9 (1994).

277. Blum, W. F., Horn, N., Kratzsch, J., Jorgensen, J. O., Juul, A., Teale, D., Mohnike, K. & Ranke, M. B. Clinical studies of IGFBP-2 by radioimmunoassay. *Growth Regul* **3**, 100-4 (1993).

278. Hermanns, W., Liebig, K. & Schulz, L. C. Postembedding immunohistochemical demonstration of antigen in experimental polyarthritis using plastic embedded whole joints. *Histochemistry* **73**, 439-46 (1981).

279. Caulfield, J. B. Effects of varying the vehicle for OsO4 in tissue fixation. *J Biophys Biochem Cytol* **3**, 827-30 (1957).

280. Frith, C. H. Histology, adrenal gland, mouse. In *Monographs of Pathologyof Laboratory Animals. Endocrine System* (Jones, T. C., Mohr, U., and Hunt, R. D., eds). pp. 8 - 12 (1983).

281. Delesse, M. A. Procede mecanique pour determiner la composition des roches. C. R. Acad. Sci. (Paris). **25**, 544-545 (1847).

282. Weibel, E. R. *Stereological Methods. I. Practical Methods for Biological Morphometry*. Academic Press, London. (1979).

283. Swinyard, C. A. Methods for volumetric determination of fresh endocrine glands. *Anatomical Records* **74**, 71 - 78 (1939).

284. Sterio, D. C. The unbiased estimation of number and sizes of arbitrary particles using the disector. *J Microsc* **134**, 127-36. (1984).

285. Gundersen, H. J. G. Notes on the estimation of the numerical density of arbitrary profiles: The edge effect. *J. Microsc.* **111**, 219-223 (1977).

286. Gundersen, H. J. Stereology of arbitrary particles. A review of unbiased number and size estimators and the presentation of some new ones, in memory of William R. Thompson. *J Microsc* **143 (Pt 1)**, 3-45 (1986).

287. Nyengaard, J. R. Stereologic methods and their application in kidney research. *J Am Soc Nephrol* **10**, 1100-23. (1999).

288. Kriz, W. & Koepsell, H. The structural organization of the mouse kidney. *Z. Anat. Entwickl.-Gesch.* **144**, 137-163 (1974).

289. Kriz, W. & Bankir, L. A standard nomenclature for structures of the kidney. The Renal Commission of the International Union of Physiological Sciences (IUPS). *Kidney Int* **33**, 1-7. (1988).

290. Herbach, N. Clinical and pathological characterization of a novel transgenic mouse model of diabetes mellitus expressing a dominant negative glucose-dependent insulinotropic polypeptide receptor (GIPR[dn]). Thesis, University of Munich. (2002).

291. Glagolev. On the geometrical methods of quantitative mineralogic analysis of rocks. *Trans. Inst. Econ. Min.* **53** (1933).

292. Bachmann, S., Sakai, T., Kriz, W. Nephron and collecting duct structure in the kidney. In: *Monographs on Pathology of Laboratory Animals* (Jones, T. C., Mohr, U., Hunt, R. D. (eds.) Springer Verlang Berlin Heidelberg New York London Paris Tokyo. (1986).

293. Hirose, K., Osterby, R., Nozawa, M. & Gundersen, H. J. Development of glomerular lesions in experimental long-term diabetes in the rat. *Kidney Int* **21**, 889-95 (1982).

294. Gundersen, H. J. Estimators of the number of objects per area unbiased by edge effects. *Microsc Acta* **81**, 107-17 (1978).

295. el Nahas, A. M. The role of growth hormone and insulin-like growth factor-I in experimental renal growth and scarring. *Am J Kidney Dis* **17**, 677-9. (1991).

296. Nakane, P. K. & Pierce, G. B., Jr. Enzyme-labeled antibodies for the light and electron microscopic localization of tissue antigens. *J Cell Biol* **33**, 307-18 (1967).

297. Hossenlopp, P., Seurin, D., Segovia-Quinson, B., Hardouin, S. & Binoux, M. Analysis of serum insulin-like growth factor binding proteins using western blotting: use of the method for titration of the binding proteins and competitive binding studies. *Anal Biochem* **154**, 138-43 (1986).

298. Fukuda, I., Hizuka, N., Takano, K., Asakawa-Yasumoto, K., Shizume, K. & Demura, H. Characterization of insulin-like growth factor II (IGF-II) and IGF binding proteins in patients with non-islet-cell tumor hypoglycemia. *Endocr J* **40**, 111-9 (1993).

299. Ketelslegers, J. M., Maiter, D., Maes, M., Underwood, L. E. & Thissen, J. P. Nutritional regulation of the growth hormone and insulin-like growth factor-binding proteins. *Horm Res* **45**, 252-7 (1996).

300. Kasiske, B., L., Keane, W., F. Laboratory assessment of renal disease: clearence, urinanalysis, and renal biopsy. In: *The Kidney, 5th ed*. (Brenner B., M., edt), W. B. Saunders Company, Philadelphia. 1137-1174 (1996).

301. Bohle, A., Mackensen-Haen, S., von Gise, H., Grund, K. E., Wehrmann, M., Batz, C., Bogenschutz, O., Schmitt, H., Nagy, J., Muller, C. & et al. The consequences of tubulo-interstitial changes for renal function in glomerulopathies. A morphometric and cytological analysis. *Pathol Res Pract* **186**, 135-44 (1990).

302. Levey, A. S., Perrone, R. D. & Madias, N. E. Serum creatinine and renal function. *Annu Rev Med* **39**, 465-90 (1988).

303. Salomon, F., Cuneo, R. & Sonksen, P. H. Growth hormone and protein metabolism. *Horm Res* **36 Suppl 1**, 41-3 (1991).

304. Knochel, J., P., Agarwal, R. Hypophosphatemia and hyperphosphatemia. In: *The Kidney, 5th ed*. (Brenner B., M., edt), W. B. Saunders Company, Philadelphia. 1086-1136 (1996).

305. Halse, J. & Haugen, H. N. Calcium and phosphate metabolism in acromegaly. *Acta Endocrinol (Copenh)* **94**, 459-67 (1980).

306. Corvilain, J. & Abramow, M. Effect of Growth Hormone on Tubular Transport of Phosphate in Normal and Parathyroidectomized Dogs. *J Clin Invest* **43**, 1608-12 (1964).

307. Hirschberg, R., Brunori, G., Kopple, J. D. & Guler, H. P. Effects of insulin-like growth factor I on renal function in normal men. *Kidney Int* **43**, 387-97 (1993).

308. Hirschberg, R., Ding, H. & Wanner, C. Effects of insulin-like growth factor I on phosphate transport in cultured proximal tubule cells. *J Lab Clin Med* **126**, 428-34. (1995).

309. Sutton, R., A., L., Dirks, J., H. Disturbances of calcium and magnesium metabolism. In: *The Kidney, 5th ed*. (Brenner B., M., edt), W. B. Saunders Company, Philadelphia. (1996).

310. Aloia, J., Powell, D., Mendizibal, E. & Roginsky, M. Parathyroid function in acromegaly. *Horm Res* **6**, 145-9 (1975).

311. Berry, C. A., Ives, H. E., Floyd, C. R., Jr. Renal transport of glucose, amino acids, sodium, chloride, and water. In: *The Kidney, 5th ed*. (Brenner B., M., edt), W. B. Saunders Company, Philadelphia. 334-370 (1996).

312. Dirsch, V. M., Wolf, E., Wanke, R., Schulz, R., Hermanns, W. & Vollmar, A. M. Effect of chronic GH overproduction on cardiac ANP expression and circulating ANP levels. *Mol Cell Endocrinol* **144**, 109-18 (1998).

313. Bengtsson, B. A., Brummer, R. J. & Bosaeus, I. Growth hormone and body composition. *Horm Res* **33**, 19-24. (1990).

314. Cecim, M., Bartke, A., Yun, J. G., Wagner, T. E. Growth allometry of transgenic mice expressing the mouse metallothionein/bovine growth hormone gene. *Transgene* **1**, 125-132 (1993).

315. Usala, A. L., Madigan, T., Burguera, B., Sinha, M. K., Caro, J. F., Cunningham, P., Powell, J. G. & Butler, P. C. Brief report: treatment of insulin-resistant diabetic ketoacidosis with insulin-like growth factor I in an adolescent with insulin-dependent diabetes. *N Engl J Med* **327**, 853-7 (1992).

316. Zierler, K. L. & Rabinowitz, D. Effect of Very Small Concentrations of Insulin on Forearm Metabolism. Persistence of Its Action on Potassium and Free Fatty Acids without Its Effect on Glucose. *J Clin Invest* **43**, 950-62 (1964).

317. Kamel, K., S., Halperin, M., L., Faber, M., D., Steigerwalt, S., P., Heilig, C., W., Narins, R., G. Disorders of potassium balance. In: *The Kidney, 5th ed*. (Brenner B., M., edt), W. B. Saunders Company, Philadelphia. (1996).

318. Lewinski, A., Bartke, A., Esquifino, A., Sewerynek, E. & Steger, R. W. Adrenal catecholamine content: effects of congenital GH, PRL and TSH deficiency and of hormone replacement therapy in the male mouse. *Exp Clin Endocrinol* **87**, 176-82. (1986).

319. Fottner, C., Hoeflich, A., Wolf, E. & Weber, M. M. Role of the insulin-like growth factor system in adrenocortical growth control and carcinogenesis. *Horm Metab Res* **36**, 397-405 (2004).

320. Slootweg, M. C., Ohlsson, C., Salles, J. P., de Vries, C. P. & Netelenbos, J. C. Insulin-like growth factor binding proteins-2 and -3 stimulate growth hormone receptor binding and mitogenesis in rat osteosarcoma cells. *Endocrinology* **136**, 4210-7 (1995).

321. Weber, M. M., Kiess, W., Beikler, T., Simmler, P., Reichel, M., Adelmann, B., Kessler, U. & Engelhardt, D. Identification and characterization of insulin-like growth factor I (IGF-I) and IGF-II/mannose-6-phosphate (IGF-II/M6P) receptors in bovine adrenal cells. *Eur J Endocrinol* **130**, 265-70 (1994).

322. Conlon, I. J., Dunn, G. A., Mudge, A. W. & Raff, M. C. Extracellular control of cell size. *Nat Cell Biol* **3**, 918-21. (2001).

323. Coelho, C. M. & Leevers, S. J. Do growth and cell division rates determine cell size in multicellular organisms? *J Cell Sci* **113 (Pt 17)**, 2927-34 (2000).

324. Alessi, D. R. Discovery of PDK1, one of the missing links in insulin signal transduction. Colworth Medal Lecture. *Biochem Soc Trans* **29**, 1-14 (2001).

325. Toker, A. & Newton, A. C. Cellular signaling: pivoting around PDK-1. *Cell* **103**, 185-8 (2000).

326. Lawlor, M. A., Mora, A., Ashby, P. R., Williams, M. R., Murray-Tait, V., Malone, L., Prescott, A. R., Lucocq, J. M. & Alessi, D. R. Essential role of PDK1 in regulating cell size and development in mice. *Embo J* **21**, 3728-38. (2002).

327. Ottenweller, J. E., Meier, A. H., Russo, A. C. & Frenzke, M. E. Circadian rhythms of plasma corticosterone binding activity in the rat and the mouse. *Acta Endocrinol (Copenh)* **91**, 150-7 (1979).

328. Henkel, H. M. Hypophysial and adrenal changes in growth hormone trangenic mice: an investigation by immumohistochemistry, morphometry and radioimmunoassay. Thesis, University of Munich. (1995).

329. Weidenfeld, J. & Feldman, S. Glucocorticoid feedback regulation of adrenocortical responses to neural stimuli: role of CRF-41 and corticosteroid type I and type II receptors. *Neuroendocrinology* **58**, 49-56 (1993).

330. Guler, H. P., Zapf, J., Scheiwiller, E. & Froesch, E. R. Recombinant human insulin-like growth factor I stimulates growth and has distinct effects on organ size in hypophysectomized rats. *Proc Natl Acad Sci U S A* **85**, 4889-93 (1988).

331. Shea, B. T., Hammer, R. E. & Brinster, R. L. Growth allometry of the organs in giant transgenic mice. *Endocrinology* **121**, 1924-30 (1987).

332. Seyer-Hansen, K., Hansen, J. & Gundersen, H. J. Renal hypertrophy in experimental diabetes. A morphometric study. *Diabetologia* **18**, 501-5 (1980).

333. Hammerman, M. R. & Miller, S. B. Renal cellular biology of growth hormone and insulin-like growth factor I. *Pediatr Nephrol* **5**, 505-8 (1991).

334. Ernst, F., Hetzel, S., Stracke, S., Czock, D., Vargas, G., Lutz, M. P., Keller, F. & Jehle, P. M. Renal proximal tubular cell growth and differentiation are differentially modulated by renotropic growth factors and tyrosine kinase inhibitors. *Eur J Clin Invest* **31**, 1029-39 (2001).

335. Senthil, D., Choudhury, G. G., Abboud, H. E., Sonenberg, N. & Kasinath, B. S. Regulation of protein synthesis by IGF-I in proximal tubular epithelial cells. *Am J Physiol Renal Physiol* **283**, F1226-36 (2002).

336. Schuller, A. G., Groffen, C., van Neck, J. W., Zwarthoff, E. C. & Drop, S. L. cDNA cloning and mRNA expression of the six mouse insulin-like growth factor binding proteins. *Mol Cell Endocrinol* **104**, 57-66 (1994).

337. Rabkin, R. & Schaefer, F. New concepts: growth hormone, insulin-like growth factor-I and the kidney. *Growth Horm IGF Res* **14**, 270-6 (2004).

338. Gröne, H.-J. Experimentielle Modelle der renalen tubulären Inaktivitätsatrophie und der zystischen Tubuluszellhyperplasie. Funktionelle und morphologische Charakteristika und klinische Relevanz. *Verh Dtsch Ges Pathol* **73**, 706-721 (1989).

339. Konda, R., Sato, H., Hatafuku, F., Nozawa, T., Ioritani, N. & Fujioka, T. Expression of hepatocyte growth factor and its receptor C-met in acquired renal cystic disease associated with renal cell carcinoma. *J Urol* **171**, 2166-70 (2004).

340. Dubey, R. K., Jackson, E. K., Rupprecht, H. D. & Sterzel, R. B. Factors controlling growth and matrix production in vascular smooth muscle and glomerular mesangial cells. *Curr Opin Nephrol Hypertens* **6**, 88-105. (1997).

341. Haas, C. S., Schocklmann, H. O., Lang, S., Kralewski, M. & Sterzel, R. B. Regulatory mechanism in glomerular mesangial cell proliferation. *J Nephrol* **12**, 405-15. (1999).

342. Norstedt, G. & Palmiter, R. Secretory rhythm of growth hormone regulates sexual differentiation of mouse liver. *Cell* **36**, 805-12 (1984).

343. Johnson, D., al-Shawi, R. & Bishop, J. O. Sexual dimorphism and growth hormone induction of murine pheromone-binding proteins. *J Mol Endocrinol* **14**, 21-34 (1995).

344. Cavaggioni, A. & Mucignat-Caretta, C. Major urinary proteins, alpha(2U)-globulins and aphrodisin. *Biochim Biophys Acta* **1482**, 218-28 (2000).

8 Appendix

8.1 Staining procedures for paraffin embedded sections

8.1.1 Hemalaun & Eosine (H&E)

1. Mayer's hemalaun (Applichem, Germany)   5 min
2. Rinse in tap water   5 min
3. 0.5% HCl-alcohol   until slides have cleared
4. Rinse in tap water   5 min
5. Eosine Y (Merck, Germany)   dip 2-7 times
6. Rinse in distilled water   3 times, 3 sec

8.1.2 Periodic acid-Schiff stain (PAS)

1. 1% periodic acid (Applichem, Germany)   10 min
2. Rinse in tap water   10 min
3. Rinse in distilled water   3 times, 3 sec
4. Schiff's reagent (Merck, Germany)   30 min
5. Rinse in tap water   5 min
6. Mayer's hemalaun (Applichem, Germany)   2 min
7. Rinse in tap water   5 min
8. 1% HCl alcohol   1 sec
9. Rinse in tap water   5 min

8.2 Staining procedures for plastic embedded sections

8.2.1 Hemalaun & Eosine (H&E)

1. Mayer's hemalaun (Applichem, Germany)   30 min
2. Rinse in tap water   10 min
3. 1% HCl-Alcohol   1 sec
4. Rinse in tap water   10 min

5. Dry
6. Eosine Y (Merck, Germany)   5 min
7. Distilled water   3 times, 3 sec

8.2.2 Periodic acid-Schiff stain (PAS)

1. 1% periodic acid (Applichem, Germany)   15 min
2. Distilled water   3 times, 3 sec
3. Schiff's reagent (Merck, Germany)   30-60 min
4. Rinse in tap water   30 min
5. Dry
6. Mayer's hemalaun (Applichem, Germany)   35 min
7. Rinse in tap water   10 min
8. 1% HCl alcohol   1 sec
9. Rinse in tap water   10 min
10. Dry

8.2.3 Periodic acid silver methenamine (PASM) PAS stain

1. 1% periodic acid (Applichem, Germany)   15 min
2. Distilled water   3 times, 3 sec
3. Dry
4. Silver-methenamine solution containing:

    3% Methenamine solution   50 ml
    5% Silver nitrate (Applichem, Germany)   2.5 ml
    2% Sodium tetraborate decahydrate (Borax)   6 ml
    Distilled water   45 ml
    Pre-heat to 60° C in a water bath   5 min

Staining: shake in a closed water bath at 60°C   15-50 min
(staining intensity has to be controlled repeatedly)
5. Distilled water   3 times, 3 sec
6. 1.5% Sodium thiosulphate solution   2 min
7. Rinse in tap water   5 min

8. Dry

9. Schiff's reagent (Merck, Germany)   60 min

10. Rinse in tap water   30 min

11. Dry

12. Mayer's hemalaun (Applichem, Germany)   25 min

13. Rinse in tap water   10 min

14. 1% HCl alcohol   1 sec

15. Rinse in tap water   10 min

16. Dry

Curriculum vitae

Thomas Fisch
Unterhachinger Straße 53
D-81737 München
eMail: thomas_fisch@gmx.de

Date of birth	17.12.1973
Place of birth	Fürstenfeldbruck

1980 – 1984	Grundschule am Pfanzeltplatz, Munich
1984 – 1993	Asam Gymnasium, Munich
09.07.1993	Allgemeine Hochschulreife

1993 – 1994	Civil service, Department of Medicine II, Klinikum Grosshadern, Ludwig-Maximilian-University, Munich

1994 – 2000	Student of veterinary medicine, Ludwig-Maximilian-University, Munich
29.08.2000	Final exams
14.11.2000	Approbation

15.10.2000	Begin of this doctorate at the Institutes of Veterinary Pathology and Molecular Animal Breeding and Biotechnology/Gene Center, Ludwig-Maximilian-University, Munich